EIDO International Doctor School

DOCTORAL DISSERTATION

Control of the structure of marine picoplankton communities by turbulence and nutrient supply dynamics

Jose Luis Otero Ferrer

2020

Universidade Vigo

EIDO
Escola Internacional
de Doutoramento

Universidade Vigo

International Doctoral School

José Luis Otero Ferrer

DOCTORAL DISSERTATION

"Control of the structure of marine picoplankton communities by turbulence and nutrient supply dynamics"

Supervised by:

Beatriz Mouriño Carballido

Pedro Cermeño Ainsa

2020

The work leading to this PhD Thesis was carried out in the framework of the CHAOS (Control of tHe structure of marine phytoplAnkton cOmmunities by turbulence and nutrient supply dynamicS, CTM2012-30680) project granted to B. Mouriño-Carballido by Spanish Ministry of Economy, Industry and Competitivity (MINECO).

The PhD candidate was supported by a FPI fellowship (CTM2012-30680) from the MINECO. Research short stays in the IIM-CSIC (Barcelona) (2 month) and the Japan Agency for Marine-Earth Science and Technology (Tokio, 3 months) were funded by the MINECO (EEBB-I-15-09468, EEBB-I-16-11485, respectively).

Chapter 2 of the present PhD Thesis is published as: Otero-Ferrer, J. L., Cermeño, P., Bode, A., Fernández-Castro, B., Gasol, J. M., Morán, X. A. G., Marañon, E., Moreira-Coello, V., Varela, M. M., Villamaña, M., and Mouriño-Carballido, B.: Factors controlling the community structure of picoplankton in contrasting marine environments, Biogeosciences, 15, 6199-6220, https://doi.org/10.5194/bg-15-6199-2018, 2018.

A summarized version of chapter 3 is currently in preparation for submission as an article entitled "Competitive dynamics of the cyanobacterium *Synechococcus* sp. and the picoeukaryote *Micromonas pusilla* under dynamical nutrient supply conditions" authored by Otero-Ferrer J.L., Mouriño-Carballido B., Vallina S., Smith L., Marañon E., Cermeño P.

A summarized version of chapter 4 is currently under revision in Nature Geosciences entitled "Estimation of the vertical supply of nitrate turbulent diffusion in contrasting marine environments" authored by Mouriño-Carballido B., Otero-Ferrer J.L, Blazquez-Maseda M., Fernández-Castro B., Aguiar-González B., Chouciño P., Graña R., Villamaña M., Moreira-Coello V.

" I presume that the numerous lower pelagic animals persist on the infusoria, which are known to abound in the open ocean: but on what, in the clear blue water, do these infusoria subsist?

Charles Darwin, 1845.

Acknowledgements/Agradecimientos

Mucho ha cambiado desde que empecé la tesis en 2014, en el calendario se ve una fecha muy lejana, sin embargo, parece que fue ayer cuando llegué a Vigo. Durante este camino, he crecido profesional y personalmente, sin duda siempre estaré agradecido de esta etapa de mi vida en GOB. Especialmente quería agradecer a mis directores de tesis, Bea y Pedro, por confiar en mí y darme esta oportunidad. Al resto del laboratorio simplemente gracias por haberme acogido, me llevo recuerdos de grandes momentos y buenas amistades.

Gracias finalmente a mis hermanos y a mis padres por haberme apoyado en toda esta etapa. También quería agradecer a Vicente, a Carlos, a Chelo y a Eli su apoyo en esta recta final, estoy seguro de que sin vosotros este momento no hubiera sido posible.

Vigo, 7 de enero de 2020

Contents

Figures

Tables

Chapter 1

Introduction

Phytoplankton and the biological carbon pump

Phytoplankton are responsible for about 90% of the primary production that takes place in the ocean, which represents almost half of the primary production of the biosphere, and therefore they play a key role in the exchange of carbon dioxide (CO_2) and other radiatively active gases between the ocean and the atmosphere (Field et al. 1998; Falkowski 2012). Though most of marine primary production is recycled almost instantaneously within the sunlit layer of the ocean, a fraction of this primary production sinks into the deep ocean. This downward export flux creates a deficit of carbon (C) in the upper ocean which is compensated by the diffusive drawdown of CO_2 from the atmosphere, the so called biological pump (Figure 1.1) (Volk and Hoffert 2013; Sarmiento and Gruber 2013). The strenght of the pump is dependent on the structure of plankton communities (Boyd et al. 2013; Guidi et al. 2016), and controlled by the relative rates of primary production and organic C remineralization (Kwon et al. 2009). About 10% of this newly produced organic C in the surface ocean is exported through gravitational sinking of particles. Finally, after multiple transformations, a fraction of the exported material reaches the deep ocean where it is sequestered over timescales of hundreds to millions of years. Therefore, the biological pump is a first order contributor to the global ocean's capacity to act as a C sink (Takahashi et al. 2009).

Due to their large cells sizes and mineral ballasts that increase sinking rates, large-sized phytoplankton, chiefly diatoms and coccolithophores, are thought to be the main responsible for the strengthening of the biological C pump (Sarthou et al. 2005; Cermeno et al. 2008; Agustí et al. 2015). However, previous evidence suggests that small autotrophic picoplankton could contribute to organic C export and the biological C pump either through physical subduction of surface waters into the deep ocean (Omand et al. 2015), through cell attachment to large settling particles and/or through consumption and organic C channeling towards upper trophic levels (Richardson and Jackson 2007). The functioning of the biological C pump can be then quantified in terms of the *f*-ratio, defined as the ratio of new production to the sum of new plus regenerated production (Eppley and Peterson 1979). The extent to which autotrophic picoplankton contributes to new production and the biological C pump remains largely unresolved.

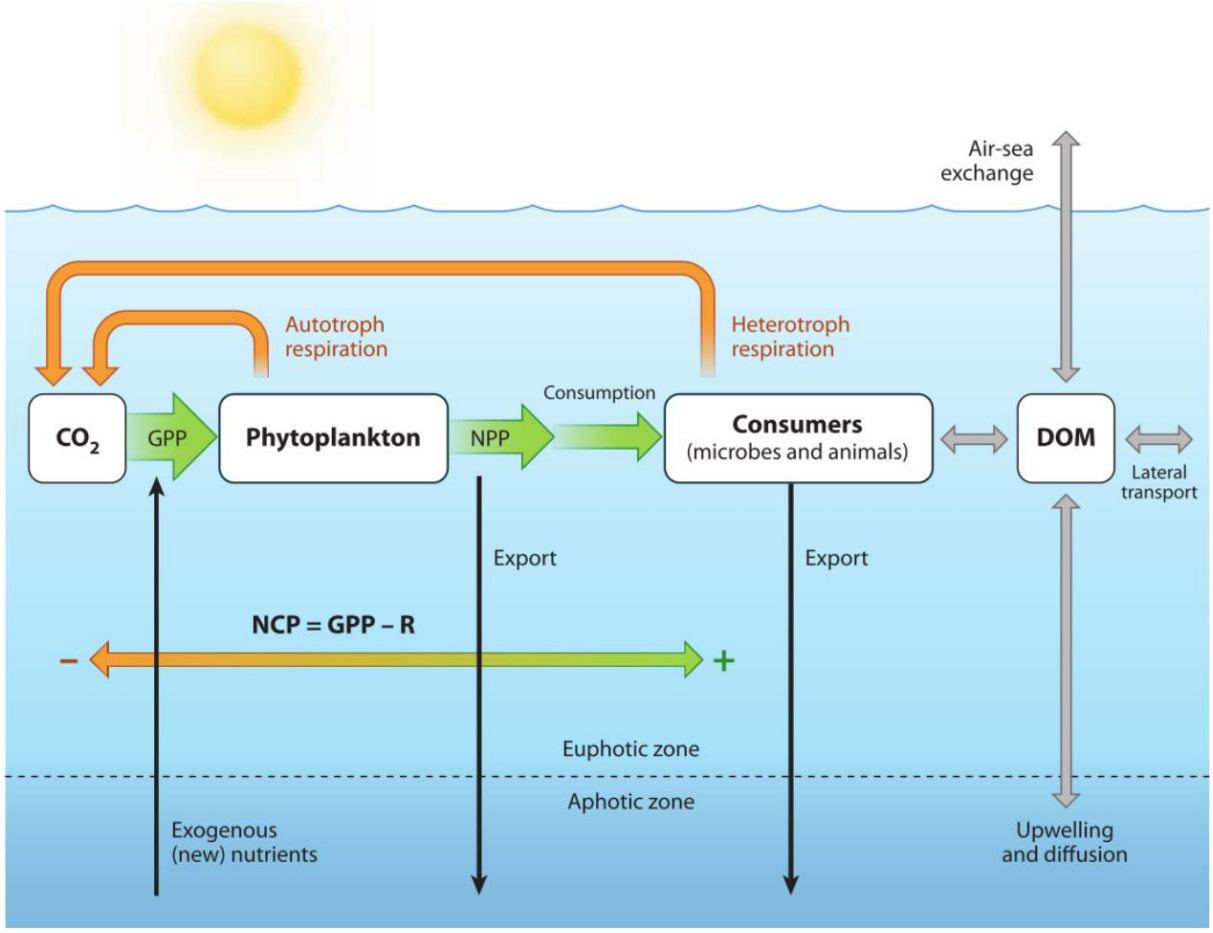

Figure 1.1 *The biological carbon pump. Reproduced from Ducklow and Doney (2013).*

Relevance of nitrogen and supply mechanisms

Phytoplankton require many different chemical elements in order to build the molecules essential to life. As reported in the classical Redfield (1958) paper there is a reasonable degree of uniformity in the measured chemical composition of plankton in the different oceans, although different phytoplankton species can have different chemical composition, which can also vary regionally (Galbraith and Martiny 2015).

Nitrogen is the primary limiting nutrient in most tropical and subtropical regions of the open ocean (Figure 1.2), as well as in temperate and polar seas during periods of seasonal stratification (Moore et al. 2013). Due to the relevance of nitrogen in marine ecosystems most of the important processes of the biological C pump can be defined in terms of nitrogen. Primary production can be supported by nitrogen inputs recently supplied from outside the photic layer (named new production, usually in the form of nitrate), or by nitrogen remineralized within the photic layer (regenerated production, usually as urea or amonia) (Dugdale et al. 1967). In most

ocean regions only a small fraction of photosynthesis is based on new nitrogen, being most phytoplankton production supported by recycled nitrogen (Yool et al. 2007; Berthelot et al. 2018). When large temporal and spatial scales are considered and for fixed stoichiometry of the organic matter, new production will be equivalent to the amount of organic carbon that can be exported to the deep ocean (export production), where it will remain isolated for long periods of time (Lewis et al. 1984).

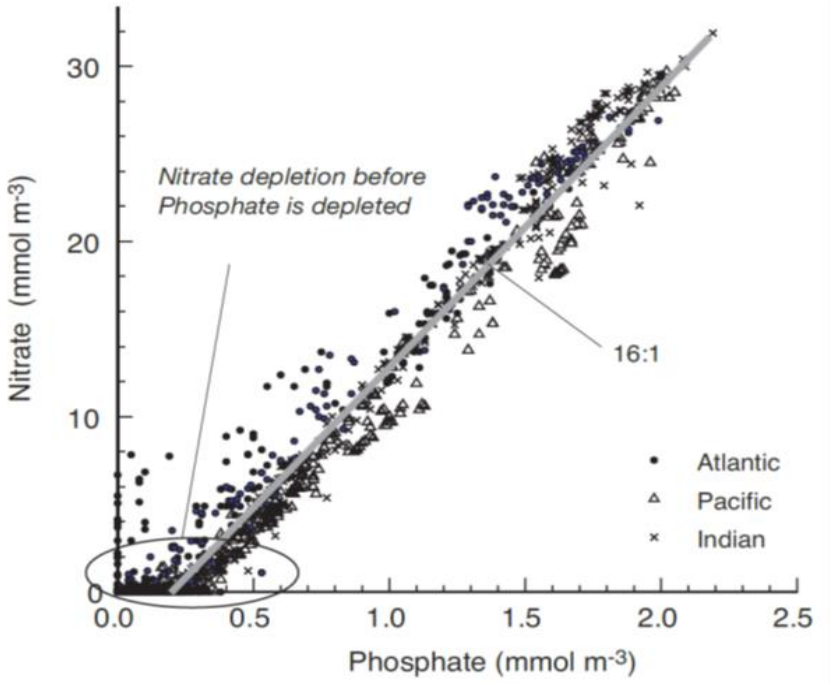

Figure 1.2 *Plot of near-surface concentrations of phosphate versus nitrate from selected WOCE cruises and the full set of GEOSEC cruises. The grey line with a slope of 16:1 represents the Redfield N:P proportion. Note that in most regions of the world ocean, nitrate becomes depleted before phosphate. Reproduced from Sarmiento and Gruber (2006)*

Mechanisms contributing to new production include biological nitrogen fixation, atmospheric deposition, and vertical and horizontal transport of organic and inorganic forms of nitrogen. Recent studies suggests that biological nitrogen fixation, the transformation of atmospheric N_2 to reduced bioavailable ammonium, is the main mechanism that supplies new nitrogen to the ocean (Voss et al. 2013). Due to its high abundances and N_2 fixation rates, the colonial cyanobacteria *Trichodesmium* that inhabits warm, stratified and oligotrophic regions (Langlois et al. 2005), has been traditionally considered the major marine diazotroph (Capone et al. 1997, 2005). However, the large diversity of marine diazotrophs and their wide distribution (Zehr et al. 2000, 2003; Riemann et al. 2010; Farnelid et al. 2011; Moreira-Coello et al. 2019) expanded the environments where biological N_2 fixation may be an important process (Moisander et al. 2010). The comparison of studies quantifying the relevance of nitrogen fixation as a supply

mechanism of new nitrogen has given rise to a wide range of results (Capone et al. 2005; Mouriño-Carballido et al. 2011; Painter et al. 2013; Sandel et al. 2015; Fernández-Castro et al. 2015; Moreira-Coello et al. 2017; Caffin et al. 2018). Atmospheric nitrogen deposition, that has increased in recent years as a consequence of human activity (Duce et al. 2008; Paerl et al. 2016), constitutes a significant source of new nitrogen which can alters the structure and metabolism of coastal and open ocean planktonic microbial communities (Paerl 1997; Paerl et al. 2002; Marañón 2010; Martínez-García et al. 2010). Another mechanism that can provide organic and inorganic nitrogen to the photic layer is horizontal and vertical transport, including the transport of surface Ekman (Williams and Follows 1998) and mesoscale and submesoscale eddies (McGillicuddy et al. 1998; McGillicuddy 2016; Lévy et al. 2018). Finally, over large regions of the tropical and subtropical open ocean and in temperate coastal regions during summer stratification vertical turbulent diffusion of nitrate is an important mechanism of new nitrogen supply (Lewis et al. 1984; Mouriño-Carballido et al. 2011; Painter et al. 2013; Fernández-Castro et al. 2015).

Quantifying the transport of nutrients from the deep ocean into the surface euphotic layer by turbulent diffusion requires calculating the magnitude of vertical diffusivity (Kz), which can be derived from observations of microstructure turbulence (Figure 1.3). Methodological difficulties for quantifying turbulence in the field motivated the estimation of nutrient turbulent diffusion by using constant values of Kz (Capone et al. 2005), and empirical diffusivity parameterizations (Planas et al. 1999). However, the increased commercialization of microstructure turbulence profilers has facilitated the collection of microstructure turbulence observations, and revealing an important variability of Kz in the upper layer (Hibiya et al. 2007; Mouriño-Carballido et al. 2011, 2016; Jurado et al. 2012; Cuypers et al. 2012; Fernández-Castro et al. 2014; Villamaña et al. 2017; Bendtsen and Richardson 2018). In other studies the amount of dissolved inorganic nutrients in the photic layer has been considered as an estimator of nutrient availability for phytoplankton cells (Agawin et al. 2000; Flombaum et al. 2013). In this regard, recent studies have proposed several estimators of global and local nitrate fields by using sea surface temperate, mixed layer depth, and surface chlorophyll-a (Switzer et al. 2003; Arteaga et al. 2015; Liang et al. 2018).

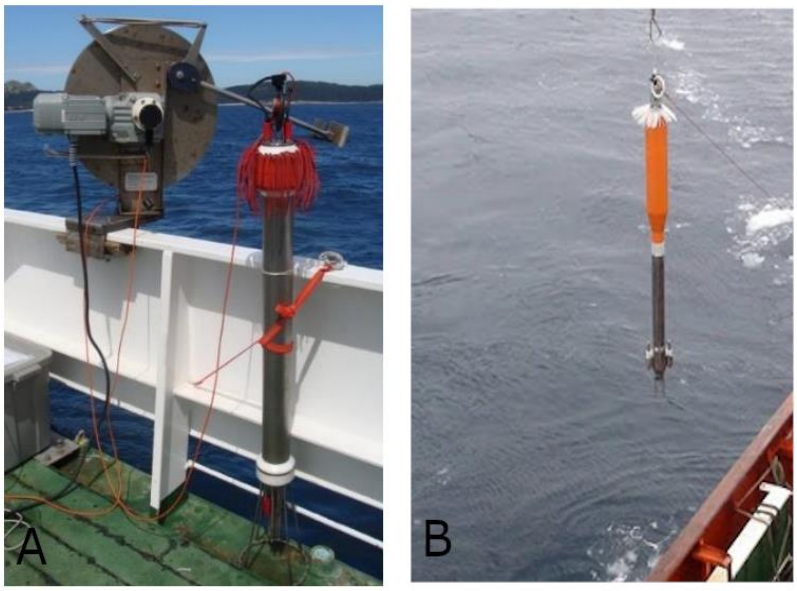

Figure 1.3 *A) MSS and B) TurboMAP multiparameter high resolution profilers for the measurement of microstructure turbulence in aquatic environments.*

The smallest size-fraction: picoplankton

The study of marine microbial distribution patterns has been constrained by the technological limits in observing and identifying of small-size organisms. The advent of epifluorescence microscopy during the 70´s (Hobbie et al. 1977; Zimmermann 1977; Porter and Feig 1980) as well as the introduction of automated cell counting by Coulter Counter and Flow Cytometry techniques (Sheldon and Parsons 1967) enabled the detection and enumeration of different microbial plankton organisms from field samples (Olson et al. 1985). These technological advances gave rise during the 80's to the sequential discovery of the smaller autotrophic organisms inhabiting aquatic ecosystems; *Synechococcus* (Waterbury et al. 1979), the picoeukaryotes (Johnson and Sieburth 1982) and *Prochlorococcus* (Chisholm et al. 1988). Subsequenlty, DNA-based fluorescent dyes were used to distinguish *Prochlorococcus* from non-photosynthetic bacteria (Monger and Landry 1993) and divide heterotrophic prokaryotes in two groups based on the hight (HNA) or low (LNA) nucleic acids content (Gasol and Del Giorgio 2000; Marie and Partensky 2006). Photosynthetic picoplankton dominates the biomass (Figure 1.4) and primary production of phytoplankton communities in oligotrophic tropical and subtropical regions (Chisholm 1992). In contrast,they are a minor component of phytoplankton communities in nutrient-replete polar and temperate seas and coastal environments, where phytoplankton communities are usually dominated by large-sized species (Finkel et al. 2010; Marañón et al. 2015).

The discovery of picoplankton led to a paradigm shift in plankton ecology by introducing the concept of microbial food web. In a microbial food web most of the recently photosynthesised biomass is rapidly recycled within the surface ocean by communities of microbial heterotrophs. The functioning of these microbial food webs contrasts with the functioning of the classical trophic chain in which most of the photosynthesized biomass is channeled towards upper trophic levels and eventually stripped out of the system. Whereas the classical trophic chain is characteristic of phytoplankton communities dominated by large-sized organisms, the microbial food web is more prevalent when phytoplankton communities are dominated by small-sized cells (Azam et al. 1983; Fenchel 2008). Despite that most of the picophytoplankton biomass is recycled through microbial food webs, previous studies have suggested that photosynthetic picoplankton could also play a role in the export of C to the deep ocean (Richardson and Jackson 2007; Lomas and Moran 2011; Guidi et al. 2016). As a result, the role ofpicophytoplankton in the export of C has attracted considerable interest during the last decade given that they account for much of the biomass and primary production in vast regions of the global ocean, and that its overall contribution to phytoplankton biomass and primary production could increase in future climate warming scenarios (Laufkötter et al. 2016).

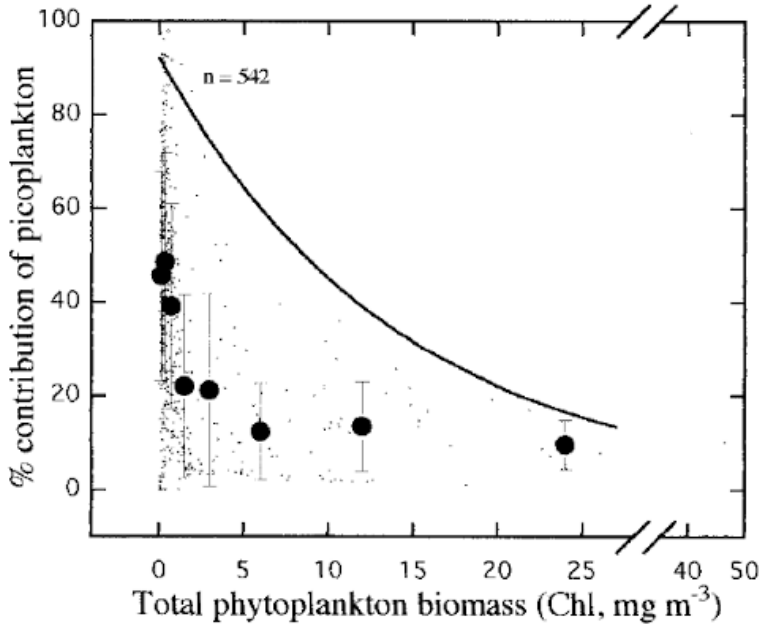

Figure 1.4 *The relationship between the percent contribution of picophytoplankton fraction to total phytoplankton biomass (mg Chl m^{-3}). Solid symbols represent the mean percentage within increasing bins and their standard error, and the solid line indicates the envelope determined by fitting a curve to the maxima of the bin intervals. Reproduced from Agawin et al., (2000).*

Although closely related phylogenetically, *Synechococcus* and *Prochlorococcus* exhibit distinct physiological traits (Moore et al. 1995), divergent evolutionary strategies (Scanlan and West 2002), and disparate geographic distributions (Zubkov et al. 2000). *Prochlorococcus* tend to be restricted to relatively warm (above 15 degrees Celsius) and nutrient-poor waters, extending from the surface down to 150 m, along the 40ºN–40ºS latitudinal band (Partensky et al. 1999; Johnson et al. 2006). *Synechococcus* exhibit a wider geographic and thermal distribution, including high-nutrient waters and, occasionally, reaching polar latitudes (Paulsen et al. 2016); their vertical distribution is shallower than that of *Prochlorococcus* (Partensky et al. 1999; Li 2002). The contribution of picoeukaryotes to picoplankton biomass is generally smaller than the contribution of picocyanobacteria (Zubkov et al. 2000; Buitenhuis et al. 2012), except in coastal regions where their contribution usually increases (Grob et al. 2007). In general, LNA prokaryotes dominate heterotrophic prokaryotic biomass in the oligotrophic open ocean, whereas HNA cells dominate in coastal regions (Li et al. 1995; Bouvier et al. 2007). These contrasting spatial distributions suggest that the picophytoplankton subgroups occupy different ecological niches or, according to the classical definition proposed by Hutchinson (1957), distinct multidimensional hyper-volumes of environmental factors in which viable populations develop. By describing the overlaps of environmental factors, realized niche partitioning can be defined, and the factors controlling the distribution of picoplankton subgroups can be identified. However, despite decades of experimental and field observations, the relative importance of the factors driving the variability in the growth and the spatial distribution of the different picophytoplankton subgroups remains largely unknown.

Environmental control factors in the distribution and activity of picoplankton

Aside from the effect of trophic controls, the distribution of microbial plankton is primarily determined by seawater temperature, light, and nutrients (Li 2002, 2009; Barton et al. 2015). Quantifying their relative influence on the spatial and temporal distribution of the different picophytoplankton subgroups is complicated by the fact that the above mentioned factors are often correlated in the ocean (Finkel et al. 2010). This shortcoming can be circumvented by using experimental approaches in the laboratory, where the influence of each independent factor is isolated. Alternatively, it can be approached by combining large datasets of hydrographic and

biological observations collected from contrasting marine environments, which allow us to characterize the suite of variables that best define the organism's ecological niches.

In order to study the significance of temperature and nutrient concentrations in determining the contribution of picophytoplankton to total phytoplankton biomass and production, Agawin et al. (2000) reviewed the available literature from oceanic and coastal estuarine areas. Although the number of observations for which both temperature and nutrient concentration were available was too small to statistically separate their effects, these authors hypothesized that the dominance of picoplankton in warm, oligotrophic waters was due to differences between picophytoplankton and larger phytoplankton cells in their capacity to use nutrients and grow. Bouman et al. (2011) investigated how vertical stratification controls the community structure of picophytoplankton in subtropical regions. They found that photosynthetic picoeukaryotes dominate in weakly stratified ocean systems, whereas *Prochlorococcus* and cyanobacteria are more prevalent in strongly stratified ocean environments . More recently, Flombaum et al. (2013) used a compilation of flow cytometry data from all major ocean regions and concluded that the distributions of *Prochlorococcus* and *Synechococcus* were controlled by temperature and photosynthetically active radiation (PAR, 400–700 nm wavelength), with nitrate concentration playing a negligible role. The analysis of Flombaum et al. (2013) was concentrated on data from tropical and subtropical domains. In these regions, surface nitrate concentrations are almost depleted and their variabilities cannot be interpreted as changes in their availability, which mainly depends on external inputs by turbulent diffusion (Mouriño-Carballido et al. 2016). It is also believed that fine-scale turbulence can enhance the nutrient uptake and subsequent growth of larger phytoplankton (Lazier and Mann 1989; Karp-Boss et al. 1996; Guasto et al. 2012), especially in regions with low nutrient levels and strong grazing pressure (Barton et al. 2014).

As far as I know, only one study has previously used estimates of nitrate supply, derived from observations of microstructure turbulence, to investigate the role of nitrate availability in controlling the composition of picoplankton communities (Mouriño-Carballido et al. 2016). These authors, using local data from the northwestern Mediterranean Sea, found that the different picophytoplankton subgroups exhibited contrasting responses to nitrate supply and that, as a consequence, the ratio of prokaryotic to picoeukaryotic photoautotrophic biomass decreased with increasing nitrate supply (Figure 1.5). However, whether these patterns are general and

widespread in the ocean remains largely uncertain, given the lack of datasets including concurrent measurements of turbulent diffusion nutrient fluxes and picophytoplankton community composition.

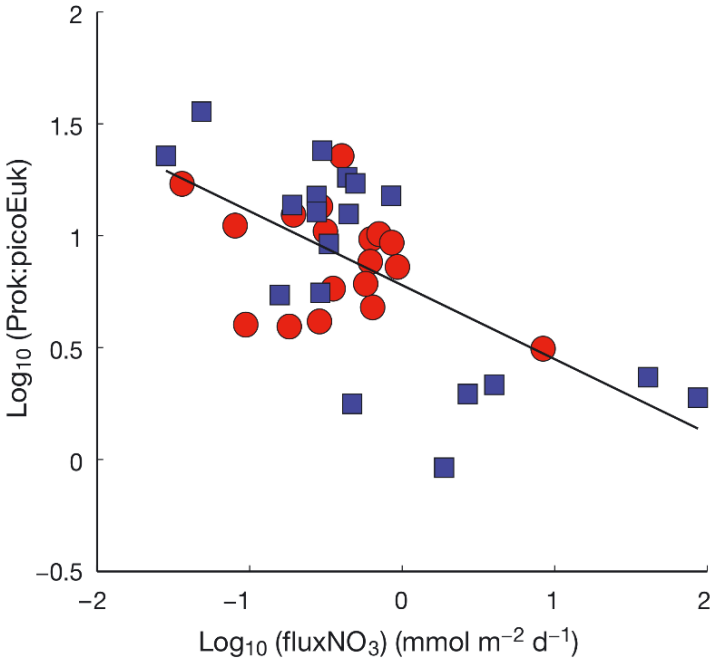

Figure 1.5 *Ratio of prokaryote to small picoeukaryote photic layer depth-integrated biomass versus vertical diffusive flux of nitrate. Reproduced from Mouriño-Carballido et al. (2016).*

Effects of competition on picoplankton community composition

Ecological niche differentiation is possible whenever habitats exhibit some degree of environmental heterogeneity across space and/or through time. In marine plankton ecosystems, a significant source of environmental heterogeneity lies in the temporal fluctuation of nutrient supplies or nutrient supply dynamics, which has been demonstrated to contribute to sustain the diversity of phytoplankton assemblages (Sommer 1989; Fawcett et al. 2011; Smeti et al. 2016). Hutchinson (1961) realized that phytoplankton communities are much more diverse than predicted by the principle of competitive exclusion. This discrepancy between field observations and theoretical expectations led him to propose the so called Paradox of the Plankton. The principle of competitive exclusion establishes that the total number of species that coexist in a given habitat cannot exceed the total number of limiting resources (MacArthur 1972; Tilman 1980, 1982) and, therefore, the outstanding diversity of marine phytoplankton communities, much greater than the number of limiting resources, has been argued to be paradoxical. This apparent inconsistency between field observations and theoretical models has been explained as a result

of the permanent environmental variability of aquatic plankton ecosystems. In steady-state, the minimum resource level that can support a species population, also known as *R**, determines the outcome of competition:

$$R^* = \frac{D}{(\mu_{max} - D)} * K_s$$

where *D* is the mortality rate, which is equivalent to the dilution rate in a continuous culture steady-state system, μ_{max} is the species' maximum growth rate, and K_s is the half saturation constant for resource acquisition, that is the resource level at which the maximum resource acquisition rate takes half of its value. At steady-state, species tend to reduce the nutrient concentration in the bulk medium to values as low as their *R** and, as a consequence, the species with the lowest *R** is predicted to win the competition. However, the outcome of this competition process might change if the system deviates from the steady-state, which is a common feature of ocean plankton environments. Experimental studies and numerical competition models support this theoretical background for large-sized phytoplankton (Tilman 1977, 1982; Sommer 1986; Stolte and Riegman 1995; Takeya et al. 2004; Winkler et al. 2017). Margalef (1978) proposed a conceptual model, his famous mandala, to explain the ecological succession of dinoflagellates, coccolithophores and diatoms based on nutrient concentration and ocean turbulence, recognizing that these three distinct phytoplankton functional groups respond differently to variable nutrient supply regimes. Grover (1991) proposed the variable internal stores model, which accounts for temporal differences in species distributions as a result of their different capabilities to store nutrients in the interior of the cell. The ability of phytoplankton to store nutrients allows them to decouple the processes of nutrient acquisition and growth, giving a competitive advantage when nutrient supply is intermittent. This model was employed by Tozzi et al. (2004) to simulate the population dynamics of diatoms and coccolithophores, illustrating the classical opportunist versus generalist scheme. Following Tozzi et al. (2004) the theoretical model, Cermeño et al. (2011) showed that pulsed nutrient regimes lead to a higher competitive advantage of diatoms over coccolithophores in laboratory photobioreactors. Their study illustrates the way these two phytoplankton functional groups compete along gradients of ocean turbulence. Many studies have considered the effect of nutrient supply dynamics on the interspecific competition of large-sized phytoplankton species, yet, its effect on the different groups making up the picophytoplankton size fraction has received much less attention (Mouriño-Carballido et al. 2016; Villamaña et al. 2019b).

The extent to which *Synechococcus* or picoeukaryotes dominate the picophytoplankton community biomass has been suggested to influence the strength of the biological pump. Whereas *Synechococcus*-dominated microbial food webs tend to be more efficient at recycling organic matter, the picoeukaryotes are thought to play a more significant role in the downward export of organic carbon (Corno et al. 2007; Fawcett et al. 2011), as well as a source of food for upper trophic levels (Reckermann and Veldhuis 1997). Thus, understanding the mechanisms that control the relative contribution of *Synechococcus* and picoeukaryotes to picophytoplankton communities is crucial to improve our ability to predict the response of these communities to environmental changes and anticipate their ensuing biogeochemical impact (Richardson and Jackson 2007; Lomas and Moran 2011).

Hypothesis, objetives and thesis outline

Nutrient concentration is commonly used as a proxy of nutrient availability for phytoplankton. Recent studies suggest that picophytoplankton community distributions are controlled by temperature and light, discarding any potential role of nutrient concentration. However, nutrient concentration is often a poor predictor of nutrient availability, which is dependent on the relative rates of nutrient supply and biological consumption (Mouriño-Carballido et al. 2011). Nevertheless, quantifying the relative influence of temperature, light and nutrient availability on the spatial and temporal distribution patterns of the different picoplankton functional groups has become particularly complicated given that, in the ocean, all these factors are often correlated (Finkel et al. 2010). This shortcoming can be circumvented using experimental approaches in the laboratory or ecological models, wherein the influence of each independent factor can be isolated. **The main hypothesis of this thesis is that nutrient supply (steady-state versus dynamical supply) controls the composition of marine picoplankton communities.**

In order to test this hypothesis, this thesis tackles the following objectives:

1. To quantify the role of temperature, light, and nitrate fluxes as factors controlling the distribution of autotrophic and heterotrophic picoplankton subgroups.
2. To describe the ecological niches of the various components of the picoplankton community.
3. To explore the effect of nitrate supply dynamics on the competitive dynamics of two model marine picophytoplankton species, namely, the cyanobacterium *Synechoccocus sp.* and the picoeukaryote *Micromonas pusilla*.
4. To build a prediction model and obtain the first climatology of nitrate diffusion into the euphotic zone.
5. To predict the change in the structure of picophytoplankton communities (the cyanobacteria to picoeukaryotes ratio) in a future global change scenario.

In order to accomplish these goals, I used a multi-scale approach by combining i) field observations of physical, chemical and biological properties collected during 17 oceanographic cruises covering tropical and subtropical ocean regions, temperate seas and a coastal upwelling ecosystem, ii) laboratory experiments of competitive interactions between selected picophytoplankton strains, and iii) an ecological model that simulates the competition of phytoplankton

under many differrent nutrient supply scenarios.

This document is structured as follows. Chapter II evaluates the main physical factors that control picoplankton community structure in contrasting ocean environments. Chapter III evaluates the competitive dynamics of *Synechococcus* and *Micromonas pusilla*, a model oligotrophic picoeukaryote, in a bench-scale commercial photobioreactor. Chapter IV reports global and regional proxies of nitrate supply and infers global estimates of present-day and future ocean distributions of picoplankton subgroups based on the regression models reported in Chapter II. Finally, the main conclusions of this thesis are presented in Chapter V.

Chapter 2

Factors controlling the community structure of picoplankton in contrasting marine environments

The research work presented in this chapter is published as:
Otero-Ferrer, J. L., Cermeño, P., Bode, A., Fernández-Castro, B., Gasol, J. M., Morán, X. A. G., Marañon, E., Moreira-Coello, V., Varela, M. M., Villamaña, M., and Mouriño-Carballido, B.: Factors controlling the community structure of picoplankton in contrasting marine environments, Biogeosciences, 15, 6199-6220, https://doi.org/10.5194/bg-15-6199-2018, 2018.

Abstract

The effect of inorganic nutrients on planktonic assemblages has traditionally relied on concentrations rather than estimates of nutrient supply. We combined a novel dataset of hydrographic properties, turbulent mixing, nutrient concentration, and picoplankton community composition with the aims of (i) quantifying the role of temperature, light, and nitrate fluxes as factors controlling the distribution of autotrophic and heterotrophic picoplankton subgroups, as determined by flow cytometry, and (ii) describing the ecological niches of the various components of the picoplankton community. Data were collected at 97 stations in the Atlantic Ocean, including tropical and subtropical open-ocean waters, the northwestern Mediterranean Sea, and the Galician coastal upwelling system of the northwest Iberian Peninsula. A generalized additive model (GAM) approach was used to predict depth-integrated biomass of each picoplankton subgroup based on three niche predictors: sea surface temperature, averaged daily surface irradiance, and the transport of nitrate into the euphotic zone, through both diffusion and advection. In addition, niche overlap among different picoplankton subgroups was computed using nonparametric kernel density functions. Temperature and nitrate supply were more relevant than light in predicting the biomass of most picoplankton subgroups, except for *Prochlorococcus* and low-nucleic-acid (LNA) prokaryotes, for which irradiance also played a significant role. Nitrate supply was the only factor that allowed the distinction among the ecological niches of all autotrophic and heterotrophic picoplankton subgroups. *Prochlorococcus* and LNA prokaryotes were more abundant in warmer waters (>20 °C) where the nitrate fluxes were low, whereas *Synechococcus* and high-nucleic-acid (HNA) prokaryotes prevailed mainly in cooler environments characterized by intermediate or high levels of nitrate supply. Finally, the niche of picoeukaryotes was defined by low temperatures and high nitrate supply. These results support the key role of nitrate supply, as it not only promotes the growth of large phytoplankton, but it also controls the structure of marine picoplankton communities.

Introduction

Picoplankton, including archaea, bacteria, and picoeukaryotes are the smallest (cell diameter <2 µm) and most abundant organisms in marine ecosystems. Photosynthetic picoplankton often dominate marine phytoplankton biomass and primary production in oligotrophic tropical and subtropical regions (Chisholm 1992), whereas they are typically a minor component in nutrient-replete coastal environments, usually dominated by large-sized plankton species (Finkel et al. 2010; Marañón 2015). However, due to the large temporal and spatial variability in the structure and composition of the microbial community in shelf seas (Sherr et al. 2005), picoplankton, together with nanoplankton, can dominate the microbial community under certain conditions (Morán 2007; Espinoza-González et al. 2012). In addition, picoplankton contributes overwhelmingly to the recycling of organic matter (Azam et al. 1983; Fenchel 2008), and previous studies suggest that photosynthetic picoplankton could also play a role in the export of carbon to the deep ocean (Richardson and Jackson 2007; Lomas and Moran 2011; Guidi et al. 2016). As a result, picoplankton is considered a key component of the current carbon cycle and likely more important in future climate warming scenarios (Laufkötter et al. 2016). When analyzed using flow cytometric techniques, two genera of picocyanobacteria (*Prochlorococcus* and *Synechococcus*), one or two subgroups of autotrophic picoeukaryotes of different sizes (small and large), and two subgroups of heterotrophic prokaryotes, based on their high (HNA) or low nucleic acid (LNA) content, can be distinguished (Gasol and Del Giorgio 2000; Marie and Partensky 2006). Although closely related phylogenetically, *Synechococcus* and *Prochlorococcus* exhibit distinct physiological traits (Moore et al. 1995), divergent evolutionary strategies (Scanlan and West 2002), and disparate geographic distributions (Zubkov et al. 2000). *Prochlorococcus* tend to be restricted to relatively warm (above 15 ∘C) and nutrient-poor waters, extending from the surface down to 150 m, along the 40º N–40º S latitudinal band (Partensky et al. 1999; Johnson et al. 2006). *Synechococcus* exhibit a wider geographic and thermal distribution, including high-nutrient waters and occasionally reaching polar latitudes (Paulsen et al. 2016); their vertical distribution is shallower than that of *Prochlorococcus* (Partensky et al. 1999; Li 2002). The contribution of picoeukaryotes to picoplankton biomass is generally smaller than the contribution of picocyanobacteria (Zubkov et al. 2000; Buitenhuis et al. 2012) except in coastal regions where their contribution usually increases (Grob et al. 2007). In general, LNA prokaryotes dominate heterotrophic prokaryotic biomass in the oligotrophic open ocean, whereas HNA cells dominate in coastal regions (Li et al. 1995; Bouvier et al. 2007).

These contrasting spatial distributions suggest that the picoplankton subgroups occupy differential ecological niches or, according to the classical definition proposed by (Hutchinson 1957), distinct multidimensional hyper-volumes of environmental factors in which viable populations develop. By describing the overlaps of environmental factors, realized niche partitioning can be defined, and the factors controlling the distribution of picoplankton subgroups can be identified. However, despite decades of experimental and field observations, the relative importance of the factors driving the variability in the growth and the spatial distribution of picoplankton subgroups remains largely unknown.

Aside from the effect of trophic controls, the distribution of microbial plankton is primarily determined by seawater temperature, light, and nutrients (Li 2002, 2009; Barton et al. 2015). Quantifying their relative influence on the spatial and temporal distribution of the different picoplankton subgroups is complicated by the fact that the abovementioned factors are often correlated in the ocean (Finkel et al. 2010). This shortcoming can be circumvented by using experimental approaches in the laboratory, where the influence of each independent factor is isolated. Alternatively, it can be approached by combining large datasets of hydrographic and biological observations collected from contrasting marine environments, which allow us to characterize the suite of variables that best define the organism's ecological niches.

In order to study the significance of temperature and nutrient concentrations in determining the contribution of picophytoplankton to total phytoplankton biomass and production, Agawin et al. (2000) reviewed the available literature from oceanic and coastal estuarine areas. Although the number of observations for which both temperature and nutrient concentration were available was too small to statistically separate their effects, these authors hypothesized that the dominance of picoplankton in warm, oligotrophic waters was due to differences between picophytoplankton and larger cells in their capacity to use nutrients and in their intrinsic growth rate. Bouman et al. (2011) investigated how vertical stratification controls the community structure of picophytoplankton in subtropical regions. According to their results, photosynthetic picoeukaryotes dominate in weakly stratified waters, whereas in strongly stratified waters, *Prochlorococcus* cyanobacteria are prevalent. More recently, Flombaum et al. (2013), using a compilation of flow cytometry data from all major ocean regions, concluded that *Prochlorococcus* and *Synechococcus* abundance distributions were controlled by temperature and photosynthetically active radiation (PAR, 400–700 nm), discarding the role of nitrate concentration. However, in tropical and subtropical domains, the most well-represented regions in the

study of Flombaum et al. (2013) surface nitrate is almost depleted and the variability in its concentration can be widely disconnected from changes in its availability for phytoplankton, which depends more on the supply from deeper waters by turbulent diffusion (Mouriño-Carballido et al. 2016). It is also believed that fine-scale turbulence can enhance the nutrient uptake and subsequent growth of larger phytoplankton (Lazier and Mann 1989; Jumars et al. 2009; Guasto et al. 2012), especially in regions with low nutrient levels and strong grazing pressure (Barton et al. 2014).

As far as we know, only one study has previously used estimates of nitrate availability, derived from observations of microstructure turbulence, to investigate the role of nutrient availability in controlling the composition of picoplankton communities (Mouriño-Carballido et al. 2016). These authors, using local data from the northwestern Mediterranean Sea, found that different autotrophic picophytoplankton subgroups exhibit contrasting responses to nitrate supply and that as a result the ratio of prokaryotic to picoeukaryotic photoautotrophic biomass decreased with increasing nitrate supply. However, whether these patterns are general and widespread in the ocean remains largely uncertain, given that no concomitant datasets including measurements of turbulent diffusion nutrient flux and picoplankton subgroup structure have been available to date.

Here we extend the analysis described in Mouriño-Carballido et al. (2016) by combining a dataset of picoplankton community composition, hydrographic properties, turbulent mixing, and inorganic nutrient concentrations collected at a total of 97 stations. Observations were made in contrasting environments of the Atlantic Ocean in order to quantify the role of temperature, light, and nitrate availability in the composition of the picoplankton community and to describe the ecological niches of each picoplankton subgroup.

Material & Methods

This study includes data collected at 97 stations from three contrasting environments covering the tropical and subtropical Atlantic Ocean (T), the northwestern Mediterranean Sea (M), and the Galician coastal upwelling ecosystem (G), between October 2006 and December 2015 (Table 2.1 & Figure 2.1). Two cruises (CARPOS October–November 2006 and TRYNITROP April–May 2008) sampled 26 stations located in the tropical and subtropical Atlantic Ocean. Three other cruises carried out in the Mediterranean Sea (FAMOSO1 March 2009, FAMOSO2

April–May 2009, and FAMOSO3 September 2009) sampled 19 stations during three contrasting hydrographic conditions, covering from winter mixing to summer stratification. Finally, 52 stations were sampled in the Galician coastal upwelling ecosystem during the HERCULES1 July 2010, HERCULES2 September 2011, HERCULES3 July 2012, DISTRAL February–November 2012, ASIMUTH June 2013, CHAOS August 2013, and NICANOR February 2014–December 2015 cruises. Additional information about the sampling design of these cruises is presented in (Mouriño-Carballido et al. 2011, 2016; Aranguren-Gassis et al. 2011; Cermeño et al. 2016; Villamaña et al. 2017; Moreira-Coello et al. 2017).

Table 2.1 *Details of the data included in this study. Domain referred to the tropical and subtropical Atlantic Ocean (T), the Mediterranean Sea (M), and the Galician coastal upwelling (G). N indicates the number of stations sampled at each cruise. Duration (mean ± standard deviation, in minutes) is the time used for the turbulence profiler deployment in each station. Depth (mean ± standard deviation, in meters) is the maximum depth reached by the microstruture profiler.*

Domain	Region	N	Cruise	Vessel	Date	Duration	Depth
T	NE Atlantic	8	CARPOS	Hespérides	14/10/06-22/11/06	57 ± 24	137 ± 15
T	Atlantic	18	TRYNITROP	Hespérides	14/04/08 - 02/05/08	45 ± 12	219 ± 19
M	Liguro-Provençal Basin	6	FAMOSOI	Sarmiento de Gamboa	14/3/09 - 22/3/09	66 ± 5	259 ± 38
M	Liguro-Provençal Basin	10	FAMOSO II	Sarmiento de Gamboa	30/4/09-13/05/09	94 ± 4	273 ± 2
M	Liguro-Provençal Basin	3	FAMOSOIII	Sarmiento de Gamboa	16/09/09 - 20/09/09	133 ± 3	323 ± 24
G	Ría de A Coruña	1	HERCULES I	Lura	07/06/2010	20 ± 4	35 ± 2
G	Ría de A Coruña	5	HERCULES II	Lura	28/09/11 - 29/09/11	11 ± 8	33 ± 26
G	Ría de A Coruña	13	HERCULESIII	Lura	16/07/12 - 20/07/12	8 ± 5	41 ± 29
G	Ría de Vigo	9	DISTRAL	Mytilus	14/02/12 - 06/11/12	110 ± 76	38 ± 1
G	Ría de Vigo	2	CHAOS	Mytilus	20/08/13 - 27/08/13	1515 ± 6	41 ± 29
G	Ría de A Coruña	12	NICANOR	Lura	27/02/14 - 17/12/15	33 ± 5	62 ± 3
G	Rías de Vigo & Pontevedra	10	ASIMUTH	Ramón Margalef	17/06/13 - 21/06/13	10 ± 4	28 ± 10

At each station, information about hydrographic properties, turbulent mixing, nitrate concentration, and picoplankton community composition was collected. Light conditions for each sampling station were considered to be the 5-day averaged daily surface PAR obtained from

satellite data (http://globcolour.info; last access: 18 October 2018). Light attenuation coefficients were obtained from vertical profiles of PAR estimated with LI-COR sensors using the Beer–Lambert law equation (Kirk 1994). Depth of the euphotic layer was calculated as the depth at which PAR was 1 % of its surface value. For those cruises for which PAR profiles were not available (ASIMUTH, CHAOS, and NICANOR), which sampled stations in the outer part of the Galician rias, the depth of the photic layer was calculated by considering light attenuation coefficients derived from surface chlorophyll a data, following the algorithms proposed by Morel et al. (2007) for Case-1 waters:

$$log_{10}Zeu = 1.524 - 0.460[Chl] - 0.00051[Chl]^2 + 0.0282[Chl]^3$$

where Zeu is the depth of the photic layer and Chl is the chlorophyll-a in the surface.

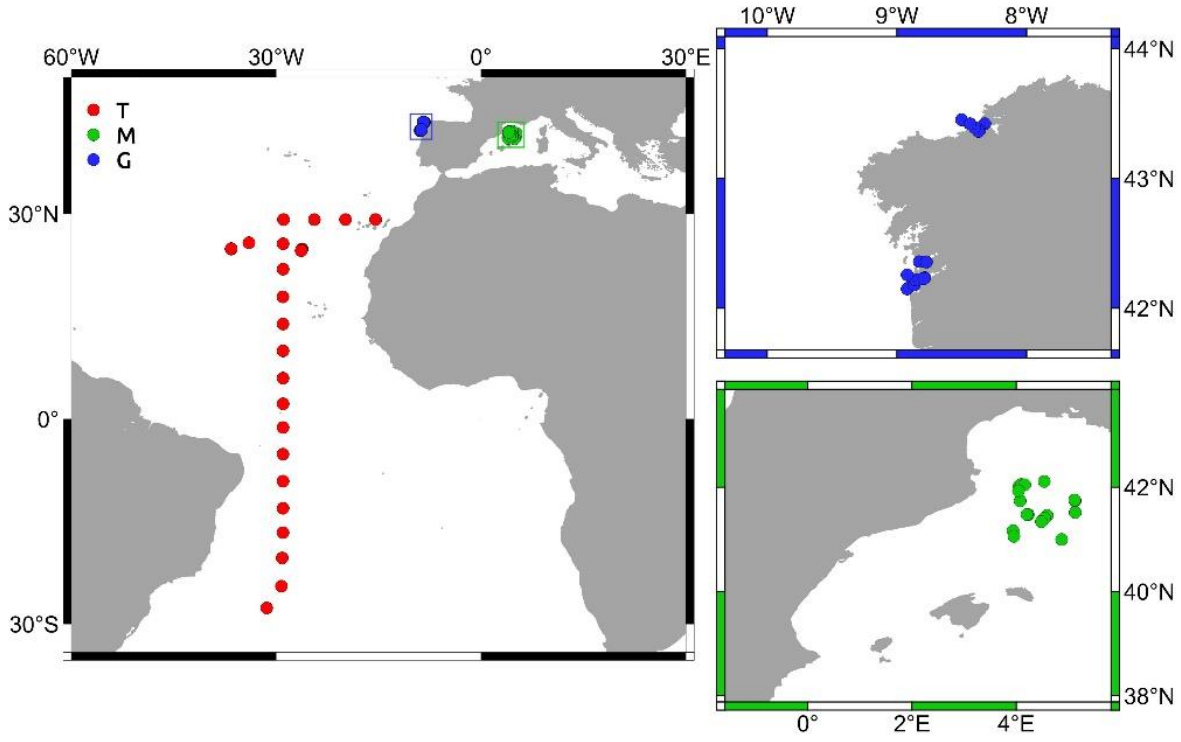

Figure 2.1 *Location of the stations sampled in the tropical and subtropical Atlantic ocean (T), the Mediterranean Sea (M), and the Galician coastal upwelling (G). Small panels provide details about those stations sampled in M (green) and G (blue).*

A comparison of the estimation of the base of the euphotic zone by using the Morel et al. (2007) equation and the data collected by a radiometer during the HERCULES cruise is shown in Figure 2.2.A.

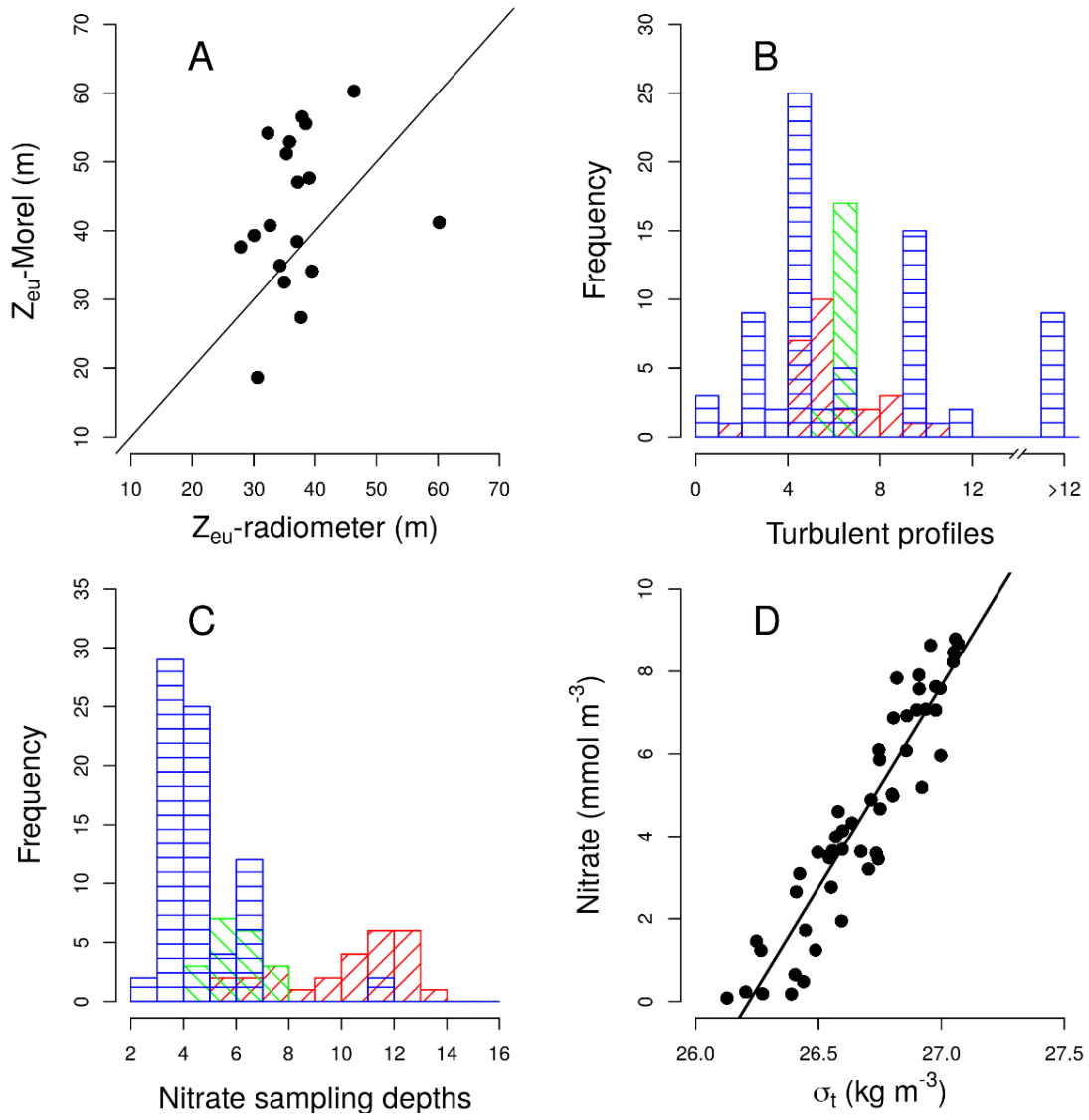

Figure 2.2 ***(A)*** *Pair scatter plot representing the relationship between the euphotic zone depth (Z_{eu}) computed using the Morel et al. (2007) equation and the data collected by a radiometer during the HERCULES cruises; the solid line represents 1:1 relationship.* ***(B)*** *Frequency histogram of the number of turbulence profiles deployed at each station and domain.* ***(C)*** *Frequency histograms of the number of samples collected for the determination of nitrate concentration at each station and domain: tropical and subtropical Atlantic Ocean (red), the Mediterranean (green), and the Galician coastal upwelling (blue).* ***(D)*** *Pair scatter plot representing the relationship between nitrate concentration and density built by using all samples collected during the NICANOR sampling period.*

Hydrography and turbulent mixing

Hydrographic properties and turbulent mixing were derived from a microstructure turbulent profiler (Prandke and Stips 1998a) equipped with a high-precision conductivity–temperature–depth (CTD) probe, two microstructure shear sensors (type PNS06), and also a sensor to measure the horizontal acceleration of the profiler. Measurements of dissipation rates of turbulent kinetic energy (ε) were conducted to the bottom, or to 137–323 m over deep waters (Table 2.1). The number of microstructure turbulence profiles used for computing nitrate fluxes at each station were always deployed successively. Sets include 2–11 in the tropical and subtropical Atlantic (37 ± 18 min), 6–7 in the Mediterranean (76 ± 22 min), and 3–402 in the Galician coastal upwelling (65 ± 246 min) (Figure 2.2.B). Episodic bursts of turbulence can induce episodic inputs of nutrient supply, which can be easily missed in sets of a low number of profiles. In coastal regions where short-term variability in mixing processes is expected to be higher, the dataset includes two high-frequency samplings carried out in the outer part of Ría de Vigo (Galician upwelling ecosystem) in August 2013 (CHAOS cruises). During these cruises two 25 h series of turbulent microstructure and current observations were carried out during spring and neap tides. Turbulent kinetic energy dissipation at the interface between upwelled and surface waters was enhanced by 2 orders of magnitude during the ebbs, as the result of the interplay of the bidirectional upwelling circulation and the tidal current shear (Fernández-Castro et al. 2018). Diffusive nitrate fluxes due to the enhanced dissipation observed during spring tide could be responsible for about half of the phytoplankton primary production estimated in this system during periods of upwelling relaxation–stratification (Villamaña et al. 2017).

The profiler was balanced to have negative buoyancy and a sinking velocity of 0.4 to 0.7 m s^{-1}. The frequency of data sampling was 1024 Hz. The sensitivity of the shear sensors was checked after each use. Due to significant turbulence generation close to the ship, only the data below 5 (HERCULES1, HERCULES2, HERCULES3, DISTRAL, ASIMUTH, CHAOS, and NICANOR) and 10 m (CARPOS, TRYNITROP, FAMOSO1, FAMOSO2, FAMOSO3) were considered reliable. Data processing and calculation of dissipation rates of (ε) were carried out with the commercial software MSSpro. The squared Brunt–Väisälä frequency (N^2) was computed from the CTD profiles according to the equation

$$N^2 = -(g\rho_w)(\partial\rho\partial z)(s^{-2})$$

where g is the acceleration due to gravity (9.8 m s^{-2}), ρ_w is seawater density (1025 kg m^{-3}), and

$\partial\rho/\partial z$ is the vertical potential density gradient. Vertical diffusivity (Kz) was estimated as

$$Kz = \Gamma \frac{\varepsilon}{N^2} (m^2 s^{-1}),$$

where Γ is the mixing efficiency, here considered to be 0.2 (Osborn 1980).

Nutrient supply

Samples for the determination of nitrate (NO_3) + nitrite (NO_2) were collected from 5 ± 2 (Galician coastal upwelling), 7 ± 1 (Mediterranean), and 11 ± 2 (tropical and subtropical Atlantic Ocean) different depths in rinsed polyethylene tubes and stored frozen at −20 °C until analysis on land, according to standard methods using the automated colorimetric technique (Hansen and Koroleff 1999). The frequency histogram of sampling depths collected for nitrate concentration in each region is indicated in Figure 2.2.C, whereas the maximum sampling depth at which the microstructure turbulence profiler was deployed is indicated in Table 2.1. At one station carried out during the NICANOR cruises, where nitrate concentrations were not available, concentration values were obtained by using a nitrate–density relationship built by using all samples (n=52) collected during the NICANOR sampling period. The relationship showed a linear behavior (NO_3 =9.7788×σt−256.38; Adj-R^2=0.87; *p-value*<0.001) for density ranging between 26.1 and 27.1 kg m^{-3} (Figure 2.2.D). Vertical diffusive fluxes of nitrate into the euphotic zone were calculated following Fick's law as

$$FluxNO_3 = K_z \Delta NO_3$$

where ΔNO_3 is the nitrate vertical gradient obtained by linear fitting of nitrate concentrations in the nitracline, determined as a region of approximately maximum and constant gradient, and (K_z) is the averaged turbulent mixing over the same depth interval. In the Galician coastal upwelling, nitrate diffusive fluxes were estimated over a fixed depth interval using the same procedure (10–40 m) except at the shallowest stations at which we compute the surface–bottom flux.

Most stations carried out in the Galician coastal upwelling were conducted inside three different rias (Ría de Vigo, Ría de Pontevedra, and Ría de A Coruña). The rias are coastal embayments affected by seasonal wind-driven coastal upwelling of cold, nutrient-rich North Atlantic Central Water (Wooster et al. 1976; Fraga 1981; Alvarez-Salgado et al. 1993). The

Galician rias, despite being, in general, longer and narrower than many open bays in upwelling areas, they resemble them in that its primary hydrographic and circulation features are determined by the extension of wind-driven flow on the external continental shelf throughout the bay (Alvarez-Salgado et al. 2009). Fertilization in the rias occurs essentially by coastal upwelling, with fresh and rain water inputs being residual (2 %) (Fernández et al. 2016). The total nitrate supply in the Galician rias was computed as the sum of nitrate vertical diffusion plus nitrate vertical advection due to coastal upwelling. A simplified estimate of nitrate supply through vertical advection due to upwelling was computed considering the Galician rias as single boxes divided into two layers (Alvarez-Salgado et al. 1993), the deeper one influenced by upwelled inflowing waters and the surface layer dominated by the outgoing flow. Assuming that the bottom layer volume is conservative and stationary, the vertical advective flux (Q_Z, $m^3\ s^{-1}$) would be equivalent to the incoming bottom flux (Q_B, $m^3\ s^{-1}$), computed as the product of the upwelling index (I_W, $m^3\ s^{-1}\ km^{-1}$) and the lengths of the mouth of the rias (ca. 10–11.5 km). I_W was averaged over the 3-day period before each cruise from wind data recorded by meteorological buoys located in Cabo Vilán (HERCULES, NICANOR) and Cabo Silleiro (DISTRAL, ASIMUTH, CHAOS, ASIMUTH), or modeled by the Fleet Numerical Meteorology and Oceanography Center (FNMOC) model when buoy data were not available (http://www.indicedeafloramiento.ieo.es; last access: 18 October 2018). Finally, the transport of nitrate into the euphotic zone through vertical advection was computed as

$$NO_3 Advective flux = Qz \frac{A_{basin}}{[NO_3]_D}$$

where A_{basin} is the surface area of the Galician rias, Q_Z is the vertical advective flux, and $[NO_3]_D$ is the averaged nitrate concentration at the base of the euphotic layer. A_{basin} is 141 km^2 for Ría de Pontevedra (ASIMUTH), 174 km^2 for Ría de Vigo (CHAOS, ASIMUTH, DISTRAL), and 145 km^2 for Ría de A Coruña (HERCULES, NICANOR) (see Villamaña et al. 2017; Moreira-Coello et al. 2017, for details).

Flow cytometry

Picoplankton samples (1.8 mL) for the determination of picoplankton abundance and cell properties were taken from three to nine depths and measured immediately onboard (TRYNITROP),

or preserved with paraformaldehyde plus glutaraldehyde (*P+G*) and frozen at −80 °C until analysis in the laboratory (the other cruises). Unfortunately, due to problems with sample preservation, only heterotrophic or autotrophic picoplankton subgroup data were available for the DISTRAL and ASIMUTH cruises, respectively. Two aliquots from the same sample were used for the study of picophytoplankton (0.6 mL) and heterotrophic prokaryotes (0.4 mL), analyzed at high (mean 60 µL min^{-1}) and low (mean 18 µL min^{-1}) flow rates for 4 and 2 min, respectively. Before the analysis, the DNA of heterotrophic prokaryotes was stained with nucleic-acid-specific fluorescent dye (SYTO-13 or SYBR1). A FACSCalibur flow cytometer (Becton, Dickinson and Company) equipped with a laser emitting at 488 nm was used to measure and count picoplankton. Autotrophic cells were separated into two groups of cyanobacteria (*Synechococcus* and *Prochlorococcus*) and one group of small picoeukaryotes, based on their fluorescence and light scatter signals (size scatter, SSC), as explained in Calvo-Díaz and Morán (2006). Two groups of heterotrophic prokaryotes (LNA and HNA) were distinguished based on their relative green fluorescence, which was used as a proxy for nucleic acid content (Gasol and Del Giorgio 2000; Bouvier et al. 2007).

In order to estimate biovolume (BV), we used an empirical calibration between SSC and cell diameter (Calvo-Díaz and Morán 2006), assuming spherical shape for all groups. The following volume-to-carbon conversion factors were used for picoautotrophic groups: 230 fg C BV for *Synechococcus*, 240 fg C BV for *Prochlorococcus*, and 237 fg C BV for picoeukaryotes (Worden et al. 2004). For bacteria, BV was converted into carbon biomass by using the allometric relationship: 108.8 fg C $BV^{0.898}$ (Gundersen et al. 2002). More details about the processing and analysis of flow cytometry samples are provided in Calvo-Díaz and Morán, 2006, (TRYNITROP), Gomes et al. 2015 (FAMOSO) and (Moreira-Coello et al. 2017) (NICANOR). Abundance data obtained at different depths for each station were combined to compute depth-integrated biomass for the photic layer.

Generalized additive models

A generalized additive model (GAM) approach was used to predict depth-integrated biomass of each picoplankton subgroup, the contribution of LNA prokaryotes to heterotrophic picoplankton, the cyanobacteria-to-picoeukaryote ratio, and the autotrophic-to-heterotrophic ratio based on observations and estimates of three environmental factors: sea surface temperature

(SST), daily surface PAR, and the transport of nitrate into the euphotic zone (NO_3 flux), including both diffusive and advective processes. GAMs assume that the effect of each predictor on the response variable can be described by smoothed functions whose effects are additive. Due to the large number of zero observations, data overdispersion, and the need for a single parsimonious model to make predictions for a large number of groups, we assumed that the depth-integrated biomass of each picoplankton subgroup, relative contribution values, and biomass ratios all followed negative binomial distributions. Those niche descriptors that did not follow normal distributions were log transformed. The complete model structure for the biomass of each picoplankton subgroup was

$$yj = I + s(SST) + s(PAR) + s(log(NO3Flux)) + Error$$

where y_j represents the depth-integrated biomass for each picoplankton subgroup j, and s a cubic regression spline used for fitting the observations to the model (Wood 2017).

Generalized models include a function linking the mean value of y_j and the predictors. For those response variables that followed a negative binomial distribution, the used link function was the natural logarithm. The LNA contribution to total heterotrophic prokaryotes was adjusted using a Gaussian distribution and an identify link (Wood et al. 2016). The inclusion of the different predictors to explain the response variable (the biomass of each picoplankton subgroup, its relative contribution, and biomass ratios) was assessed via stepwise model selection using the minimum Akaike information criterion (Hastie and Tibshirani 1993).

Smooth terms were tested using a Bayesian test (Marra and Wood 2012) to prevent overfitting. GAMs were evaluated based on explanatory power (explained variance) and goodness of fit (GOF). GOF was assessed via quantile–quantile (QQ) plots of Pearson residuals (Figure 2.3). All calculations were carried out using the mgcv package (Wood 2011) in R (R Core Team, 2015).

Niche overlap analysis

The estimation of niche overlap among different picoplankton subgroups based on nonparametric kernel density functions (NO_K) was calculated following Mouillot et al. (2005):

$$NO_{K_{i,j,t}} = 1 - 12\int |fit(x) - fjt(x)|dx$$

where NO_K is the niche overlap between picoplankton subgroups *i* and *j* for the environmental factor *t*, and f_{it} and f_{jt} are the kernel population density functions of factor *t* for species *i* and *j*, respectively. In order to correct the correlation among niche predictors, we used the estimator in a dependent sample (EDS) proposed by Kark et al. (2002).

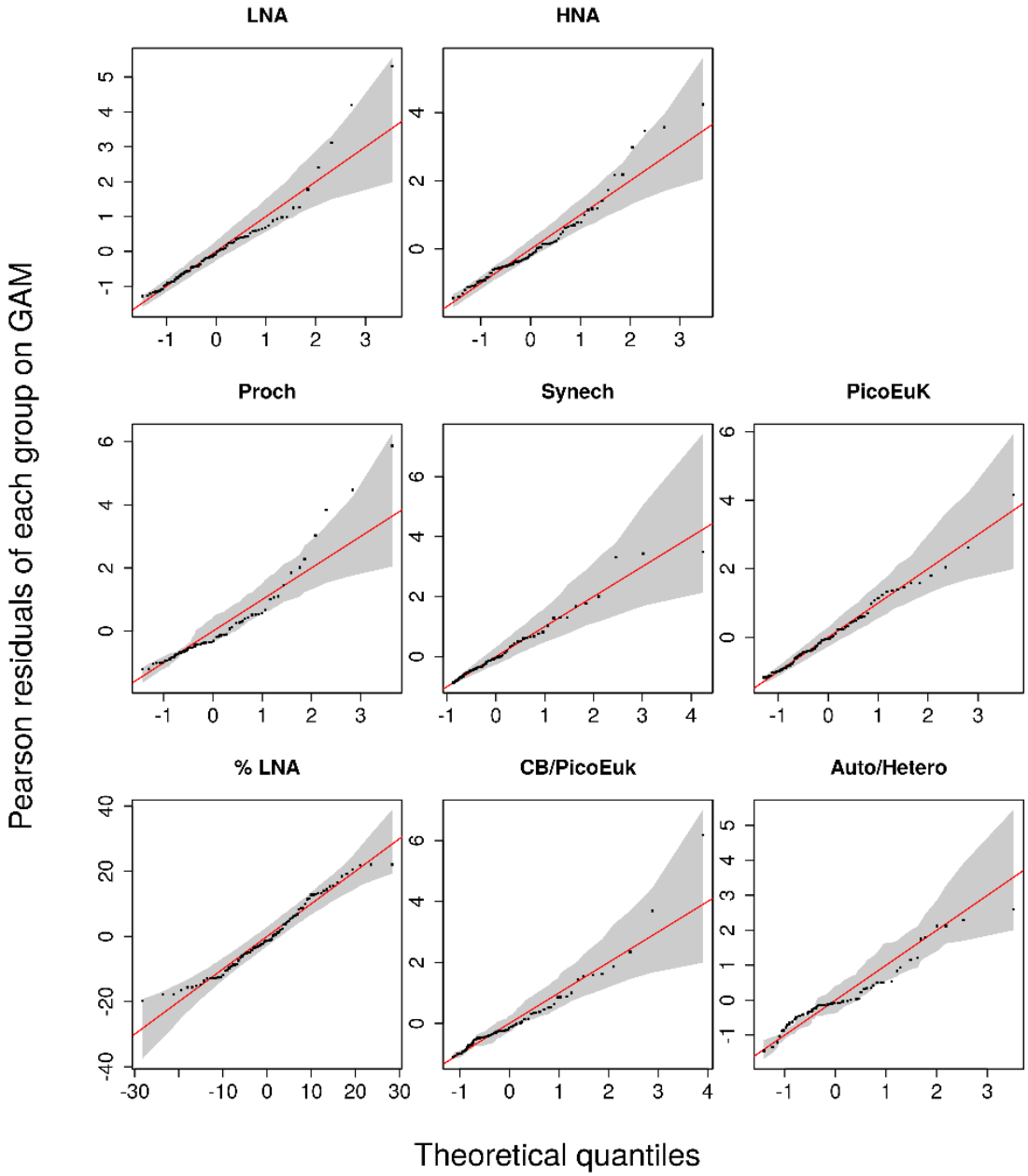

Figure 2.3 *Quantile–quantile (QQ) plots between the observations and the selected GAM models for each picoplankton subgroup, the contribution of LNA to heterotrophic picoplankton (%LNA), the cyanobacteria-to-picoeukaryote ratio (CB/ PicoEuk), and the autotrophicto-heterotrophic biomass ratio (Auto / hetero). The y axes represent the Pearson residuals and the x axes the negative binomial theoretical quantiles. Solid red lines indicate the theoretical quantile of the models and grey shadows the 95 % confidence intervals.*

To assess the statistical niche differences between subgroups, null model permutation tests were performed to verify whether the niche overlaps were significantly lower than 100 % (Geange et al. 2011). When the contribution of depth-integrated biomass for each picoplankton subgroup exceeded that expected by chance (one-third for autotrophic and one-half for heterotrophic picoplankton), niche predictors for each station were selected. Statistical null distributions (the distribution of the statistic test under the null hypothesis of no niche differentiation) were generated by calculating pseudo-values through randomly permuting group labels in the corresponding dataset over 10 000 runs. The distributions of the average niche overlaps for the null model were then computed. Niche overlap calculations and associated null model tests were performed using the density function and the source code provided as supporting information in (Geange et al. 2011). All calculations were performed using R (R Core Team 2015).

Results

Environmental variables and picoplankton biomass

The database covered a wide environmental gradient from oligotrophic to eutrophic conditions. Stations sampled in the tropical and subtropical Atlantic Ocean (T) were, on average, characterized by warm surface waters (26 ± 2 °C, mean ± SD) where the supply of nitrate through vertical diffusion from deeper waters (0.7 ± 1.6 mmol N m^{-2} d^{-1}) and surface chlorophyll *a* were low (0.1 ± 0.1 mg m^{-3}) (Figure 2.4 & Table 2.2). The Mediterranean Sea, sampled from March to September, was characterized by cooler surface waters (16 ± 4 °C) and intermediate values of both nitrate vertical diffusive supply (41 ± 113 mmol N m^{-2} d^{-1}) and also surface chlorophyll *a* (0.9 ± 0.9 mg m^{-3}). Finally, the stations sampled in the Galician coastal upwelling system, which included year-round samples, were characterized by relatively cold surface waters (16 ± 2 °C), enhanced rates of nitrate supply (30 ± 46 mmol N m^{-2} d^{-1}), and high values of surface chlorophyll *a* (2.2 ± 2.5 mg m^{-3}). No statistically significant differences were observed in averaged surface PAR among the three regions.

Differences in picoplankton biomass and composition were also observed among the three domains. Averaged photic layer depth-integrated total picoplankton biomass (including both LNA and HNA prokaryotes, *Prochlorococcus*, *Synechococcus*, and picoeukaryotes) was higher in the tropical and subtropical Atlantic (1052 ± 215 mg C m^{-2}) and the Mediterranean (1038 ± 485 mg C m^{-2}), compared to the Galician coastal upwelling (216 ± 36 mg C m^{-2}) (Table

2.2). In the tropical and subtropical Atlantic, the contribution of *Prochlorococcus* to total picoplankton biomass was 41 %, followed by LNA (27 %) and HNA (22 %) prokaryotes, with smaller contributions of *Synechococcus* and picoeukaryotes (<5 % each). In the Mediterranean, picoplankton biomass was on average dominated by *Synechococcus* (50 %), followed by LNA and HNA prokaryotes (~17 % for each group), picoeukaryotes (10 %), and *Prochlorococcus* (5 %). Finally, HNA (55 %) and LNA (21 %) prokaryotes dominated in the Galician coastal upwelling system, followed by picoeukaryotes (11 %), *Synechococcus* (6 %), and *Prochlorococcus* (1 %).

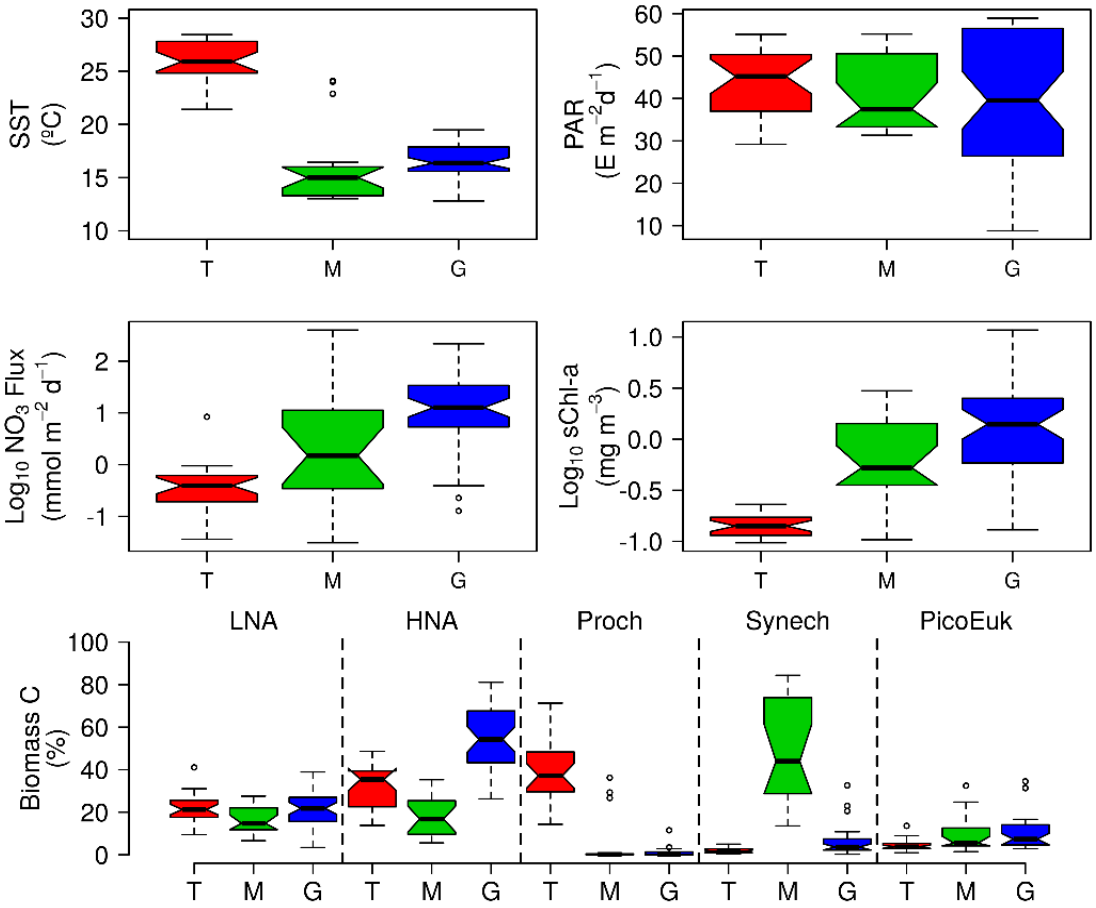

Figure 2.4 *Box-and-whisker plots of sea surface temperature (SST), surface photosynthetic active radiation (PAR), nitrate supply (NO_3 Flux), surface chlorophyll a concentration (sChl a), and contribution to total picoplankton biomass of low (LNA) and high (HNA) nucleic acid content bacteria, Prochlorococcus (Proch), Synechococcus (Synech), and small picoeukaryotes (PicoEuk) computed for the tropical and subtropical Atlantic Ocean (T), the Mediterranean (M), and the Galician coastal upwelling (G). In each box, the central mark indicates the median, the notches the 95 % confidence interval for the median, and the bottom and top edges of the box the 25th and 75th percentiles, respectively. The whiskers extend to the most extreme data points not considered outliers, and the outliers are plotted individually using white circles.*

Table 2.2 *Mean ± standard deviation of sea surface temperature (SST), surface photosynthetic active radiation (PAR), mixed-layer depth (MLD), photic layer depth (1 % PAR), surface nitrate concentration (sNO3), nitrate gradient, vertical diffusivity (K), nitrate supply (NO3 flux), surface chlorophyll (sChl a), photic layer depth-integrated chlorophyll a (Chl a); biomass (B), abundance (A), and contribution (C) to total picoplankton biomass (Total Pico B); and surface abundance (s) of LNA and HNA bacteria, Prochlorococcus, Synechococcus and picoeukaryotes computed for the tropical and subtropical Atlantic Ocean (T), the Mediterranean (M), and the Galician coastal upwelling (G). MLD was estimated from an increase in water column density of 0.125 Kg m−3 relative to surface values. A nonparametric one-way ANOVA (Kruskal–Wallis) was performed to test the null hypothesis that independent groups come from the same distribution. The Bonferroni multiple comparison test was applied a posteriori to analyze the differences between every pair of groups (⁎p-value < 0.05; ⁎⁎p-value < 0.01; ⁎⁎⁎p-value < 0.001).*

Variables (Units)	**T**	**M**	**G**	**KW p-value**	**Post hoc Bonferroni**
SST (ºC)	26 ± 2	16 ± 4	16 ± 2	0.001***	T>G>M
PAR (E m^{-2} d^{-1})	43 ± 23	42 ± 13	39 ± 17	0.69	
MLD (m)	61 ± 30	61 ± 71	12 ± 10	0.001**	T,M>G
1% PAR (m)	109 ± 23	62 ± 13	37 ± 17	0.001**	T>M>G
sNO_3 (µmol m^{-3})	90 ± 77	2414 ± 1635	1601 ± 1604	0.001***	T<M,G
NO_3 gradient (µmol m^{-4})	146 ± 158	90 ± 40	105 ± 100	0.71	
K (m^2 s^{-1}) $x10^{-3}$	0.2 ± 0.3	5.3 ± 13.9	0.5 ± 0.8	0.24	
NO_3 flux (mmol m^{-2} d^{-1})	0.7 ± 1.6	41 ± 113	30 ± 46	0.001***	T<M<G
sChl-a(mgm^{-3})	0.1 ± 0.1	0.9 ± 0.9	2.2 ± 2.5	0.01**	T<M<G
Chl-a (mg m^{-2})	31 ± 6	70 ± 99	81 ± 66	0.001***	T<G
sLNA A (cell ml^{-1}) $x10^5$	4.4 ± 2.4	3.7 ± 2.5	2.1 ± 1.1	0.001***	T>M>G
sHNA A (cell ml^{-1}) $x10^5$	3.0 ± 1.8	4.0 ± 4.5	3.6 ± 2.3	0.13	
sProchlA (cell ml^{-1}) $x10^3$	144 ± 132	2.2 ± 4.4	1.0 ± 2.8	0.001***	T>M,G
sSynechA (cell ml^{-1}) $x10^3$	18 ± 66	75 ± 81	5.7 ± 6.9	0.001***	T<M>G
sPicoEuk A (cell ml^{-1}) $x10^3$	2.5 ± 9.4	6.8 ± 8.4	5.7 ± 6.9	0.001***	T<M,G
LNA A (cell m^{-2}) $x10^{12}$	40 ± 20	22 ± 8	6.4 ± 4	0.001***	T,M>G
HNA A (cellm^{-2}) $x10^{12}$	27 ± 1	22 ± 1	9.4 ± 0.8	0.001***	T>M>G
Prochl A (cell m^{-2}) $x10^{11}$	156 ± 121	10 ± 23	0.5 ± 1	0.001***	T>M,G
Synech A (cell m^{-2}) $x10^{11}$	7 ± 15	50 ± 49	2 ± 2	0.001***	T<M>G
PicoEukA (cell m^{-2}) $x10^{11}$	1.7 ± 3	2.8 ± 2	1 ± 2	0.001***	T<M>G
LNA B (mg C m^{-2})	253 ± 105	170 ± 97	43 ± 34	0.001***	T>M>G
HNA B (mg C m^{-2})	216 ± 127	168 ± 105	108 ± 73	0.02*	T>M>G
Prochl B (mg C m^{-2})	482 ± 516	36 ± 84	1.3 ± 4	0.001***	T>M,G
Synech B (mg C m^{-2})	43 ± 83	576 ± 530	19 ± 26	0.001***	T,M>G
PicoEuk B (mg C m^{-2})	59 ± 102	86 ± 59	43 ± 59	0.001***	T<M>G
Total Pico B (mg C m^{-2})	1052 ± 215	1038 ± 485	216 ± 36	0.001***	T,M>G
LNA C (%)	27 ± 10	18 ± 8	21 ± 9	0.001***	T>M,G
HNA C (%)	22 ± 12	17 ± 10	55 ± 15	0.001***	T,M<G
Prochl C (%)	41 ± 16	5 ± 12	1 ± 2	0.001***	T,M<G
Synech C (%)	4 ± 5	50 ± 24	6 ± 7	0.001***	T,G>M
PicoEuk C (%)	5 ± 5	10 ± 9	11 ± 9	0.001***	T<M,G

Vertical distributions of temperature, nitrate concentration, and the biomass of autotrophic and heterotrophic picoplankton groups for each domain are shown in Figure 2.5.

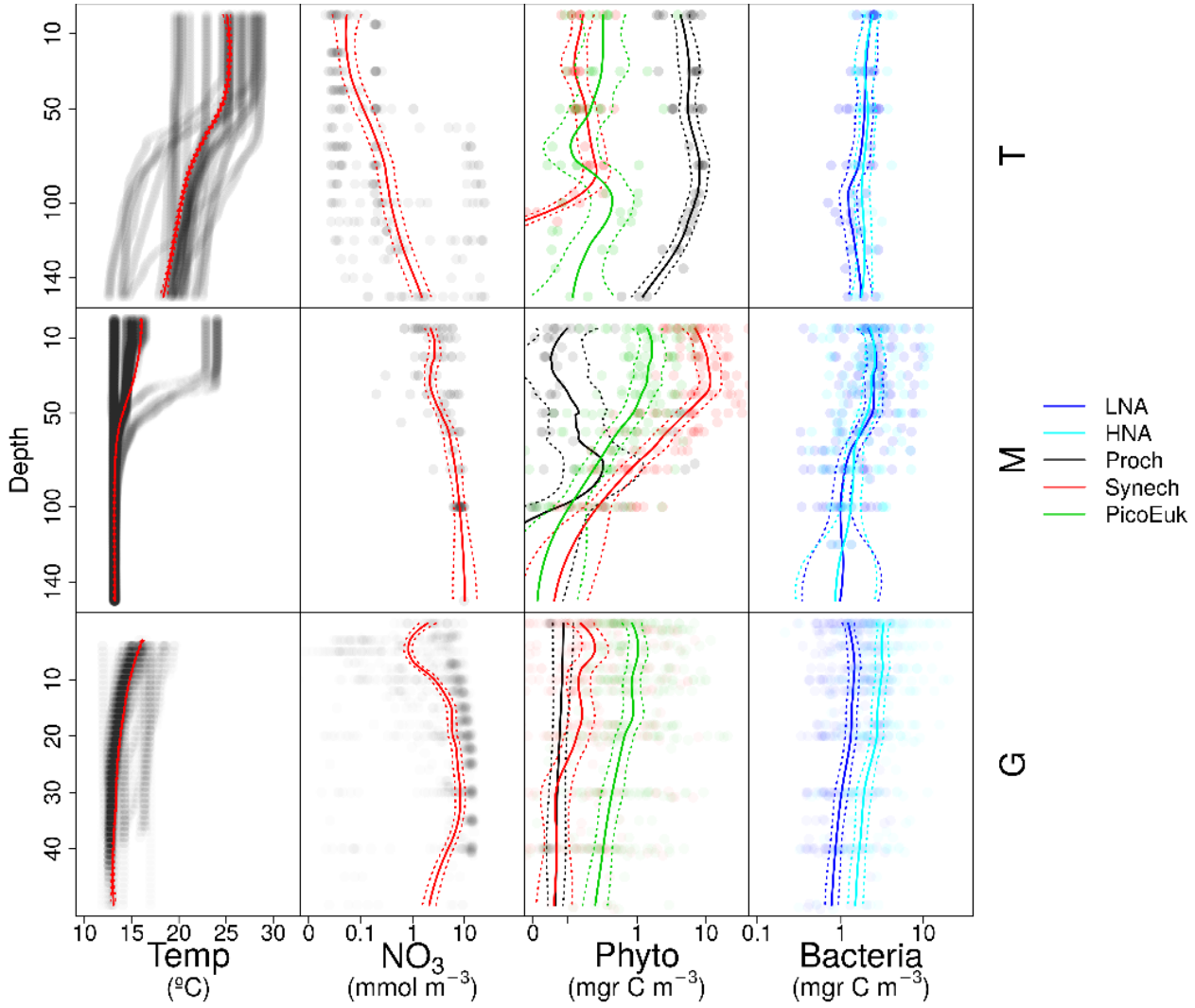

Figure 2.5 *Vertical distribution of temperature (Temp), nitrate (NO_3), and picoplankton biomass of autotrophic (Phyto) and heterotrophic (Bacteria) groups for each domain: tropical and subtropical Atlantic Ocean (T), the Mediterranean (M), and the Galician coastal upwelling (G). Points represent raw data and the solid line the locally weighted scatter plot smoothing (LOESS). Dashed lines indicate 95 % confidence intervals. Dot and line color intensity indicates the number of overlapping observations.*

The role of environmental factors in picoplankton composition

In order to explore the role of temperature, light, and nitrate supply in the composition of the picoplankton community, we first used generalized linear models to investigate simple linear relationships among each of these factors and the depth-integrated biomass of each picoplankton subgroup, the contribution of LNA prokaryotes to heterotrophic picoplankton biomass, the ratio of cyanobacteria (*Prochlorococcus* and *Synechococcus*) to picoeukaryote, and the autotrophic-to-heterotrophic picoplankton ratio (Figure 2.6 & Table 2.3).

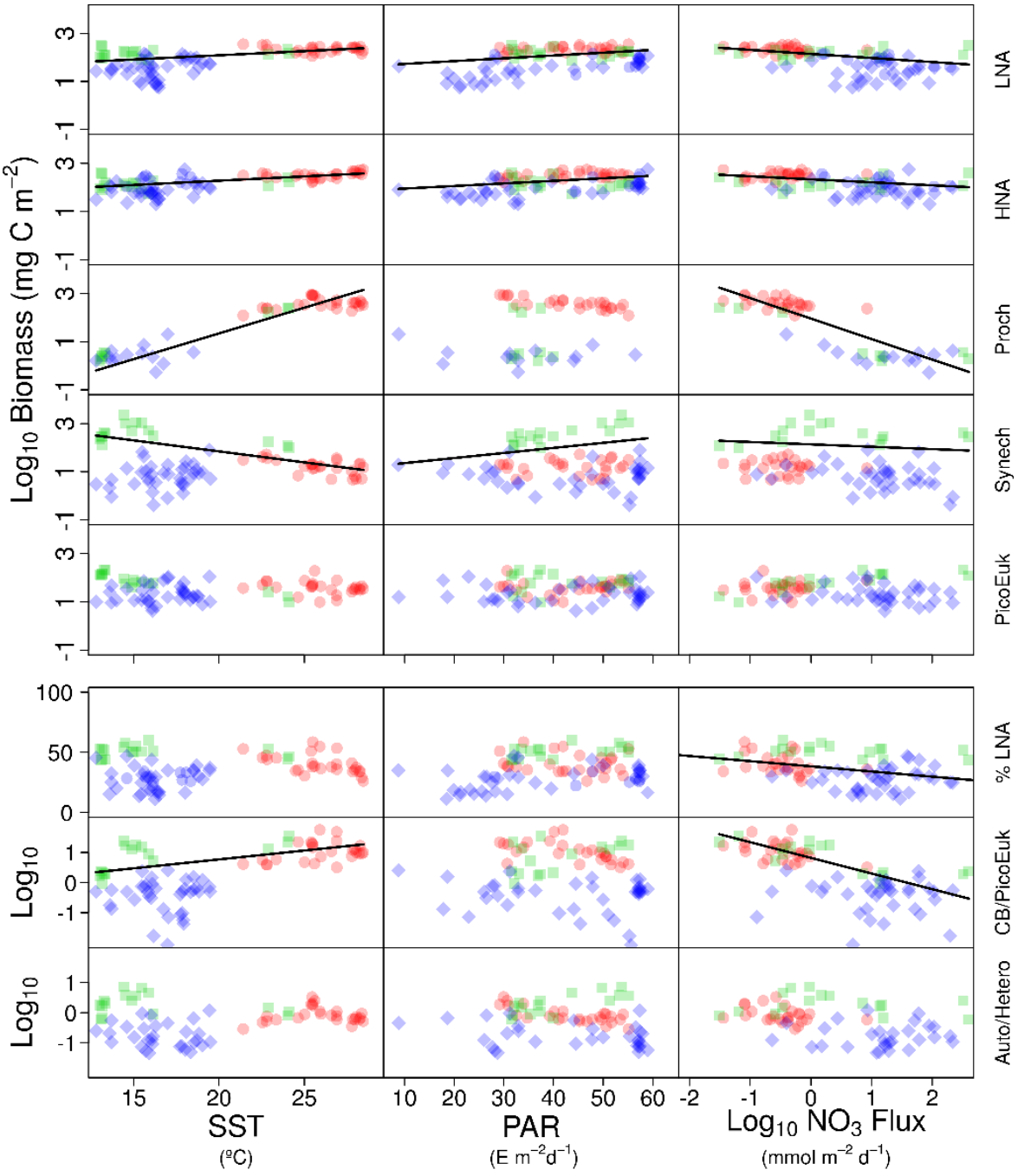

Figure 2.6 *Pair scatter plots representing the relationship among log-transformed depth-integrated biomass for each picoplankton subgroup, the contribution of bacteria with a low nucleic acid content to heterotrophic picoplankton biomass (%LNA), the ratio of cyanobacteria (Prochlorococcus + Synechococcus) to picoeukaryote depth-integrated biomass (CB/ PicoEuK), and the ratio of autotrophic to heterotrophic picoplankton biomass (Auto / hetero) versus sea surface temperature (SST), surface photosynthetically active radiation (PAR), and nitrate flux (NO3 flux). Significant linear relationships are indicated as solid (p value < 0.01) black lines. Samples collected at different regions are indicated as red dots (tropical and subtropical Atlantic Ocean), green squares (Mediterranean), and blue diamonds (Galician coastal upwelling).*

Table 2.3 *Simple (R^2) and adjusted squared correlation coefficients (Adj-R^2) for simple linear regression and multiple generalized additive models (GAMs) built to predict depth-integrated biomass for each picoplankton subgroup, the contribution of LNA bacteria to total heterotrophic picoplankton biomass (% LNA), the ratio of cyanobacteria (Prochlorococcus + Synechococcus) to picoeukaryote depth-integrated biomass (CB/ PicoEuK), and the ratio of autotrophic (CB + PicoEuk) to heterotrophic bacteria (LNA + HNA) biomass based on sea surface temperature (SST), surface photosynthetically active radiation (PAR), and nitrate supply (NO_3 flux). Negative binomial distribution was assumed. Multiple model selection was based on stepwise regression and the Akaike information criterion. Only significant (p value < 0.05) results are shown. Percentage of total effects represents the contribution of each environmental factor to the variability explained by each GAM model.*

Group	R^2 simple linear			Adj-R^2 multiple regression	Percentage of total effects		
	SST	PAR	NO3 flux		SST	PAR	NO3 flux
LNA	0.39	0.01	0.34	0.55	0.30	0.35	0.35
HNA	0.47	0.05	0.18	0.53	0.52	0.48	
Proch	0.01		0.01	0.86	0.72	0.28	
Synech	0.11	0.01		0.52	0.53	0.16	0.31
PicoEuk				0.23	0.51		0.49
% LNA		0.05	0.12	0.49	0.39	0.26	0.35
CB/PicoEuk	0.25		0.28	0.40		0.38	0.62
Auto/Hetero				0.29	0.39		0.61

All picoplankton groups except picoeukaryotes exhibited statistically signif cant relationships with SST. This relationship was negative for *Synechococcus* and positive for all the other subgroups (Figure 2.7.). Only LNA and HNA prokaryotes and *Synechococcus* exhibited significant, positive relationships with surface radiation. All groups except the picoeukaryotes were negatively correlated with nitrate fluxes. The contribution of LNA prokaryotes to heterotrophic picoplankton biomass only exhibited a significant negative relationship with nitrate fluxes, whereas the cyanobacteria-to-picoeukaryote ratio was positively correlated with surface temperature and negatively correlated with nitrate fluxes. Finally, the ratio of autotrophic to heterotrophic biomass was not linearly correlated with any of the studied environmental factors. In order to exclude cross correlation among the three environmental factors and consider the possibility of nonlinear relationships, we subsequently fitted the data to GAMs (Table 2.3 & Figure 2.7).

Temperature was the only factor included in the models built for predicting the depth-integrated biomass of all picoplankton subgroups. HNA prokaryotes exhibited a positive relationship with temperature above 19 ºC, whereas *Prochlorococcus* and LNA prokaryotes showed a nearly sigmoid curve relationship with a transition between ca. 16 and 25 ºC (Figure 2.8). The relationship between the biomass of both *Synechococcus* and picoeukaryotes and tem-

perature showed a negative trend until ~20 ºC and remained relatively constant above this temperature. PAR was included in the models of all picoplankton groups except picoeukaryotes.

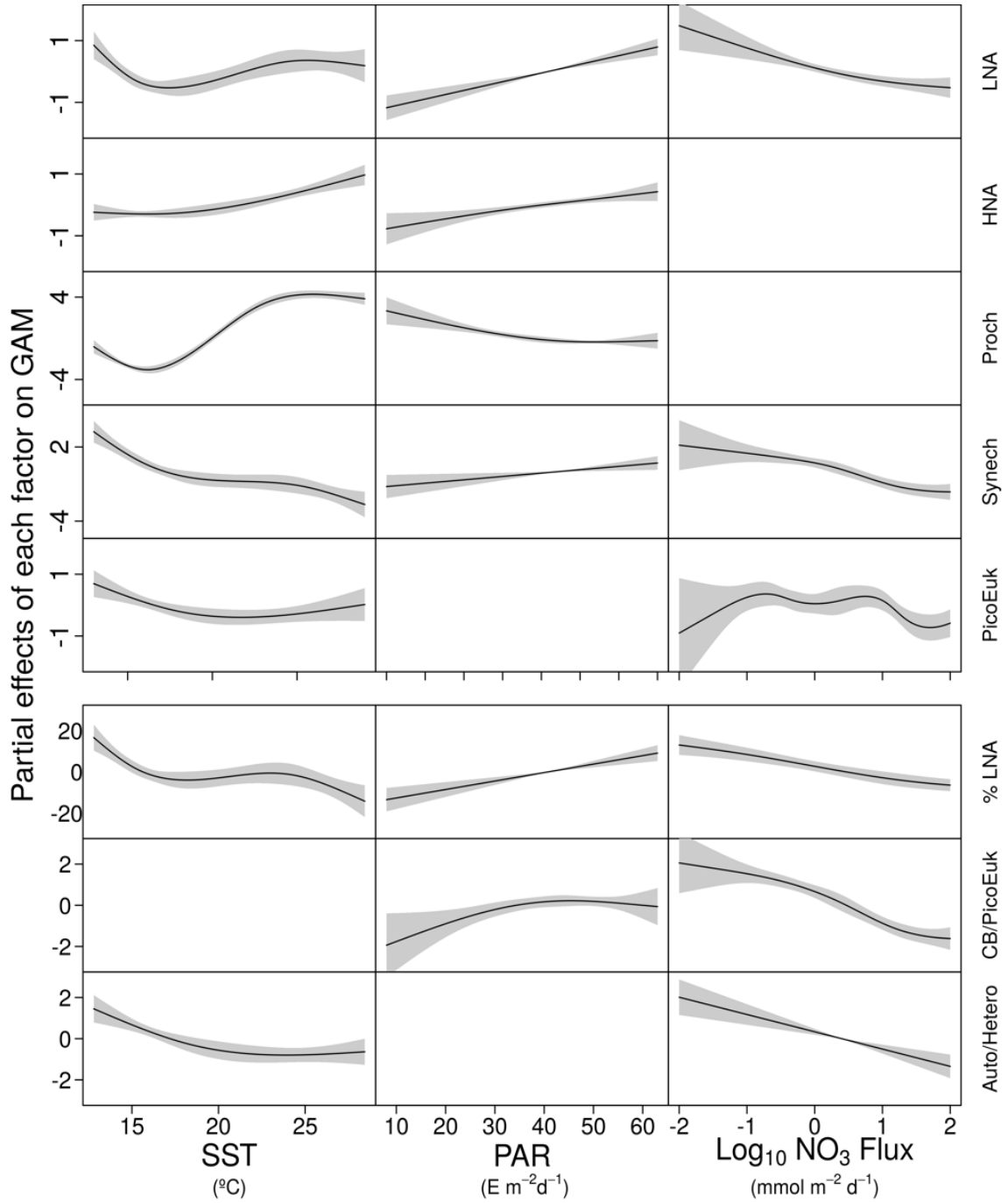

Figure 2.7 *GAM-predicted effects of the response variables (biomass and contribution of picoplankton subgroups) as a smooth function of sea surface temperature (SST), photosynthetically active radiation (PAR), and nitrate flux (NO_3 flux). All terms were centered at zero. Significant linear relationships are indicated as solid (p value < 0.01) black lines. Shaded regions represent the 95 % confidence intervals of the smooth spline functions. Intercept values were 4.6 (LNA), 5.1 (HNA), 2.1 (Prochlorococcus), 3.6 (Synechococcus), 3.7 (picoeukaryotes), 36.4 (contribution of LNA to heterotrophic picoplankton, %LNA), 1.4 (cyanobacteria-to-picoeukaryote ratio, CB/PicoEuk), and −0.1 (autotrophic-to-heterotrophic biomass ratio, Auto / hetero).*

Whereas the biomass of *Prochlorococcus* exhibited a saturation-type relationship with PAR, heterotrophic prokaryotes and *Synechococcus* showed a linear positive relationship. Finally, only LNA prokaryotes, *Synechococcus*, and picoeukaryotes exhibited statistically significant relationships with nitrate supply. This relationship was negative for LNA prokaryotes and *Synechococcus*, whereas picoeukaryotes showed a unimodal function, peaking at ~1 mmol $NO_3\ m^{-2}\ d^{-1}$. Nitrate flux was the only factor selected in the models to predict the contribution of LNA prokaryotes to heterotrophic picoplankton biomass and both the cyanobacteria-to-picoeukaryote biomass ratio and the autotrophic-to-heterotrophic biomass ratio. This relationship was negative in the three models. Temperature was also negatively correlated with the contribution of LNA prokaryotes to heterotrophic biomass and the ratio of autotrophic to heterotrophic biomass. Finally, PAR showed a positive correlation with the contribution of LNA prokaryotes to heterotrophic biomass and the cyanobacteria-to-picoeukaryote biomass ratio.

Ecological niches for picoplankton groups

By using nonparametric kernel density functions, we investigated the overlapping in the ecological niches of the autotrophic and heterotrophic picoplankton subgroups defined by using the three variables previously considered together with surface nitrate concentration (Figure 2.8). Photic layer depth-integrated biomass of each picoplankton group was used for this analysis.

These results revealed three ecological niches in the distribution of picoplankton subgroups. *Prochlorococcus* and LNA prokaryotes were more abundant in warm waters, where nitrate supply was low. HNA prokaryotes and *Synechococcus* dominated in cooler regions with medium to high nitrate supply, and picoeukaryotes were more abundant in cold waters with high nitrate supply. A large degree of overlapping of the ecological niches for all picoplankton subgroups was observed when only surface light was considered. For each picoplankton subgroup Table 2.4 shows the partial weighted overlap of the ecological niches defined by the four factors: SST, PAR, nitrate flux, and surface nitrate concentration. According to these data only nitrate supply enabled a statistically significant separation of the niches of both heterotrophic (HNA and LNA prokaryotes) and autotrophic (*Prochlorococcus*, *Synechococcus*, and picoeukaryotes) picoplankton subgroups. Although the minimum overlap between *Prochlorococcus*

and the other autotrophic picoplankton subgroups was also well defined by temperature, only nitrate supply could statistically distinguish the niche partitioning between the two groups of heterotrophic prokaryotes (p-value<0.05) and between *Synechococcus* and picoeukaryotes (p-value<0.1).

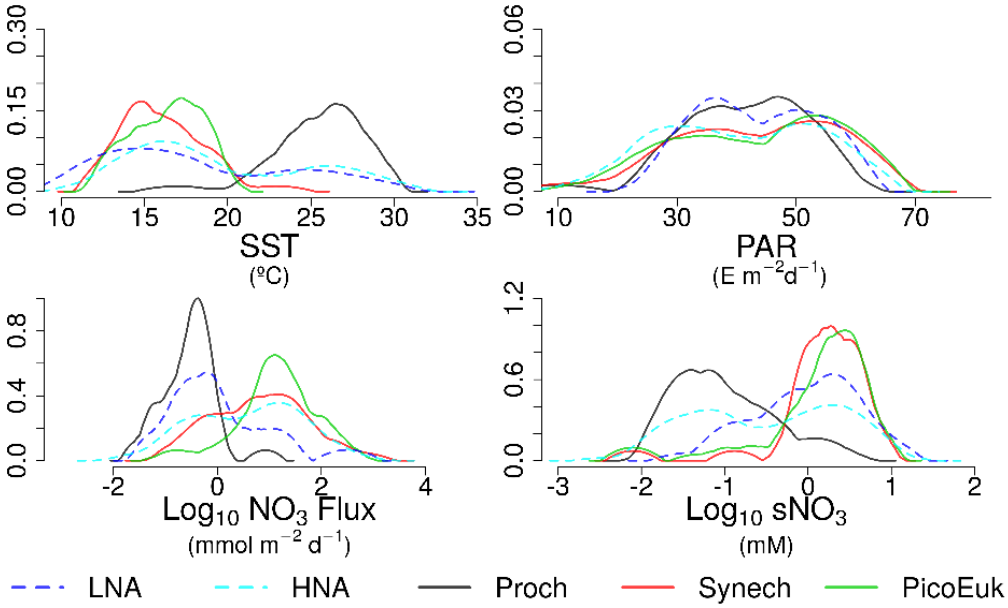

Figure 2.8 *Kernel density estimates of LNA and HNA bacteria, Prochlorococcus, Synechococcus, and picoeukaryotes based on the considered niche descriptors: sea surface temperature (SST), surface photosynthetically active radiation (PAR), nitrate flux (NO_3 flux), and surface concentration (sNO_3).*

Table 2.4 *Partial weighted niche overlap (%) for each environmental factor and picoplankton subgroup. sNO_3 represents surface nitrate concentration. Asterisks denote the existence of significant differences among niches (∗ p-value < 0.1, ∗∗ p-value < 0.05, ∗∗∗ p-value < 0.01, ∗∗∗∗ p-value < 0.001).*

		LNA	HNA	Proch	Synech	PicoEuk
SST	LNA	100				
	HNA	85	100			
	Proch			100		
	Synech			9***	100	
	PicoEuk			5***	84	100
PAR	LNA	100				
	HNA	80	100			
	Proch			100		
	Synech			80	100	
	PicoEuk			74*	94	100
NO3 Flux	LNA	100				
	HNA	69*	100			
	Proch			100		
	Synech			31***	100	
	PicoEuk			14***	77 ^	100

	LNA	100					
	HNA	73^	100				
sNO3	Proch			100			
	Synech			22***	100		
	PicoEuk			29***	89	100	

Discussion

Environmental factors and ecological niches

Picoplankton community composition and concurrent estimates of nitrate supply into the euphotic zone from highly contrasting marine environments allowed us to conclude that SST and nitrate supply are the main factors controlling the variability in the biomass of different subgroups, whereas surface light generally played a minor role. As far as we know, only one study had previously investigated the role of these environmental factors in the distribution of, in this case, the two major groups of cyanobacteria. By using a large flow cytometry dataset from all major ocean regions, Flombaum et al. (2013) concluded that temperature and light were the most important predictors of the abundances of *Prochlorococcus* and *Synechococcus*, with nitrate availability exerting a negligible effect. Although this conclusion seems to be contradictory with the results presented here, some important differences between these studies should be noted. Firstly, Flombaum et al. (2013) used bulk estimates of seawater nitrate concentration as a proxy for nitrate availability in the euphotic zone. However, in near-steady-state systems such as the subtropical gyres, where diffusive nutrient supply into the euphotic zone is slow, nitrate concentrations are kept close to the detection limit due to phytoplankton uptake. For this reason, nitrate concentrations and actual nitrate supply into the euphotic zone in the vast oligotrophic regions are often largely disconnected (Mouriño-Carballido et al. 2011, 2016). Moreover, whereas Flombaum et al. (2013) used *Prochlorococcus* and *Synechococcus* abundances determined at several depths in the upper 200 m, we used depth-integrated biomass of both autotrophic and heterotrophic picoplankton subgroups in the photic layer.

Although these results point to both temperature and nitrate supply as important factors controlling the distribution of the picoplankton subgroups (Figure 2.7 & Table 2.3), nitrate supply was the only factor that allowed the distinction among the ecological niches of autotrophic and heterotrophic picoplankton subgroups (Figure 2.8 & Table 2.4). This attempt to sort out the ecological niches of picoplankton subgroups gave rise to three distinct categories. *Prochlorococcus* and LNA prokaryotes were more abundant in warmer waters (above 20 °C) where the

availability of nitrate was low. *Synechococcus* and HNA prokaryotes prevailed mainly in cooler (below 20 °C) marine environments characterized by intermediate and high levels of nitrate supply, and finally, the niche for picoeukaryotes was characterized by low temperatures and high nitrate supply. These results underline the physiological and ecological features of the distinct picoplankton functional subgroups. These results confirm the previously reported ecological differences between the two major groups of unicellular cyanobacteria (Scanlan and West 2002; Li 2009; Partensky and Garczarek 2010).

Moreover, the ecological niche alignment of the two cyanobacteria genera with the two heterotrophic prokaryotes subgroups is consistent with taxa that prevail in oligotrophic regions (e.g., SAR11) being included in the LNA prokaryotes, whereas copiotrophic and more diverse taxa (Gammaproteobacteria, Bacteroidetes/Flavobacteria, etc.) are generally grouped under HNA (Schattenhofer et al. 2011; Vila-Costa et al. 2012). Although the relationship among stratification, mixing, and nutrient supply is not obvious (Mouriño-Carballido et al. 2016), these results are in general consistent with the patterns described by (Bouman et al. 2011). These authors, by using vertical density stratification as a proxy for the three main environmental factors influencing phytoplankton growth (temperature, light, and nutrients) in subtropical regions of the Pacific, Atlantic, and Indian oceans, described the dominance of photosynthetic picoeukaryotes in well-mixed waters and the prevalence of cyanobacteria in strongly stratified conditions.

Physiological traits of picoplankton subgroups

Although previous studies have revealed that *Prochlorococcus* may have acquired the ability to use nitrate by horizontal gene transfer, their photosynthetic activity primarily relies on regenerated forms of nitrogen (Moore et al. 2002; Malmstrom et al. 2013). These results support this view and substantiate that, after controlling for the concurrent effects of light and seawater temperature, *Prochlorococcus* biomass was uncorrelated with nitrate fluxes. However, it is important to note that we could not discriminate between high-light (HL) and low-light (LL) ecotypes and that the presence of nitrate reductase seems to be more relevant in LL (Martiny et al. 2009; Berube et al. 2015). Evolutionary adaptation to light-limiting conditions makes *Prochlorococcus* the most efficient light harvesters among Earth's photosynthetic organisms (Morel et al. 1993). Their competitive ability under light-limiting conditions could explain the negative effect of light as a predictor for *Prochlorococcus* biomass. Ultimately, the photo-physiological strategy of *Prochlorococcus* leads to (i) thermal sensitivity of photosystem II (Mackey

et al. 2013), which limits its fundamental niche to temperatures greater than 15 °C (Moore et al. 1995), and (ii) high sensitivity to ultraviolet (UV) radiation in surface waters (Sommaruga et al. 2005; Llabrés et al. 2010; Mackey et al. 2013). This could explain that, after removing the effect of light, the data analysis revealed that the effect of temperature on *Prochlorococcus* biomass showed a sigmoid relationship as temperature increased.

Synechococcus is able to use both new and regenerated forms of nitrogen (Moore et al. 2002; Mulholland and Lomas 2008), which largely explains its wider geographical distribution range (Flombaum et al. 2013). The fact that it is more abundant at intermediate levels of nitrate supply is consistent with the lower intracellular nitrogen quota of *Synechococcus* relative to *Prochlorococcus* and hence their higher growth rate under saturating nutrient conditions (Marañón et al. 2013). Conversely, the large affinity of *Prochlorococcus* to acquire nutrients (Partensky and Garczarek 2010) and absorb light under severe nutrient- and light-limiting conditions (Mella-Flores et al. 2012) precludes the supremacy of *Synechococcus* in warm and stratified oligotrophic systems (Moore et al. 2007). Although *Prochlorococcus* and *Synechococcus* are not very different in cell size and they usually coexist in oligotrophic regions, differences in adaptation to light conditions and UV stress lead to segregate their maximal distributions across space (vertical segregation) and through time (Chisholm 1992; Mella-Flores et al. 2012).

Picoeukaryotes, like *Synechococcus*, also exhibited a negative relationship with seawater temperature, again reflecting the superior competitive ability of *Prochlorococcus* under severe nutrient-limiting conditions (Moore et al. 2007). The relative dominance of cyanobacteria in oligotrophic systems results from the fact that cyanobacteria are less negatively affected by nutrient diffusion limitation than picoeukaryotes (Chisholm 1992). It is widely accepted that small cells are at an advantage over large cells in stratified open-ocean environments, where nutrient recycling dominates biogeochemical fluxes (Raven 1998). First, the surface-to-volume ratio increases with decreasing cell size, which narrows the nutrient diffusion boundary layer around the cell and facilitates the acquisition of nutrients in nutrient impoverished environments. Second, small-sized cells have lower sinking rates than their larger counterparts, which allow them to extend their chances of survival in the euphotic layer (Smayda 1980; Chisholm 1992; Kiørboe 1993).

The analysis indicates that among the picophytoplankton, picoeukaryotes were the most

responsive to nutrient fluxes. This is consistent with experimental observations under laboratory-controlled conditions revealing that, within the picoplankton size range, the maximum attainable growth rate increases with increasing cell size (Raven 1994; Marañón et al. 2013). This positive relationship between maximum growth rate and cell size in the picophytoplankton to small nanophytoplankton size range has been explained as a trade-off between intracellular nitrogen quotas (N requirements) and mass-specific nitrate uptake rates (N uptake) (Marañón et al. 2013). Whereas nitrogen uptake rate exhibits an isometric relationship with cell size, smaller picoplankton cells have substantially larger intracellular nitrogen quotas, which reduce their capability to maximize carbon-specific growth rates. Conversely, high maximum growth rates represent an advantage for picoeukaryotes, compared to any other organism, as they attenuate the effect of loss processes such as predation or the washout of plankton communities in highly dynamic, turbulent systems (Sherr et al. 2005; Echevarria et al. 2009). For instance, microzooplankton is thought to maintain the biomass of their prey under tight control, and thus slight variations in picophytoplankton growth rate may substantially alter the resulting biomass of the different picophytoplankton subgroups (Chen et al. 2009).

The unimodal relationship observed between the biomass of picoeukaryotes and nitrate supply (Figure 2.8) could seem at first contradictory with the rising hypothesis proposed by Barber and Hiscock (2006), which describes that improved growth conditions benefit all phytoplankton size classes, including picoplankton. In this regard, Brewin et al. (2014) by using data collected along the Atlantic Meridional Transect cruises showed that <2 μm size-fractionated chlorophyll was positively correlated with total chlorophyll only until a value of 1 mg m^{-3}, and then it did not show any positive relationship with total chlorophyll. It is also important to note that surface abundance of picoplankton subgroups reported in this chapter, which are consistent with previous observations (Zubkov et al. 2000; Froján et al. 2014; Teira et al. 2015), did show higher surface abundance of picoeukaryotes in the Galician coastal upwelling and the Mediterranean compared to the tropical and subtropical Atlantic (Table 2.2 & Figure 2.7). However, this pattern was diluted when depth-integrated biomasses were computed since the lower limit for the integration (the base of the photic zone) was much shallower in the coastal upwelling domain (ca. 37 m) compared to the Mediterranean (ca. 62 m) and the tropical and subtropical regions (ca. 109 m).

Heterotrophic prokaryotes also use dissolved inorganic nutrients, including nitrate, for

growth (Kirchman 1994). Consistent with this, Gasol et al. (2009) showed a positive relationship between prokaryotic abundance and a proxy for nutrient supply in a latitudinal gradient across the Atlantic. They did not partition this effect on the two subgroups that can universally be differentiated among bacteria and archaea. These results suggest that LNA prokaryotes respond less markedly to nutrient fluxes than HNA prokaryotes. The effect of nitrate supply on the biomass of LNA prokaryotes showed a linear negative relationship as nitrate supply increases, perhaps associated with their ability to survive under nutrient starving conditions (Mary et al. 2008). Under such conditions, proteorhodopsin-containing LNA prokaryotes (e.g., example SAR11) can use energy from light (Mary et al. 2008; Pinhassi et al. 2016), improving their competitiveness against non-proteorhodopsin-containing prokaryotes. Consistent with this idea, these results showed a positive relationship between the biomass of LNA prokaryotes and PAR. Li et al. (2004) already proposed the ubiquity of this bottom-up control of prokaryotic abundance in oligotrophic environments (<1 mg Chl m3). Therefore, we believe that that the underlying cause for the clear niche difference between LNA and HNA prokaryotes is more the difference in the suite of genes (Schattenhofer et al. 2011) than in cell size (Morán et al. 2015).

Outlook

Picoplankton often dominate marine phytoplankton biomass and primary production in oligotrophic regions (Chisholm 1992; Agawin et al. 2000), contribute overwhelmingly to the recycling of organic matter (Azam et al. 1983; Fenchel 2008), and could have a substantial contribution to the export of carbon to the deep ocean (Richardson and Jackson 2007). However, our limited understanding about the factors that control picoplankton community composition constrains our ability to include them in ocean biogeochemical models and predict the consequences of future global change scenarios. For the first time, by combining observations that allowed us to estimate vertical nutrient fluxes, instead of nitrate concentrations, we investigated the role of temperature, light, and nitrate supply in the distribution of the major autotrophic and heterotrophic picoplankton subgroups. Our results highlight the role of nitrate supply in the distribution of picoplankton subgroups, as it was the only factor that allowed the statistically significant distinction of the ecological niches between the autotrophic and heterotrophic picoplankton subgroups. In general, autotrophic picoplankton biomass was dominated by *Prochlorococcus* in warmer waters where the availability of nitrate was low and by *Synechococcus* and picoeukaryotes in cooler waters with medium to high nitrate availability. Similarly, LNA

prokaryotes dominated heterotrophic picoplankton biomass in regions of weak nitrate supply, whereas HNA prokaryotes dominated the heterotrophic community in regions of enhanced nutrient supply. Although our study included 97 stations sampled in contrasting environments, a larger dataset, including a broader range of environmental conditions, will be needed to accurately discern the role of temperature and nitrate supply in the field, as both factors are strongly correlated in the ocean. In this regard, by growing three phytoplankton species (the diatom *Skeletonema costatum*, the coccolithophore *Emiliania huxleyi*, and the picocyanobacteria *Synechococcus* spp.) in the lab, (Marañón et al. 2018) showed a reduced sensitivity of metabolic rates to temperature variability under nutrient-depleted conditions, suggesting that nutrient availability controls the temperature dependence of metabolism. Consistent with these results, the statistical analyses stress the relevance of nitrate supply in the distinction of the ecological niches of heterotrophic and autotrophic picoplankton subgroups. Other mechanisms of nutrient supply, such as mesoscale and sub-mesoscale turbulence, atmospheric deposition, nitrogen fixation, and more complex three-dimensional dynamics (Jenkins and Doney 2003; Bonnet et al. 2005; Estrada et al. 2014; Fernández-Castro et al. 2015) as well as the influence of trophic interactions (Van Mooy et al. 2006; Baudoux et al. 2007; Chen et al. 2009; Rusch et al. 2010) deserve further investigation.

According to our results, in a future ocean in which global change scenarios predict an increase in surface temperature and stratification (Howes et al. 2015), the resulting decrease in nitrate supply into the euphotic zone (Lewandowska et al. 2014) would lead to the dominance of autotrophic picoplankton by cyanobacteria, whereas the picoeukaryotes would decrease their contribution. Due to the smaller contribution of cyanobacteria to the transfer of carbon to the deep ocean compared to picoeukaryotes, this pattern could have important implications in the efficiency of the biological carbon pump (Corno et al. 2007).

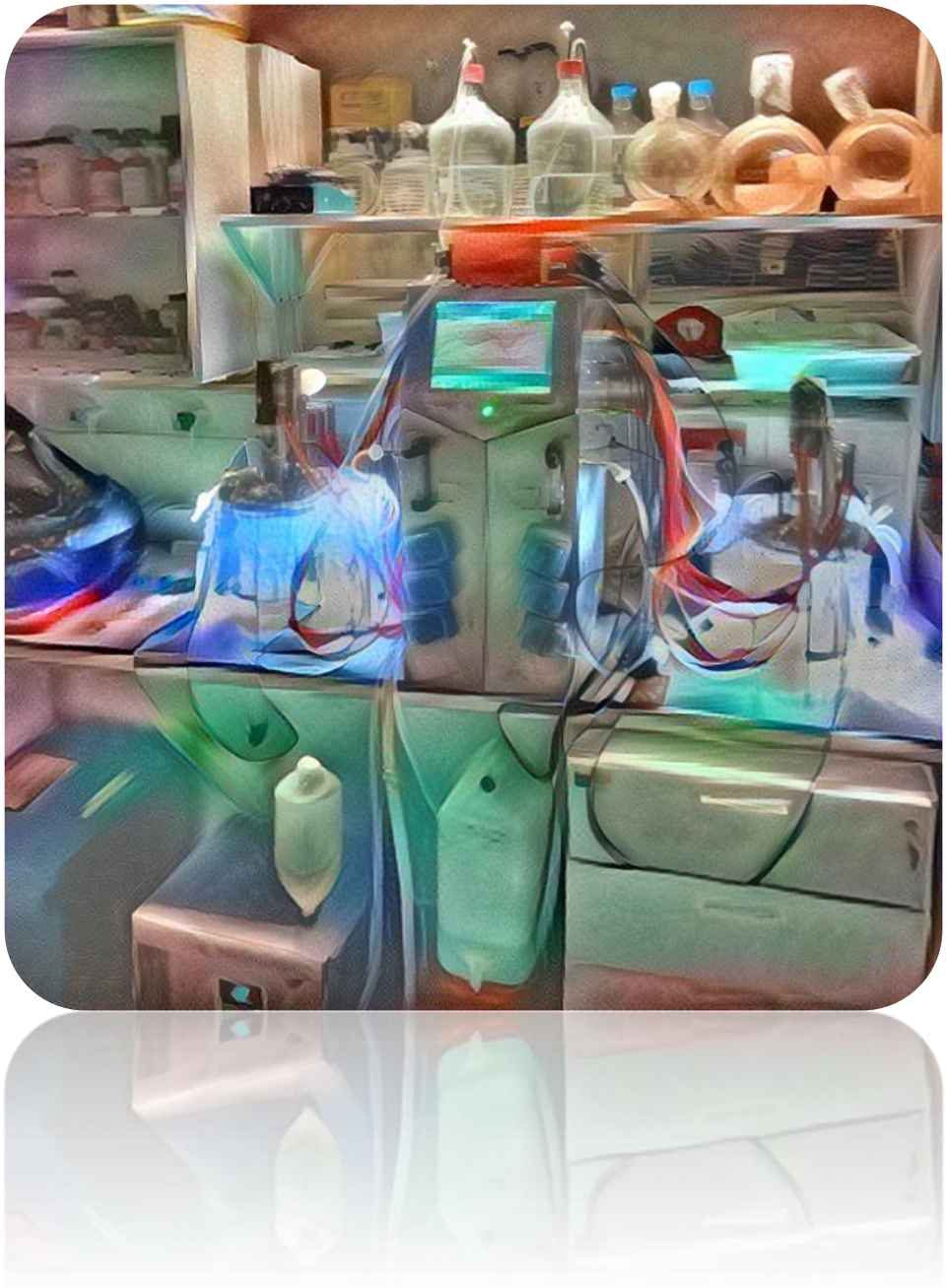

Chapter 3

Competitive dynamics of the cyanobacterium *Synechococcus* sp. and the picoeukaryote *Micromonas pusilla* under dynamical nutrient supply conditions

Abstract

Photosynthetic picoplankton (<2 μm of equivalent spherical diameter), also known as picophytoplankton, dominate autotrophic biomass and primary production in large regions of the tropical and subtropical ocean. Previous studies suggest that some groups within the picophytoplankton size fraction can contribute significantly to new production in these ocean regions. However, our understanding of the ecological mechanisms underlying the spatial and temporal distribution patterns of the different picophytoplankton subgroups is very limited. According to the resource competition theory, the species with the lowest requirement for the most limiting resource will be the best competitor in the steady-state, that is, when the condition of resource limitation is maintained over time. However, the outcome of competition might change if the system deviates from the steady-state, which is the most usual scenario in the surface ocean. Two picophytoplankton strains, one of the cyanobacterium *Synechococcus* sp., and another of the picoeukaryote *Micromonas pusilla*, were selected to perform nutrient competition experiments in bench-scale photobioreactors. These experiments were designed to simulate different nitrate supply scenarios ranging from continuous to intermittent supply (0, 0.5, 1, 2, 3 nitrate pulses per day). In the steady-state, i.e. continuous nitrate supply, *M. pusilla* was outcompeted by *Synechococcus* sp. However, regime shifts to either nitrate pulsing conditions (i.e. non steady-state) or increased culture dilution rates, led to the exclusion of *Synechococcus* sp. The rate of competitive exclusion was a linear function of the frequency of nitrate pulses. Using the physiological parameters that describe the nitrate uptake kinetics of each of the selected strains, computer model simulations of the competitive process were carried out to theoretically expand our experimental trials into a broader range of environmental conditions. Model simulations were consistent with experimental results and allowed us to identify nitrate supply scenarios that promoted species coexistence over time. These results demonstrate that nutrient supply regimes contribute to regulating the structure of picophytoplankton communities and, presumably, the magnitude of organic C export into the deep ocean.

Introduction

Synechococcus (Waterbury et al. 1979) and picoeukaryotes (Johnson and Sieburth 1982) belong to the picophytoplankton, the phytoplankton size fraction comprising organisms with a cell size below 2µm of equivalent spherical diameter (ESD). Together with *Prochlorococcus* (Chisholm et al. 1988), they dominate autotrophic biomass and primary production in tropical and subtropical ocean oligotrophic gyres (Agawin et al. 2000). While *Prochlorococcus* dominates in warm, oligotrophic and highly-stratified ocean waters, *Synechococcus* and picoeukaryotes tend to be more prominent components of the picophytoplankton communities in relatively more productive ocean environments (Partensky et al. 1999; Berthelot et al. 2018). The extent to which *Synechococcus* or picoeukaryotes dominate the picophytoplankton community biomass has been suggested to influence the strength of the biological pump, the mechanism through which plankton communities contribute to export organic carbon (C) into the deep ocean, where can be sequestered over climatically-relevant time scales (Karl et al. 2001). Whereas *Synechococcus*-dominated microbial food webs tend to be more efficient at recycling organic matter, the picoeukaryotes are thought to play a more significant role in the downward export of organic C (Corno et al. 2007; Fawcett et al. 2011), as well as a source of food for upper trophic levels (Reckermann and Veldhuis 1997). Thus, understanding the mechanisms that control the relative contribution of *Synechococcus* and picoeukaryotes to picophytoplankton communities is crucial to improve our ability to predict the response of these communities to environmental changes and anticipate their consequent biogeochemical impact (Richardson and Jackson 2007; Lomas and Moran 2011).

The ability of species to use resources efficiently confers competitive advantages under certain environmental conditions and contributes to shape the structure of biological communities. According to the Gause's law of competitive exclusion (Gause 1932), two species competing for a single limiting nutrient cannot coexist indefinitely if the condition of nutrient limitation is maintained through time (MacArthur 1972; Tilman 1980, 1982). The key parameter here is the minimum resource level that can support a species population, also known as *R**:

$$R^* = \frac{D}{(\mu_{max} - D)} * K_s \quad (1)$$

where D is the mortality rate, which is equivalent to the dilution rate in a continuous culture steady-state system, μ_{max} is the species' maximum growth rate, and K_s is the half saturation

constant for resource acquisition, that is the resource level at which the maximum resource acquisition rate takes half of its value. At steady-state, species tend to reduce the nutrient concentration in the bulk medium to values as low as their R^* and, as a consequence, the species with the lowest R^* is predicted to win the competition. However, the outcome of this competition process might change if the system deviates from the steady-state, which is the most usual scenario in the surface ocean.

Margalef (1978) showed that the input of external energy to plankton ecosystems determines the ecological succession of dinoflagellates, coccolithophores and diatoms, recognizing that these three distinct phytoplankton functional groups respond differently to variable nutrient supply regimes. Physical and biological processes such as turbulent eddies (Falkowski et al. 1991), Ekman transport (Bauer et al. 1991), nitrogen fixation (Moore et al. 2013), atmospheric deposition (Paerl 1997; Jickells et al. 2017), Rossby waves (Sakamoto 2004), internal waves (Schott et al. 1996; Villamaña et al. 2017), Langmuir circulation (Thorpe 2004) or double diffusive turbulent processes (Dietze et al. 2004; Fernández-Castro et al. 2015) bring nutrients to the surface ocean on different temporal and spatial scales and in different magnitudes, altering the natural equilibrium of plankton ecosystems, the outcome of competition processes and, as a consequence, the structure of phytoplankton communities. Experimental studies and competition models support this theoretical background for large-sized phytoplankton groups such as diatoms and green algae (Tilman 1977; Grover 1991). Grover (1991) proposed an internal stores model in which the competitive advantage under variable nutrient supply conditions is given by the ability of species to adjust their internal nutrient quotas or stores. Tozzi et al. (2004) and Cermeño et al. (2011) showed that dynamical nitrate supply regimes lead to a higher competitive advantage of diatoms over coccolithophores in computer model simulations and laboratory photobioreactors, respectively. Their results, as previously formulated in seminal competition papers, illustrated how variable nutrient supply regimes allows opportunists to exploit their higher maximum growth rates and ability to build up their internal nutrient quotas and thrive at the expense of slow growing species. While many studies have considered the effect of nutrient supply dynamics on the interspecific competition of large-sized phytoplankton (Tilman 1977, 1982; Sommer 1986; Stolte and Riegman 1995; Takeya et al. 2004; Winkler et al. 2017), its effect on the subgroups making up the picophytoplankton size fraction has received much less attention (Mouriño-Carballido et al. 2016; Villamaña et al. 2017).

In this chapter, I investigate the effect of dynamical nutrient supplies on the competitive dynamics of the cyanobacterium *Synechococcus* (equivalent spherical diameter, ESD 0.8-1.5 µm) and the chlorophyte *Micromonas pusilla* (ESD = 1.5-2 µm) under laboratory-controlled conditions and in a computer-based competition model. The former approach allowed me to test a limited set of nutrient supply scenarios, the latter approach made it possible to cover a wider range of scenarios, including those in which species were able to coexist indefinitely.

Material and methods

Experimental analyses

Two strains, one of the cianobacteria *Synechococcus* sp. and one of the picoeukaryote, *Micromonas pusilla* were selected from the Roscoff Culture Collection (RCC-450 and RCC-2366, respectively). Both strains had been originally isolated from the oligotrophic North Atlantic Subtropical West region (NASW, Figure 3.1) (Six and Thomas 2004; Worden et al. 2009). The *Synechococcus* strain was isolated from surface waters whereas *M. pusilla* was isolated from a sample collected at 100 m depth. Cultures were grown in a modified PCR-S11 medium (Rippka et al. 2000) prepared with 0.2-µm filtered and autoclaved seawater and completed with filter-sterilized PCRS-11 trace metals, nitrate, phosphate and f/2 vitamin solution (Guillard and Ryther 1962). All equipment used for medium preparation and culturing were previously soaked in 10% HCl during 24h, and then rinsed with distilled water and ultrapure de-ionized water (Milli-Q). To ensure nitrogen limitation of phytoplankton growth, the nitrogen to phosphorus (N/P) ratio was fixed to five with a final dissolved nitrate concentration of 50 µM. Temperature was set to 21ºC, in order to simulate the annual mean temperature of the sampling sites at 100 m depth as measured by ARGO floats (Figure 3.2). The photosynthetically active radiation (PAR), measured with a laboratory radiometer (QSL-2100), was saturating (Moore et al. 1995) for both groups (115µmol photons m^{-2} s^{-1}) and was provided on a 12:12h light:dark cycle. Cultures were aerated using commercial air pumps which pumped the air of the culture chamber through polycarbonate filters (Ø = 0.45 µm) in order to promote culture mixing and facilitate gas exchange.

Species populations from batch and continuous cultures systems were employed to carry out the nitrate uptake kinetics and competition experiments, respectively. Batch cultures were incubated in a culture chamber with a temperature variation of ± 1 °C and illuminated using

cool-white fluorescent PAR lamps (Sylvania lamps). The photo-bioreactor system was equipped with two 2-L double-walled borosilicate culture vessels connected to a re-circulating water system that maintained the cultures within ± 0.1 °C of the growth temperature. The dilution rate used, which in the absence of any other mortality losses equals the steady-state growth rate of the population, was 0.225 d^{-1}. , which is within the range of growth rates estimated for phytoplankton inhabiting oligotrophic regions (Marañón 2005). Fresh medium was filtered by 5 µm using PTFE "last drop" mobile phase filter (Interchim) in the header tanks (5L). Header tanks were maintained at room temperature and dark conditions to avoid light degradation of vitamins. Cultures were agitated with a stirrer shaft rotating at 50 rpm. Fresh medium was supplied to the culture vessels by high-precision peristaltic pumps (Watson Marlow 101 U/R) using high-precision silicon tubing (Watson Marlow pumpsil) and calibrated before each experiment (R^2>0.98 ± 0.001). Another set of peristaltic pumps, integrated in the main bioreactor system and activated by a level sensor, controlled outflow rates and culture volume (1.5 dm^3). PAR irradiance on each vessel was provided by white-light LED array (3M) powered by a 24v source (Mean Well). Monocultures acclimation period to culture chamber and chemostat were at least 2 generations (3 weeks).

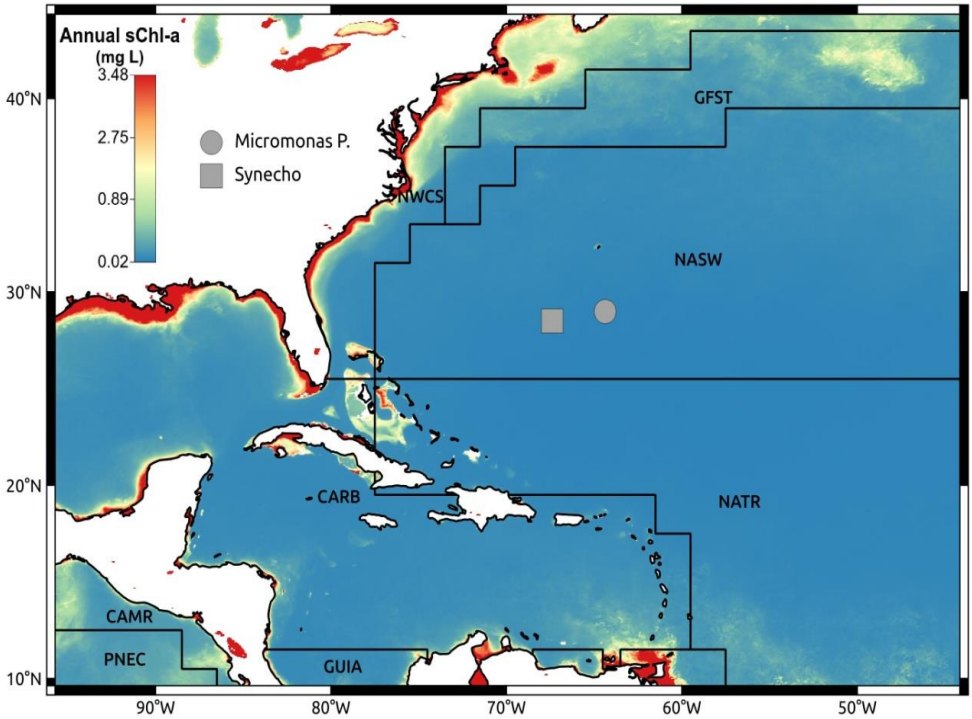

Figure 3.1 *Location of the stations were Micromonas pusilla and Synechococcus sp. were sampled in the western tropical and subtropical North Atlantic Ocean (NASW). Annual surface chlorophyll of ten years (2004-2014) is shown. Synechococcus sp. was collected in surface water and Micromonas pusilla was collected at 100 m depth.*

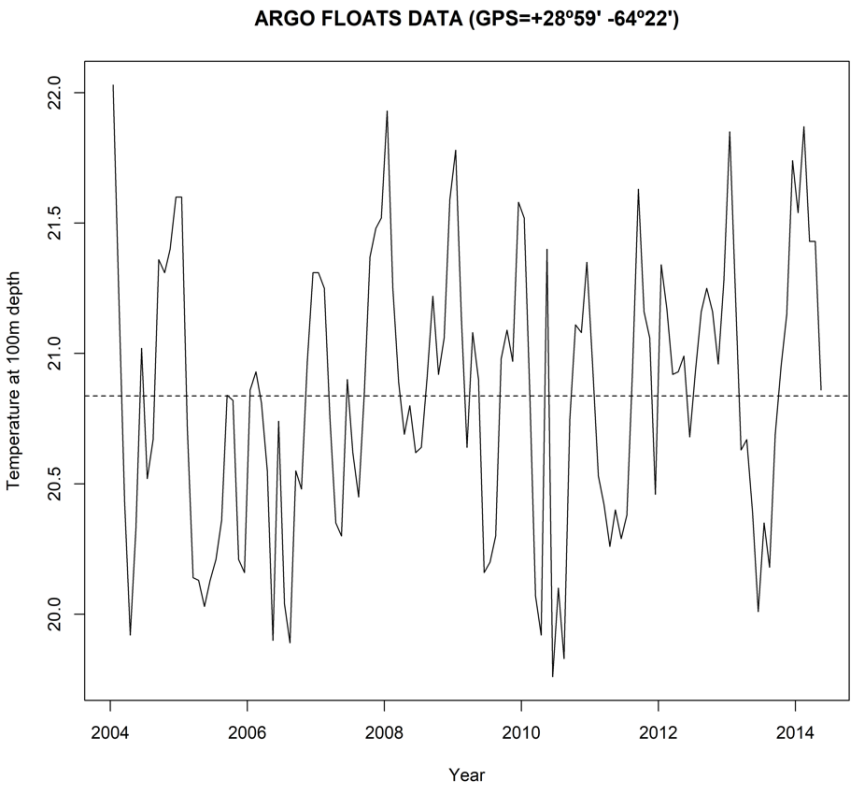

Figure 3.2 *Time series of mean temperature (ºC) at 100 m depth collected by ARGO floats in the western subtropical North Atlantic ocean over 2004-2014. Dashed line represents the mean value over the period.*

Cell abundance was measured with a FACSCalibur flow cytometer (Becton-Dickinson) equipped with a laser emitting at 488 nm was used to measure and count picoplankton. The picophytoplankton sample (0.6 ml) was analyzed at high flow rate (~mean 60 µl min^{-1}) during 4 min. The flow velocity was measured during the processing of samples by the difference in weight of sample after a given acquisition time. MilliQ water was used as sheath fluid. When culture readers exceeded more than 1000 events s^{-1}, the sample was diluted following the method proposed by Gasol (1999).Acquisition was carried out with the software CELL Quest™ (Becton Dickinson) and data analysis with CELL Quest™ and Flowing (http://flowingsoftware.btk.fi/). Cytometric samples (1.8 ml) for the determination of picoplankton abundance and cell properties were taken every other day, preserved with glutaraldehyde and quick-frozen using liquid nitrogen after 10 min of dark incubation (Marie et al. 2014). Later, they were stored at −80°C until analysis. In order to estimate biovolume, we used an empirical calibration between Size SCatter (SSC) and cell diameter (Calvo-Díaz and Morán 2006), assuming spherical shape for all groups. Finally, picophytoplankton biomass was

computed using the following conversion factors of volume to carbon: 230 fg C μm^{-3} for *Synechococcus*, and 237 fg C μm^{-3} for *M. pusilla* (Worden et al. 2004).

Both extracted chlorophyll-*a*and cell abundance (epifluorescence microscopy) were used to monitor competition during the experiments (data not shown). Chlorophyll-*a* was determined using samples (5 mL) filtered through GF/F filters (Whatman) and extracted with 90% acetone. The fluorescence signal was measured with a TD-700 Turner fluorimeter that had been calibrated with pure chlorophyll-*a*. The cells were counted using an epifluorescence microscope (Leica). Each sample was prepared using 1 ml of culture sample, then it was diluted (1:10) and fixed using filtered formaldehyde 37% (swinnex filter, Ø=0.2 µm) and incubated in dark conditions at least 2h (2% final concentration). The fixed sample was filtered using a black GTBP filter (Ø=0.2 µm), the tube was washed with Milli-Q water twice to avoid cell adhesion to the walls of plastic tube. The filters were stained with 4'-6-diamidino-2-phenylindole (DAPI)-mix (5.5 parts of Citifluor, Ltd.), 1 part of Vectashield (Vector Laboratories, Inc.) and 0.5 parts of PBS (final concentration 1 mg ml-1) for 10 min. Natural fluorescence (phycobiliproteins) of *Synechococcus* was observed under blue light, DNA of both algae were observed under UV light due to DAPI staining.

Both the maximum growth rate (μ_{max}) and cell quotas (CNH analysis) were determined under batch experiments. The maximum (Q_{max}) and minimum (Q_{min}) nitrogen and carbon quotas were estimated as the highest and lowest cell content measured throughout the growth cycle. Samples for particulate organic C and N (PON and POC, respectively) were collected from batch cultures through the growth cycle. Ten ml of culture were filtered over pre-combusted and pre-weighted GF/F filters (Whatman), which were stored at -20ºC. The carbon and nitrogen concentration were analyzed on a Thermo Electron Flash EA 1112 elemental analyzer (EA).

Maximum nutrient uptake rates (ρ_{max}) and half saturation constants (K_s) were determined on monospecific cultures grown in batch in the culture chamber. Nutrient uptake curves were estimated using short-term independent incubations. Bulk nitrate was measured in 7 incubations (0.5, 1, 1.5, 2.5, 5, 10, 25 µM) at different time intervals (0, 5, 10, 15, 20, 30, 45 min). Bulk nitrate samples were obtained by a gentle filtration of medium onto Nylon filters (Ø=0.45 µm). Samples were frozen at -20ºC until analysis in SFA (Segmented Flow Analyzer). The nitrate uptake rate for each aliquot was calculated as the slope of the linear regression of

nitrate concentration over time (Harrison et al. 1989). Both ρ_{max} and K_s were estimated assuming a Michaelis-Menten model with 2 parameters (see eq. (where ρ_{max}/α_i equals K_s). The calculations were done in R (R Core Team 2015) using the Dose-Response Curves "drc" package (Ritz and Streibig 2005). The data correspond to different sets of independent measurements from which a single nitrate uptake kinetic curve was generated for each individual population.

In order to determine the effects of nutrient supply dynamics and dilution rate on interspecific competition, the strains of the cyanobacterium *Synechococcus* sp. and the picoeukaryote *M. pusilla* were inoculated in independent photo-bioreactors (Sartorius Biostat BPlus bioreactor). After acclimation, cultures were gently mixed for competition, using a peristaltic pump and autoclaved tubing. The competition for nitrate was tested under different nitrate supply scenarios including constant and variable nitrate supplies, the latter being simulated by adding nitrate pulses to the bioreactors. For that, the inflow media (D = 0.2 d^{-1}) were supplemented with discrete pulses of nitrate (final concentration 5.8 µmol l^{-1}) from a sterile stock solution (882 µmol l^{-1}) at predetermined intervals (0.5, 1, 2 and 3 pulses d^{-1}) that represented different degrees of perturbation. The nitrate pulses were added with a sterilized pipette through a septum in the top of the bioreactor (Figure 3.3). Each pulse represented an increase of 52% of the total amount of nitrate supply per day (i.e. 11.25 µM). This procedure allowed us to rapidly increase the nitrate concentration in the media without physically altering the system's dilution rate; i.e. a total 8.5 ml of stock solution was added to the culture in each pulse, which led to a 0.57% change in culture volume (1.5-L) and that was quickly corrected by level sensor thereby avoiding any cumulative effect.

Finally, to evaluate the effect of the dilution rate on the competitive process, another experiment was performed by setting a higher dilution rate (0.35 d^{-1}). In this experiment, the system was maintained at steady-state for 8 days and then perturbed by adding nitrate pulses (23 µmol l^{-1}) at a frequency of twice per day. A higher dilution rate is expected to have accelerated all processes by increasing the growth rate of the species.

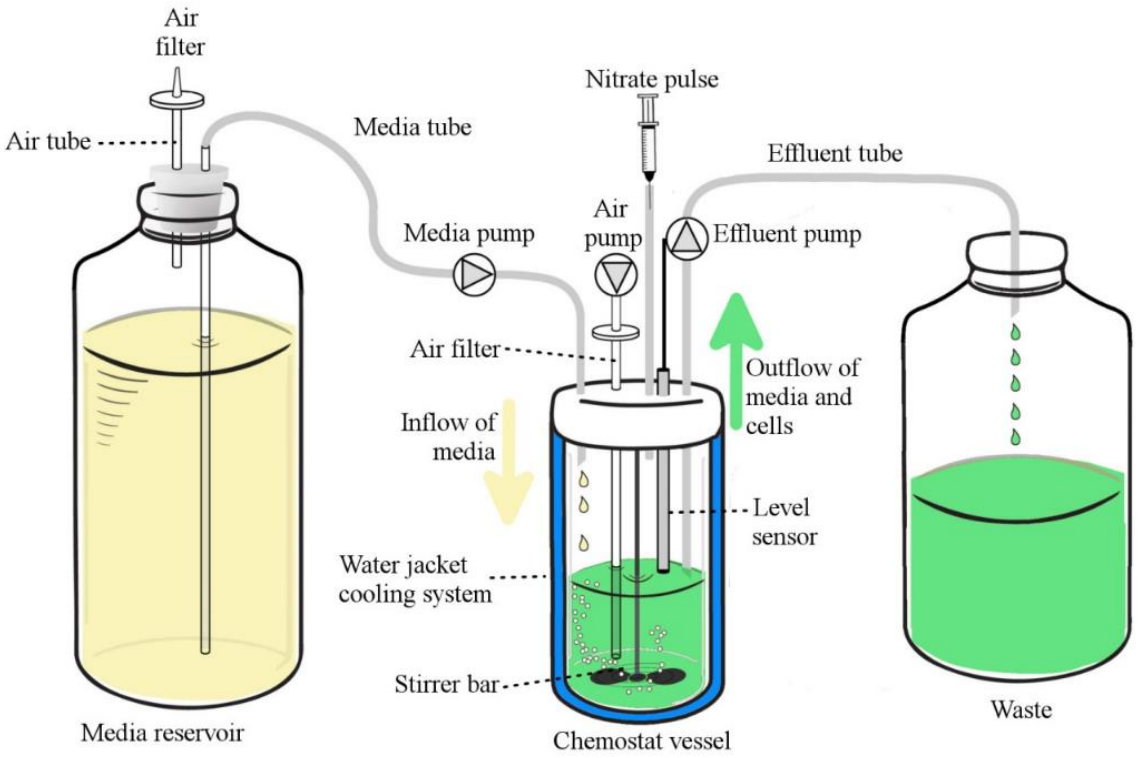

Figure 3.3 *Experimental design of competition experiments using continuous culture systems (chemostats). Media reservoir (PCR-S11) pump was calibrated (0.2 d^{-1}) before the experiment. Stirrer bar was used to homogenize the culture and avoid cell precipitation. Irradiance was provided on a 12:12 light:dark cycle (PAR = 100 µmol m^{-2} s^{-1}) and temperature was maintained at 21 (±0.1) ºC by a water cooling system. Nitrate pulses (final concentration: 5 or 23 µM) were injected using a syringe at a frequency of 0.5, 1, 2 and 3 d^{-1}.*

Competition model

Nutrient competition was numerically simulated using a modified version of Droop's canonical nutrient uptake model (Droop 1973). All parameters and their units are described in Table 3.1. The model assumes that both phytoplankton species were limited by nitrate as follows:

$$dN / dt = \mu(Q) * N - D * N \quad (2)$$

$$dQ / dt = \rho(R) - \mu(Q) * Q \quad (3)$$

$$dR / dt = S(t) - (R * D) - \rho(R) * N \quad (4)$$

$$dP / dt = (dN/dt * Q) + (dQ/dt * N) \quad (5)$$

where:

$$\rho(R) = \rho_{max} * (R / (\rho_{max} / \alpha + R)) \quad (6)$$

$$\mu(Q) = \mu_{max} * (1.0 - (Q_{max} - Q)/(Q_{max} - Q_{min})) \quad (7)$$

In the Droop's formulation, the specific growth rate (μ) of species (i) is related to the cell quota (Q) (see eq.(). The growth rate of species i (μ_i) approaches asymptotically its maximum ($\mu_{max,i}$) when the cell quota of species i (Q_i) approaches $Q_{max,i}$. The rate of change of the population density (N) is given by the difference between the growth rate of the population (μ_i) and the dilution rate (D) (see eq. 2). The nutrient uptake rate (ρ_i) is a function of external nutrient concentration (R), maximal uptake rate ($\rho_{max,i}$) and affinity (α_i), and its dynamics is well described by a hyperbolic function (see eq. 6). The parameter α_i represents the slope of the hyperbolic function and can be calculated as the quotient between $\rho_{max,i}$ and the half-saturation constant (K_s), also defined as the nutrient concentration at which ρ_i is half of $\rho_{max,i}$. The rate of change of the cell quota (Q_i) is dependent upon the nutrient uptake rate (ρ_i) and the population growth rate (μ_i) (see eq. 7).

Table 3.1 *Parameters, description and units of the phytoplankton model and nitrate uptake kinetics experiments and biochemical composition.*

Parameter	Description	Units
D_{cell}	Cell diameter	µm
V_{cell}	Cell volume	μm^3
C_{cell}	Cell carbon	fmol $cell^{-1}$
N_{cell}	Cell nitrogen	fmol $cell^{-1}$
C_{cell}:N_{cell}	Carbon to nitrogen ratio per cell	mol:mol
D	Flow (dilution) rate of chemostat	d^{-1}
R	Nitrate concentration at the cell surface	µmol N dm^{-3}
S(t)	Nutrient concentration at infinite distance (bulk concentration) at the time t	µmol N dm^{-3}
P	Biomass nitrogen	µmol N dm^{-3}
μ_{max}	Maximum growth rate	d^{-1}
Q_{min}	Minimum cell quota of N	fmol $cell^{-1}$
Q_{max}	Maximum cell quota of N	fmol $cell^{-1}$
N_O	Initial cell abundance	cells ml^{-1}
Q_0	Initial cell nitrogen quota	fmol $cell^{-1}$
ρ_{max}	Maximum nitrate uptake rate	fmol N $cell^{-1}$ d^{-1}
K_N	Half-saturation constant	µmol N dm^{-3}
α	Nutrient affinity	m^3 $cell^{-1}$ d^{-1} x 10^{-6}

The population biomass concentration is a function of cell abundance and internal quotas (see eq. 5). In the model, R, the nutrient concentration in the bulk medium varies as a function of the nutrient supply (S) and population growth rate (μ). S can be either constant (as in steady-state) or vary over time in response to spikes of nitrate of different magnitude and at different frequencies as follows:

$$S(t) = R_0 + (R_1/(D * dt)) * tpulse \quad (8)$$

where R_0 is the nutrient concentration in the reservoir (header tank), R_1 is the magnitude of the nitrate spike or pulse and *tpulse* = [t_1,t_2, t_3,...,t_{max}] is a Boolean vector of length t_{max}/dt that represents the frequency of the discrete pulses over time, being t_{max} the time of simulation (d). For multi-species communities, the rate of change of nitrate concentration (R) in the culture vessel is a function of the dilution rate (D), nutrient supply concentration, and the summation of total uptake by all populations. Note that the dilution rate multiplied by the nutrient concentration in the incoming medium ($D*S$) gives the nitrate supply rate (µM N d^{-1}), and that the dilution rate multiplied by the nitrate concentration in the culture vessel ($D*R$) gives the nitrate overflow rate (µM N d^{-1}). Then, R can be represented over time as follows:

$$dR / dt = D * (S - R) - \sum(\rho_i(R) * N_i)$$

The system of equations was implemented in MATLAB (MATLAB 2014b) and solved numerically using the Runge-Kutta algorithm (C Butcher John 1987). The Delayed Rejection Adaptive Metropolis (DRAM) algorithm (Haario et al. 2006) was used to fit values of selected model parameters to experimental observations (i.e. experiments setting a dilution rate of 0.2 d^{-1} and nitrate spikes at frequencies of 0, 0.5 and 3 d^{-1}). The other competition experiments were run subsequently for model validation. All runs were initialized with the population densities at the beginning of the laboratory-based competition experiments. A mean cell quota calculated over the time course of the experiments and an initial nutrient concentration in the bioreactor of 0.5 µM were selected.

In order to study the environmental windows of species' co-existence, we performed model simulations by considering all potential combinations of dilution rates, magnitudes of nitrate pulses and their frequencies. The simulation time was 100 days, and the differential equations were solved every 3 min (dt = 0.021 d^{-1}). Dilution rates were set in the range 0.1 to 0.4 d^{-1}. The magnitude (concentration) of the nitrate pulses spanned an order of magnitude, from 0 to 10 µM, while the frequency of nitrate pulses (spikes) varied from 0.1 to 10 d^{-1}. These selected dilution rates , magnitudes and frequencies were intended to be representative of real-world ocean processes, including mixing due to internal waves, semidiurnal and diurnal tides, deep water upwelling, and storms (Walsh et al. 1978).

Results

Physiological variables

Table 3.2 reports on the biochemical and physiological features of the selected microalgae strains. The cell diameter (D_{cell}) and biovolume (V_{cell}) were 0.95 ± 0.07 µm and 0.45 ± 0.10 μm^3, respectively, for *Synechococcus* sp., and 1.49 ± 0.11 µm and 1.77 ± 0.37 μm^3, respectively, for *M. pusilla*. μ_{max} were 0.56 ± 0.06 $d^{-1}$and 1.11 ± 0.27 d^{-1} for *Synechococcus* and *M. pusilla,* respectively. The C quota (C_{cell}) and N quota (N_{cell}) of *Synechococcus* (22.09 ± 2.53 fmol C $cell^{-1}$ and 3.2 ± 0.77 fmol N $cell^{-1}$, respectively) were roughly four times lower than those of *M. pusilla* (94.63 ± 63.60 fmol C $cell^{-1}$ and 11.65 ± 0.81 fmol N $cell^{-1}$, respectively). The maximum (Q_{max}) and minimum (Q_{min}) intracellular N quotas were 4.21 and 2.32 fmol N $cell^{-1}$, respectively, for *Synechococcus*, and 16.03 and 8.86 fmol N $cell^{-1}$, respectively, for *M. pusilla*.

The maximum nitrate uptake rates (ρ_{max}) for *Synechococcus* and *M. pusilla* were 1.85 ± 1.49 fmol N $cell^{-1}$ d^{-1} and 18.04 ± 1.73 fmol N $cell^{-1}$ d^{-1}, respectively. I found statistically significant differences between them (p-value<0.05). The half saturation constant for nitrate uptake (K_s), i.e. the nitrate concentration at which a species population attains half of its maximum nitrate uptake rate, was 0.13 ± 1.19 µM and 1.05 ± 0.42 µM for *Synechococcus* and *M. pusilla*, respectively. The nitrate affinity parameter (α), which is defined as the ρ_{max}/K_s ratio, took values of 4.23 ± 131.07 x 10^{-6} m^3cell^{-1} d^{-1} for *Synechococcus*, and 17.18 ± 8.52 x 10^{-6} $m^3cell^{-1}d^{-1}$ for *M. pusilla*. α represents the fraction of all nitrate molecules available in the bulk medium that is taken by the species population and, together with ρ_{max}, are the primary parameters that establish the opportunists and gleaners trade-off.

Assuming that the internal nutrient quotas remained invariable through time (dQ/dt=0), the Droop model parameterization can be simplified to a Monod model in which $\rho(R)/Q$ equal $\mu(Q)$. Based on this assumption, I calculated a μ_{max} for *Synechococcus* and *M. pusilla* of 0.58 ± 0.14 $d^{-1}$and 1.55 ± 0.17 d^{-1}, respectively. These estimates were slightly higher than those measured in batch culture experiments for *Synechococcus* (0.56 ± 0.06 d^{-1}) and *M. pusilla* (1.11 ± 0.27 d^{-1}).

Table 3.2 *Mean and standard deviation (n=2) of cell diameter (D_{cell}), cell volume (V_{cell}), cell carbon (C_{cell}), cell nitrogen (N_{cell}), minimum nitrogen quota (Q_{min}), maximum nitrogen quota (Q_{max}), mean C : N ratio, maximum nitrogen uptake rate (ρ_{max}), semisaturation constant (K_s) and affinity (α) for Micromonas pusilla and Synechococcus. D_{cell}, V_{cell}, C_{cell}, N_{cell}, Q_{min} and Q_{max} were measured during the exponential growth phase. ρ_{max} and K_s were determined during the stationary phase. The mean C:N ratio was computed from daily measurements obtained throughout the growth cycle in culture chamber.*

	Synechococcus	*M. pusilla*
Dcell	0.95 ± 0.07	1.49 ± 0.11
Vcell	0.45 ± 0.10	1.77 ± 0.37
μmax	0.56 ± 0.06	1.11 ± 0.27
Ccell	22.09 ± 2.53	94.63 ± 63.60
Ncell	3.20 ± 0.78	11.65 ± 0.81
Qmin	2.32	8.86
Qmax	4.21	16.03
Ccell:Ncell	6.90 ± 1.59	8.12 ± 0.79
ρmax	1.85 ± 1.49	18.04 ± 1.73
Ks	0.13 ± 1.19	1.05 ± 0.42
α	14.23 ± 131.07	17.18 ± 8.52

Competition experiments in laboratory photo-bioreactors

I initially introduced the 2 picophytoplankton species in 3 independent culture vessels under the same temperature, light, and nutrients supply regimes at a dilution rate of 0.20 (± 0.05) d^{-1}. According to theoretical predictions, *Synechococcus* (*R** = 0.07), outcompeted *M. pusilla* (*R** = 0.23), under continuous nitrate limiting conditions (Figure 3.4). The temporal pattern was characterized by a steady increase of the *Synechococcus* to *M. Pusilla* (S/M) ratio at a rate of 0.1 (± 0.07) log units d^{-1}. This result was remarkably consistent in all 3 experiments. In order to alter the steady-state continuous nitrate limitation, discrete pulses of nitrate at a final concentration of 5.8 μM were added to the bioreactor. The population dynamics were reversed when nitrate pulses were supplied at a frequency higher than 1 pulse per day. At a frequency of 1 pulse per day, the S/M ratio showed a slight decrease, though both populations increased simultaneously their abundances. On the contrary, the S/M ratio increased slightly when the frequency of nitrate pulses was reduced to 0.5 per day, being a similar response as that observed in the steady-state, no nitrate pulsing scenario. The temporal decay of the ln S/M ratio conformed consistently to a simple linear regression model (Figure 3.4.A). Plotting all treatments together, the analysis revealed that the rate of competitive exclusion of

Synechococcus increased linearly with the frequency of nitrate pulses (Figure 3.4.B). By extrapolating the results of this linear model, coexistence between species at a nitrate pulsing frequency of 0.67 pulses per day was inferred.

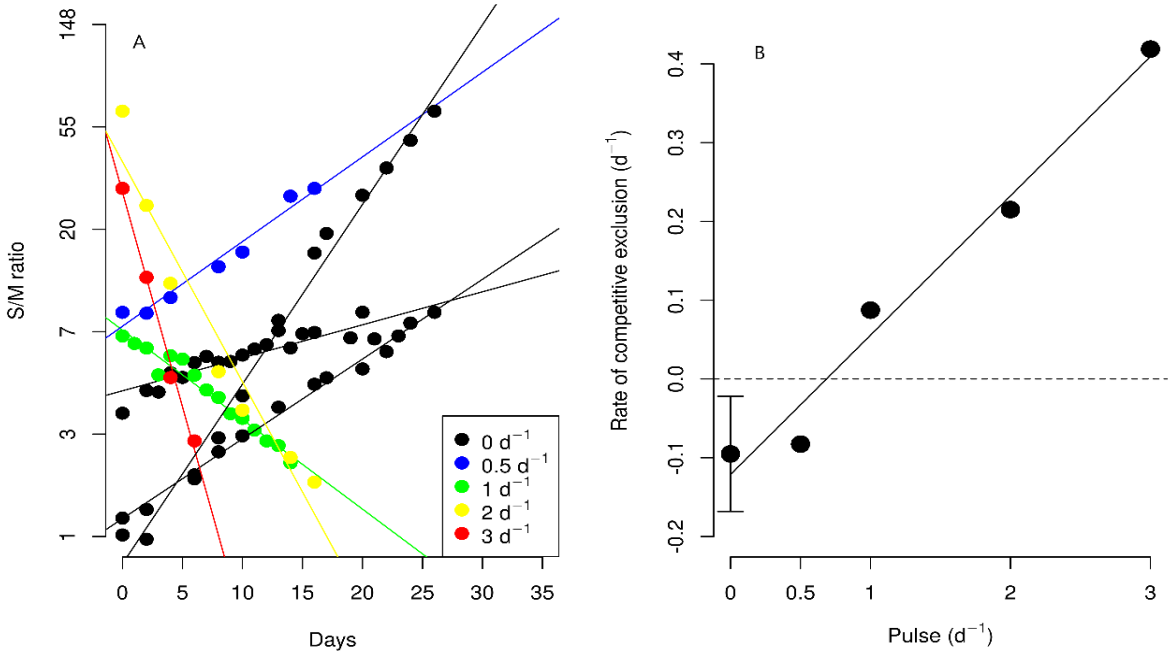

Figure 3.4 *Synechococcus/Micromonas abundance (S/M ratio) over time at different frequencies of nitrate pulses in a constant dilution rate in chemostats (D=0.22 d-1). Lines represent significant (p<0.05) linear relationships in each experiments. The temporal evolution of the S/M ratio from experiments shown in Figure 1 is shown on a logarithmic scale. The slope of the linear relationship between ln S/M ratio and time represents the rate of competitive exclusion (slopes were all different from 0, p<0.05). B: Relationship between the rate of competitive exclusion (-S/M rate) and the rate of nitrate supply (frequency of nitrate pulses). Dashed line indicates the frontier of outcome. Under it, Synechococcus outcome Micromonas pusilla and upper it, Micromonas pusilla displace Synecochoccus. The data fit to a linear regression model: y= -0.12 + 0.18x, R^2 = 0.97, p-value < 0.01.*

One additional experiment was carried out by adjusting the dilution rate to values as high as 0.35 d^{-1}, which surpasses the intersection point of growth rate curves. Excess mortality of *Synechococcus* led to a rapid dominance of *M. pusilla* regardless of whether or not nitrate pulses were added to the bioreactor (Figure 3.6). In all cases, the population dynamics exhibited similar trends when using biomass instead of abundance as a metric (Figure 3.5).

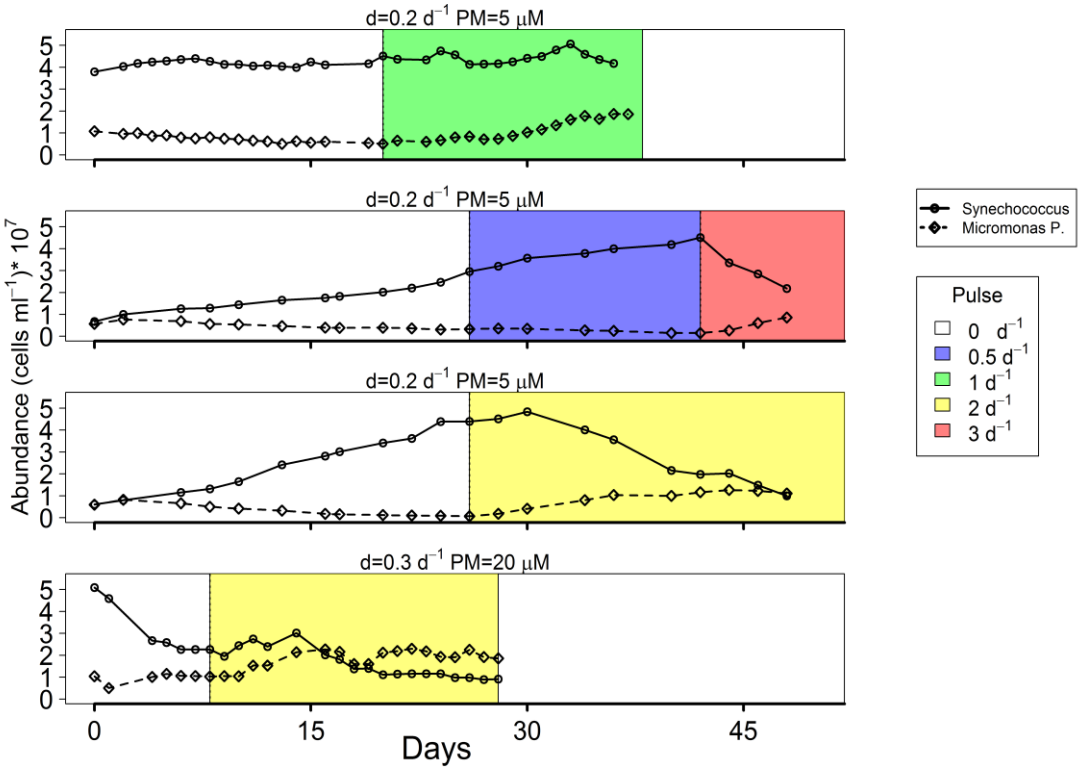

Figure 3.6 *Synechococccus and Micromonas pusilla population dynamics at a frequency of 0, 0.5, 1, 2 and 3 pulses d^{-1}. These experiments were conducted in chemostat systems at different dilution rates (d) and pulse magnitudes (PM) at predetermined time intervals.*

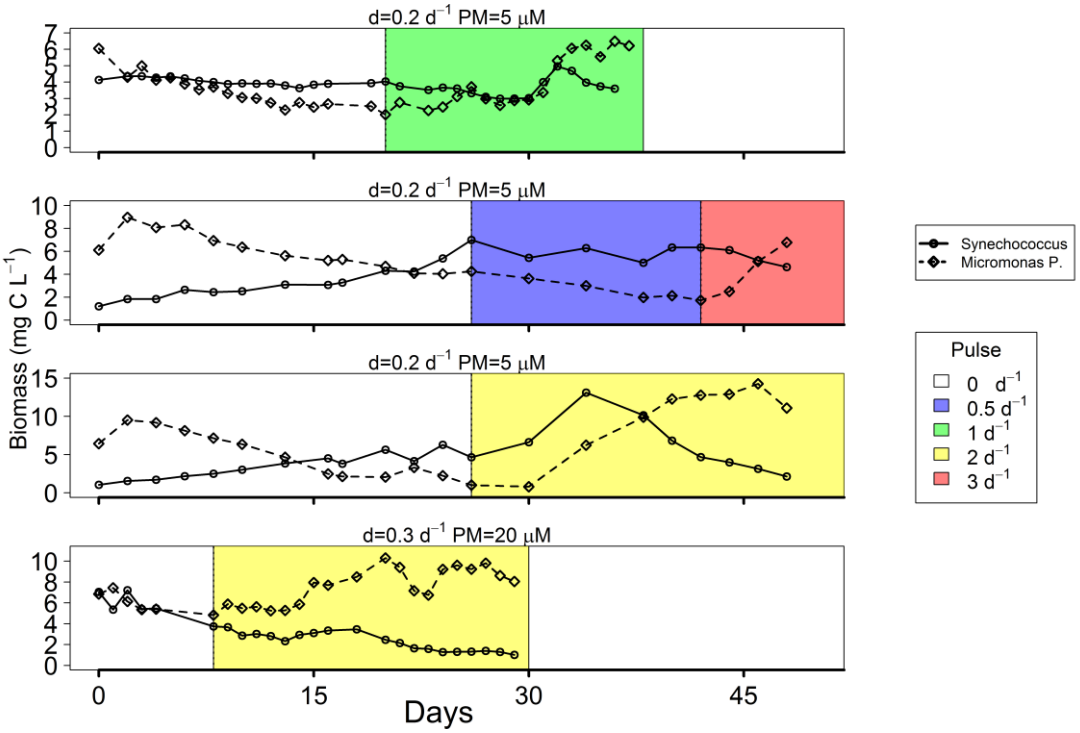

Figure 3.5 *Synechococccus and Micromonas pusilla biomass dynamics at a frequency of 0, 0.5, 1, 2 and 3 pulses d^{-1}. These experiments were conducted in chemostat systems at different dilution rates (d) and pulse magnitudes (PM) at predetermined time intervals.*

Competition model simulations

Table 3.3 reports the model parameters as calibrated by using the laboratory competition experiments. μ_{max} were 0.82 ± 0.12 d^{-1} and 1.45 ± 0.03 d^{-1} for *Synechococcus* and *M. pusilla*, respectively. Q_{max} and Q_{min} were 0.14 ± 0.01 and 0.62 ± 0.07 fmol N $cell^{-1}$ for *Synechococcus*, and 11.29 ± 0.54 and 20.31 ± 0.35 fmol N $cell^{-1}$ for *M. pusilla*. ρ_{max} for *Synechococcus* and *M. pusilla* were 0.17 ± 0.01 fmol N $cell^{-1}$ d^{-1} and 70.87 ± 8.89 fmol N $cell^{-1}$ d^{-1}, respectively. α of *Synechococcus* was 2.27 ± 0.13$m^3cell^{-1}d^{-1}$ x 10^{-6}, whereas that of *M. pusilla* was 47.47 ± 3.03$m^3cell^{-1}d^{-1}$ x 10^{-6}. K_s, calculated as the quotient of ρ_{max} and α, were 0.07 ± 0.01 µM and 1.49 ± 0.28 µM, respectively, for *Synechococcus* and *M. pusilla*. For both species, μ_{max} were higher than those estimated from ρ_{max} and Q in batch experiments. However, the Q_{max} and Q_{min} values of *M. pusilla*, as calculated by DRAM methods, fitted well with nitrate uptake kinetics experiments. The uncoupling between uptake rate and growth rate (i.e. the ρ_{max}/Q_{max} ratio) in *M. pusilla* was twice larger than in *Synechococcus* when cells grew at maximal growth rate. On the other hand, the parameters of *Synechococcus*, especially the internal quotas, were smaller than those expected from batch cultures. Nevertheless, the competition model reproduced the competitive dynamics in all experiments (Figure 3.7), although model data were slightly smoother than the dynamics observed in the laboratory experiments.

In order to define a hyperspace for coexistence of species, I used the model to explore the outcome of the competition processes in a tridimensional space by simulating combinations of the variables pulse frequency (pulses d^{-1}), pulse magnitude (µM) and dilution rate (d^{-1}). Figure 3.8 shows the contribution of *Synechococcus* to total abundance over different dilution rates. The hyperplane of coexistence was defined by a consistent coexistence in the last month of the temporal simulation. Below the coexistence hyperplane (red zone), nitrate pulses were unable to deviate the steady state dynamics enough to switch the dominance from *Synechococcus* to *M. pusilla*. By contrast, the system became much more dynamical above the hyperplane, leading to a rapid exclusion of *Synechococcus*. These patterns of dominance and coexistence were inferred from a simple competition model by adjusting the dynamics of nitrate supply and illustrate how ocean physics, chemistry and ecology interact to shape the structure of plankton communities.

Table 3.3 *Mean and standard deviation of composition, growth and metabolic rates for Micromonas pusilla and Synechococcus. Variables are cell minimum nitrogen quota (Q_{min}), maximum nitrogen quota (Q_{max}), maximum nitrogen uptake rate (ρ_{max}), half-saturation constant (K_s), maximum population growth rate (μ_{max}) and nutrient affinity (α). Parameters were either measured using batch and chemostats experiments or estimated using Delayed Rejection Adaptive Metropolis (DRAM) algorithm in competition experiments carried out on chemostats.*

Group	Parameter	Measured on batch	Estimated by DRAM
Synechococcus	μ_{max}	0.56 ± 0.06	0.82 ± 0.12
	Q_{min}	2.32	0.14 ± 0.01
	Q_{max}	4.21	0.62 ± 0.07
	ρ_{max}	1.85 ± 1.49	0.17 ± 0.01
	K_s	0.13 ± 1.19	0.07 ± 0.01
	α	14.23 ± 131.07	2.27 ± 0.13
M. pusilla	μ_{max}	1.11 ± 0.27	1.45 ± 0.03
	Q_{min}	8.86	11.29 ± 0.54
	Q_{max}	16.03	20.31 ± 0.35
	ρ_{max}	18.04 ± 1.73	70.87 ± 8.89
	K_s	1.05 ± 0.42	1.49 ± 0.28
	α	17.18 ± 8.52	47.47 ± 3.03

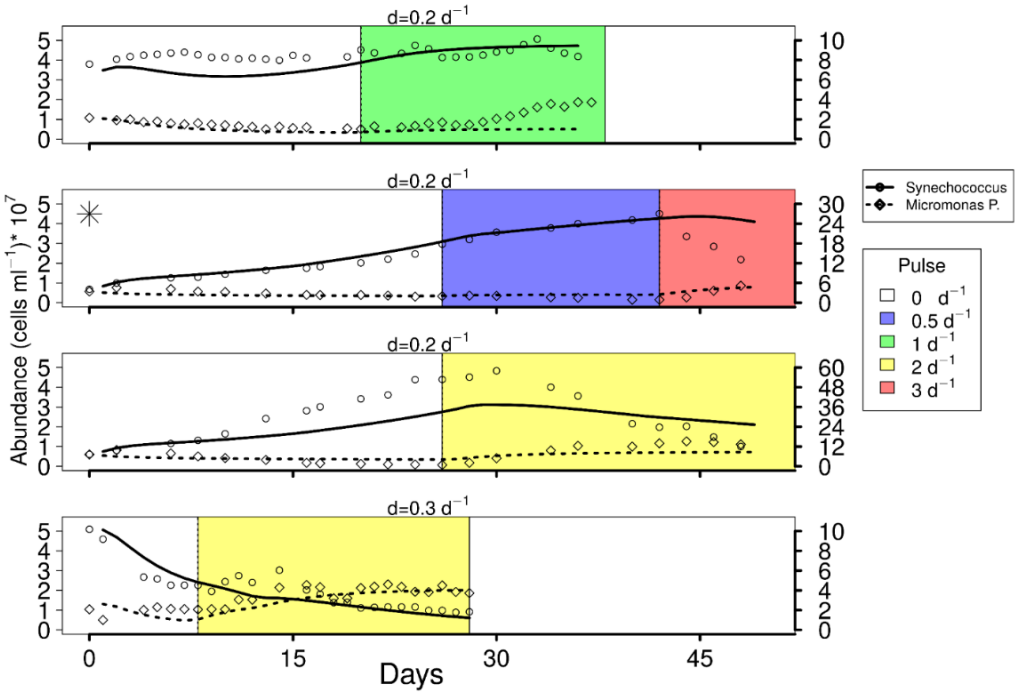

Figure 3.7 *Synechococccus and Micromonas pusilla population dynamics of competition experiments (points) and their ecological modelling comparation (line). These experiments were conducted in chemostat systems at different dilution rates (d) by adding pulses of nitrate (PM) at predetermined time intervals. Model was calibrated using the experiment indicated with a star and then tested in the other experiments.*

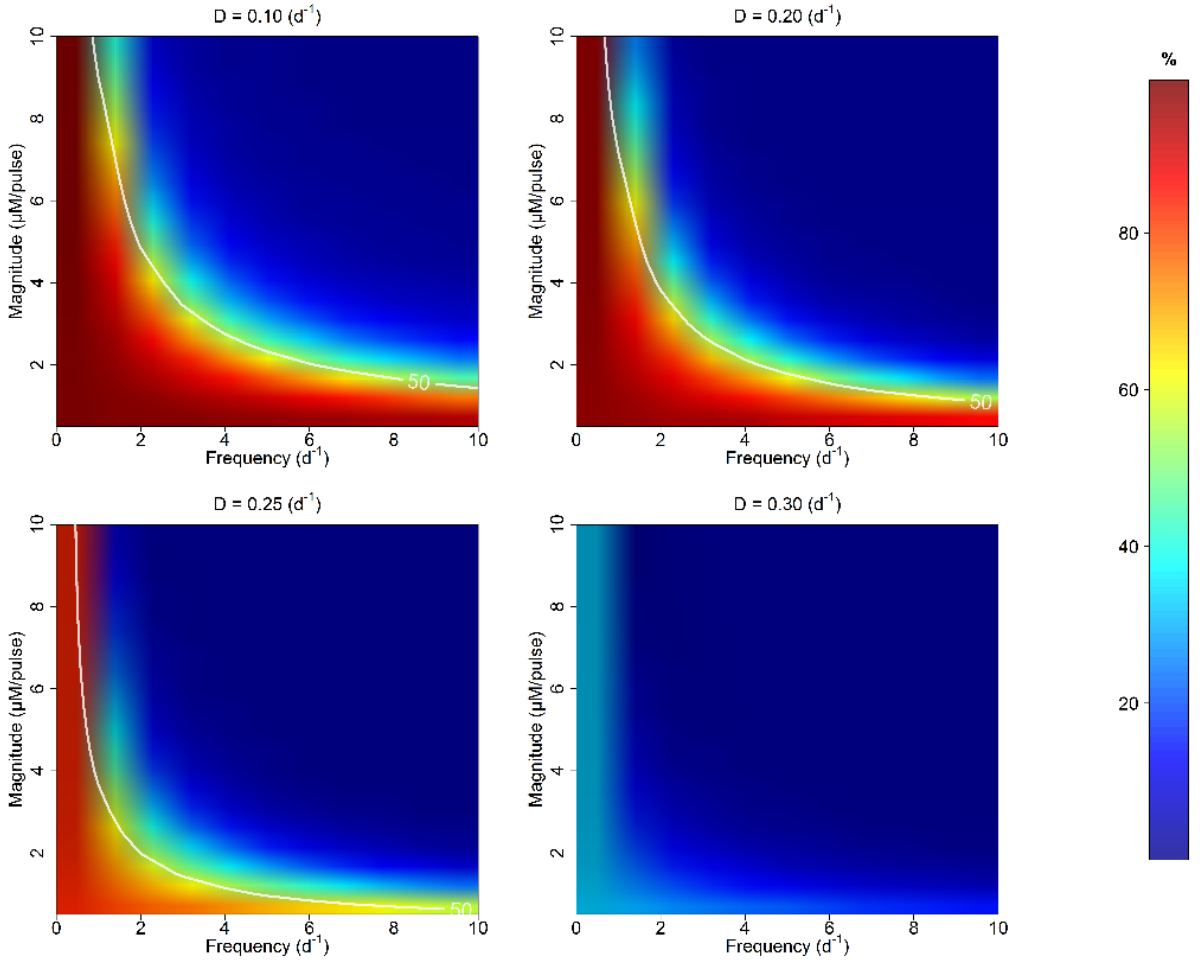

Figure 3.8 *Contribution of Synechococcus sp. to total cell density at different dilution rates, and frequency and magnitude (increase in final concentration) of nitrate pulses. Simulations using a constant dilution rate are shown. The line represented the combination of environmental conditions that allow the coexistence of populations at the corresponding dilution rate.*

Discussion

Physiological traits

The ability of phytoplankton species to use resources efficiently confers some species competitive advantages under certain environmental conditions and contributes to shape the structure of their communities. These species-specific physiological traits are the main foundation of the resource competition theory (Tilman 1982). These traits, such as the maximum nutrient uptake rate (ρ_{max}) and nutrient affinity (α), are often correlated among them giving rise to physiological trade-offs (Edwards et al. 2012). These trade-offs promote the emergence of new life-forms and innovative eco-physiological strategies and lead to the establishment of different ecological and functional niches. Cell size is a key morphometric

trait that affects virtually every aspect of phytoplankton biology from cell physiology to community ecology (Chisholm 1992; Raven 1998; Litchman and Klausmeier 2008; Finkel et al. 2010; Marañón et al. 2013). Minimalism carries on advantages and limitations to cells. For instance, the ratio between the maximum nutrient uptake rate (ρ_{max}) and the minimum intracellular nutrient quota (Q_{min}) scales positively with cell size in small phytoplankton (0.1–100 μm^3), allowing the separation of the processes of growth and nutrient uptake over time (Raven 1998; Ward et al. 2017) (citar Raven). Additionally, non-scalable components, such as membranes and genetic material, occupy an increasingly larger fraction of the cell biovolume as cell size decreases (Raven 1998), thus reducing the amount of space available for catalytic and biosynthetic units and hence, affecting their potential to achieve a higher maximum growth rate (μ_{max}). However, there also exists a positive correlation between ρ_{max} and α for nitrate uptake that can be explained by using the nutrient uptake model of Aksnes and Egge (1991). According to their formulations, two mutually exclusive strategies are permitted, namely, a high ρ_{max}/Q_{min} ratio and low α, or a low ρ_{max}/Q_{min} ratio and high α. These two contrasting eco-physiological strategies are consistent with the classical opportunists versus gleaners confrontation (Margalef 1978; Grover 1991). Cermeño et al. (2011) explored this idea using the cocolithophore *Coccolithus braadurii* and the diatom *Thalassiosira pseudonana* as two model marine phytoplankton species representative of two biogeochemically-distinct functional groups. Their analysis revealed that the coccolithophore was superior competitor under continuous nitrate supply conditions. However, the addition of nitrate pulses switched the competitive dynamics towards the dominance of the diatom. Though in the study of Cermeño et al (2011) both species *T. pseudonana* and *C. braarudii* exhibited rather similar cell sizes, yet, their distinct taxonomic affiliations were decisive to influence the competitive dynamics under the different nitrate supply regimes. Whereas the coccolithophore has inherited features proper of a relatively stable and oligotrophic open ocean environment, the diatom illustrates the classical example of opportunists, with higher maximum growth rates and the ability to store inorganic nutrients in large intracellular vacuoles, reflecting the turbulent ocean conditions in which their ancestral lineages evolved. Here, I have shown that the cyanobacterium *Synechococcus* sp. and the picoeukaryote *M. pusilla* followed rather similar competitive dynamics (Figure 3.4). This remarkable similarity in the competitive dynamics of these two picophytoplankton species is attributable to their different cell sizes, taxonomic affiliations and evolutionary origins. Under variable nitrate supplies, *Synechococcus* was

outcompeted by *M. pusilla*. The relatively large cell size of *M. pusilla* conferred competitive advantages under variable nitrate supply conditions, which enable *M. pusilla* to exploit their comparatively higher maximum growth rate and, presumably, a greater capacity to increase their internal nitrate quotas. The Droop model, in which the variable internal nutrient quotas influence the outcome of the competitive dynamics, provides a useful mechanistic framework to explain these results and constrain the set of nutrient supply scenarios which allowed both species populations to coexist. The nitrate supply dynamical scenarios recreated here led to periods of nitrate-limited growth interspersed with periods of nitrate-replete conditions (Figure 3.8). The continuous and dynamical nitrate supplies led to the selection of gleaners and opportunists, respectively. However, we also found a range of nitrate supply regimes i.e. certain frequencies of nutrient pulses, which allowed the coexistence of both species through time. These results provide a new insight into the patterns of picophytoplankton species succession, revealing an array of potential community configurations along a range of nitrate supply conditions, from steady-state, continuous nitrate supply to high frequency nitrate-pulses regimes. The affinity parameter calculated for *Synechococcus* and *M. pusilla* in nitrate uptake kinetics experiments were slightly lower and higher, respectively, than the values estimated by the DRAM algorithm. This could be explained by the different physiological status of populations under steady-state (continuous nutrient limitation) and non steady-state conditions (from nutrient excess to starvation). Limitation and starvation cause markedly different physiological responses as a result of cells being in unbalanced and balanced growth states, respectively (Mulholland and Lomas 2008; Halsey and Jones 2015). It is well known that steady-state growth is closer to conditions encountered in open-ocean environments, whereas cultures transitioning from nutrient excess into starvation are more illustrative of unstable marine environments typical of polar and temperate seas and coastal regions.

The results of the competition experiments indicate that a higher frequency of nitrate pulses increased the abundance of the picoeukaryote at the expense of the cyanobacterium (Figure 3.5). These results reveal a positive linear relationship between the frequency of nitrate pulses and the rate of competitive exclusion. This relationship implies the existence of a window of opportunity for species coexistence somewhere between steady-state and the low frequency of perturbations scenario. Using nutrient concentrations as an index of nutrient availability and turbulence, Margalef (1978) proposed a conceptual model to describe the temporal patterns of marine microphytoplankton species succession in his famous mandala.

Cullen et al. (2002) and Wyatt (2014) later provided updated versions of the classical Margalef's mandala by incorporating different groups within the picophytoplankton size fraction. More recently, Mouriño-Carballido et al. (2016) further advanced in our understanding of how the picophytoplankton subgroups fit into the scheme of the mandala by using concurrent measurements of nutrient supply rates to the euphotic zone and taxonomic composition data from the northwestern Mediterranean Sea. Mouriño-Carballido et al. showed that *Synechococcus* was the dominant group at intermediate levels of nitrate supply whereas the picoeukaryotes dominated the picophytplankton community biomass under regimes of increased nutrient supply rates. Further supporting their results, Berthelot et al. (2018) determined nutrient uptake rates of picophytoplankton from the Northeast Pacific Ocean and showed that, on average, *Synechococcus* relied on nitrate fluxes in the rage 4–6 times lower than those required by picoeukaryotes determined.

I recognize that the experimental results and model analyses reported here provide an oversimplified view of plankton communities and the mechanisms underlying their structure. My study neglects the complexity of microbial plankton communities by omitting the effects of third-party competitors, predators, viruses, etc. Furthermore, by focusing on the competition for one single nutrient, specifically nitrate, it also ignores the effect of co-limiting nutrients on the competitive dynamics of population species and species coexistence. In fact, the classical resource competition theory explains species coexistence as a result of multiple resources limitation such that, at equilibrium, the number of coexisting species should be equal to the total number of limiting resources. To further complicate interpretations, field observations have long shown that the number of species of plankton communities is much higher than the number of species predicted by the resource competition theory, the so-called Paradox of the Plankton (Hutchinson 1967). In conclusion, my results cannot be used to infer the distribution of the different picophytoplankton subgroups across the ocean nor their responses to climatically-driven changes in nutrient supply regimes. However, by oversimplifying things, this study allows a closer inspection into the details of the competition between two picophytoplankton species with global biogeochemical relevance. These results should be useful to inform models about individual processes, which are key to refine mechanistic models in their venture to produce more reliable predictions.

Biogeochemical implications

The classical view, supported by Stokes' Law (Raven 1986), considers that particle sinking speed scales with the square of particle size, and therefore large particles are more likely to escape microbial remineralization and reach the deep ocean. Taking into consideration this premise, a large segment of the oceanographic community has focused on the analysis of large-sized phytoplankton as the main responsible for the downward export of organic carbon (Tremblay et al. 1997; Agawin et al. 2000; Dunne et al. 2005). These previous studies have neglected the potential of small-sized phytoplankton fractions (i.e. nano- and picophytoplankton) as contributors to organic carbon export. However, other analyses have demonstrated that small phytoplankton cells can contribute to the downward export fluxes of organic carbon through i) sinking enhancement mechanisms such as particle aggregation and biomass processing through complex food webs (Richardson and Jackson 2007), and ii) physical mixing (Gardner et al. 1995). These mechanisms, together with the fact that the open ocean tropical and subtropical regions cover vast areas of the global ocean (Longhurst 2010), suggest that picophytoplankton could be a significant player in the organic carbon export fluxes on a planetary scale (Lomas and Moran 2011; Close et al. 2013). Within the different picophytoplankton groups, *Prochlorococcus*, the smallest and most abundant primary producer on Earth, has become adapted to severe oligotrophic conditions by minimizing their resources requirements through a drastic reduction of cell size and genome size (Partensky and Garczarek 2010). The contribution of *Prochlorococcus* to phytoplankton community biomass is overwhelming in oligotrophic regions (Zubkov et al. 2000). However, the great contribution of *Prochlorococcus* to phytoplankton community biomass in these ocean regions does not seem to be correlated with their contribution to organic carbon export fluxes. The contribution of *Prochlorococcus* to organic carbon export fluxes is extremely low (Guidi et al. 2016). On the other hand, the abundances of *Synechococcus* and photosynthetic picoeukaryotes have been shown to covary in many different ocean environments (Worden et al. 2004; Calvo-Díaz and Morán 2006; Estrada et al. 2014), suggesting that these two picophytoplankton subgroups respond idiosyncratically to different nutrient supply regimes. Using data from Hawaii ocean time series station, Corno et al. (2007) found a positive correlation between the abundance of both picoeukaryotes and prymnesiophytes and the rates of depth-integrated primary production and organic carbon export. The observation that these two groups correlated positively with the organic carbon export fluxes could be explained in part by differences in the organic carbon

content of picoeukaryotes and *Synechococcus*. Despite the small differences between these two picophytoplankton groups in cell diameter (picoeukaryotes = ~2.0 μm and *Synechococcus* = ~1.1 μm), the organic carbon content of picoeukaryotes is from 6.5-fold to 14-fold greater than that of cyanobacteria (Worden et al. 2004). This implies that picoeukaryotes possess a greater potential for organic carbon export than the cyanobacteria.

Current ocean models indicate that over the period from 1800 to 2100, nutrient supply fluxes will reduce by 40% due to the climatically-enhanced surface ocean stratification (Lewandowska et al. 2014). Ocean ecosystem models predict that these changes in ocean stratification will most critically influence the abundance of large-sized phytoplankton such as diatoms, which are better adapted to thrive in unstable ocean environments. However, the extent to which other phytoplankton such as the picophytoplankton will be impacted by these trends in ocean stratification is unknown. One can argue that their small size will buffer the reduction in nutrient supply associated with increased ocean stratification, but, will all picophytoplankton respond in the same manner? Based on the results presented in this chapter, I argue that increased ocean stratification will impact more negatively on picoeukaryotes than cyanobacteria that could even increase if ocean stratification impairs the growth of their competitors. Mesoscale and sub-mesoscale ocean processes influence nutrient supply dynamics to the euphotic zone, giving rise to a mosaic of environmental conditions and a variety of opportunities for distinct phytoplankton functional types to thrive (d'Ovidio et al. 2010; Barton et al. 2014). The low spatial resolution of current, state-of-the-art global ocean ecosystem models prevents these physical processes from being adequately represented. Thus, the implementation of global ocean ecosystem models to incorporate upper ocean dynamics at a finer spatial resolution is urgently needed. Only then, model will provide a more realistic view of microbial plankton communities and their population dynamics in response to climatically-induced ocean changes.

Chapter 4

Estimation of the vertical supply of nitrate turbulent diffusion in contrasting marine environments

Abstract

Nitrate turbulent diffusion has been traditionally considered one of the main mechanisms by which nitrogen is supplied to phytoplankton inhabiting the surface ocean. However, difficulties to quantify turbulence in the ocean have limited our knowledge about the magnitude and geographical variability of this process. Here we use a large dataset of microturbulence observations collected in contrasting marine environments to build a prediction model, and obtain the first climatology of nitrate diffusion into the euphotic zone. A model including three predictors (surface temperature, nitrate vertical gradient, and surface chlorophyll-a) explained 57% of the variance in the nitrate diffusive flux. This model was applied to climatological data to predict nitrate diffusion in the global ocean. Average nitrate diffusion for oligotrophic regions between 40ºN-40ºS (~20 Tmol N y^{-1}) was comparable to the sum of global estimates of nitrogen fixation, fluvial fluxes and atmospheric deposition, and therefore represents represents the main entry of new nitrogen in these regions. Finally, we estimated that with the predicted decreased in nitrate supply as the result of global change, a 8% increase in the ratio cyanobacteria to picoeukaryotes would occur in a future ocean, something that would have important implications, given the contribution of smallest cells to the biological carbon pump.

Introduction

Picoplankton, including archaea, bacteria and picoeukaryotes are the smallest (cell diameter <2 μm) and most abundant organisms. This group dominates the biomass and production in the vast oligotrophic ocean (Chisholm 1992; Agawin et al. 2000) and together with nanoplankton, can dominate the microbial community under certain conditions in shelf seas (Morán 2007; Espinoza-González et al. 2012). Traditionally larger cells (diatoms and coccolithophores) have been considered the main contributors to carbon exportation due to their large size and mineral content (Smayda 1971). However, recent studies suggest that photosynthetic picoplankton could also play a role in the export of carbon to the deep ocean (Richardson and Jackson 2007; Lomas and Moran 2011; Guidi et al. 2016). Moreover, the relevance of this group is predicted to increase under global change scenarios due to the increase in sea surface temperature, and the decrease in the supply of nitrogen from deeper waters (Morán et al. 2010; Flombaum et al. 2013; Agusti et al. 2019).

"Follow the nitrogen", the mantra proposed by Capone et al. (2006) for searching for life on Mars, summarizes the relevance that this element plays on life. By limiting both land and marine primary productivity, this element controls the flow of energy through the ecosystem, and the atmospheric CO_2 uptake by photosynthetic organisms. Marine primary production can be supported by nitrogen inputs recently supplied from outside the photic layer (named new production, mainly in the form of nitrate), or by nitrogen remineralized within the photic layer (regenerated production) (Dugdale et al. 1967). In steady state, when large temporal and spatial scales are considered, and for fixed stoichiometry of organic matter, new production will be equivalent to the amount of organic carbon that can be exported to the deep ocean, where it will remain isolated for time scales of the deep ocean circulation (100s-1000s years) (Lewis et al. 1986). The efficiency of the biological carbon pump can be then characterized in terms of the f-ratio, defined as the ratio of new production to the sum of new plus regenerated production (total production) (Eppley and Peterson 1979).

Nitrate turbulent diffusion has been traditionally considered one of the main mechanisms by which nitrogen is supplied to phytoplankton, particularly in permanently stratified ocean environments such as tropical and subtropical regions (Lipschultz et al. 2002), and in temperate areas during summer stratification (Rippeth 2005; Bendtsen and Richardson 2018). Quantification of nitrate diffusion requires estimates of vertical diffusivity (Kz), which can be derived from observations of microstructure, tracer release experiments and indirect methods using

acoustic Doppler (Thorpe 2007). These experimental approximations present methodological difficulties that have historically limited our knowledge about the magnitude and variability of turbulent mixing in the ocean. Alternatively, constant values of Kz have been used to estimate nitrate turbulent diffusion (Capone et al. 2005). However, the increased availability of commercial microturbulence profilers has increase the number of observations, which have revealed a large temporal and spatial variability of Kz in the upper layer of the ocean (Kunze et al. 2006; Hibiya et al. 2007; Sharples et al. 2007; Forryan et al. 2012; Cuypers et al. 2012; Fernández-Castro et al. 2014; Villamaña et al. 2017; Bouruet-Aubertot et al. 2018).

Bulk estimates of seawater nutrient concentration have been also frequently used as a proxy for nutrient availability in the euphotic zone (Agawin et al. 2000; Flombaum et al. 2013). However, nitrate concentrations and actual nitrate supply into the euphotic zone can be disconnected in near-steady-state systems, such as the subtropical gyres, where nitrate diffusion is slow, and nitrate concentrations are kept close to the detection limit due to phytoplankton uptake (Mouriño-Carballido et al. 2016).

We used microstructure turbulence observations and environmental variables collected in contrasting marine environments, to predict nitrate turbulent diffusion into the euphotic zone by using a multivariable fractional polynomial method. This model was later used to: 1) get a global estimation of the nitrate supply by turbulent diffusion in tropical and subtropical regions (40ºN – 40ºS), and 2) predict the change in the structure of picoplankton communities (the cyanobacteria to picoeukariotes ratio) in a future global change scenario.

Material and Methods

Sampling

This study includes 181 stations collected between October 2006 and December 2015 mainly in four contrasting marine environments: tropical and subtropical Atlantic, Pacific and Indian oceans (T), the Northwestern Mediterranean Sea (M), the Galician coastal upwelling ecosystem (G), and the Antartic Peninsula (A) (see Figure 4.1 & Table 4.1). Three cruises (CARPOS Oct-Nov 2006, TRYNITROP Apr-May 2008 and MALASPINA Dic 2010 – July 2011) sampled 75 stations, mainly located in the tropical and subtropical Atlantic, Pacific and Indian Oceans. Four cruises carried out in the Northwestern Mediterranean Sea (PERFILM Jun-Jul 2009, FAMOSO1 Mar 2009, FAMOSO2 Apr-May 2009, FAMOSO3 Sep 2009) sampled 34 stations

during four contrasting hydrographic conditions, covering from winter mixing to summer stratification. In the Galician coastal upwelling ecosystem 37 stations were sampled during HERCULES2 Sep 2011, HERCULES3 Jul 2012, DISTRAL-REIMAGE Feb 2012-Jan 2013, ASIMUTH Jun 2013, STRAMIX Aug 2013, CHAOS Aug 2013, and NICANOR Feb 2014-Dec 2015 cruises. In this region all stations considered were deeper than 40 m. One cruise sampled 10 stations located in the Antartic Peninsula (COUPLING Jan-2010). Finally, the PERFILC cruise sampled 27 stations, in the Bay of Biscay in July 2008. Because no samples were collected for the determination of nitrate during the PERFILM and PERFILC cruises (see below), hydrographic and microstructure turbulence profiles collected during both cruises were averaged and assigned to the mean geographical location of all the stations conducted during each cruise (Figure 4.1)**.** Additional information about the sampling design of these cruises is described in Aranguren-Gassis et al. (2011, CARPOS), Mouriño-Carballido et al. (2011, TRYNITROP), Fernández-Castro et al. (2015, MALASPINA), Mouriño-Carballido et al. (2016, FAMOSO), Cermeño et al. (2016, DISTRAL), Teira et al. (2012, COUPLING), Villamaña et al. (2017, CHAOS), Díaz et al. (2019, ASIMUTH), Villamaña et al. (in preparation 2019, STRAMIX) and (Moreira-Coello et al. 2017).

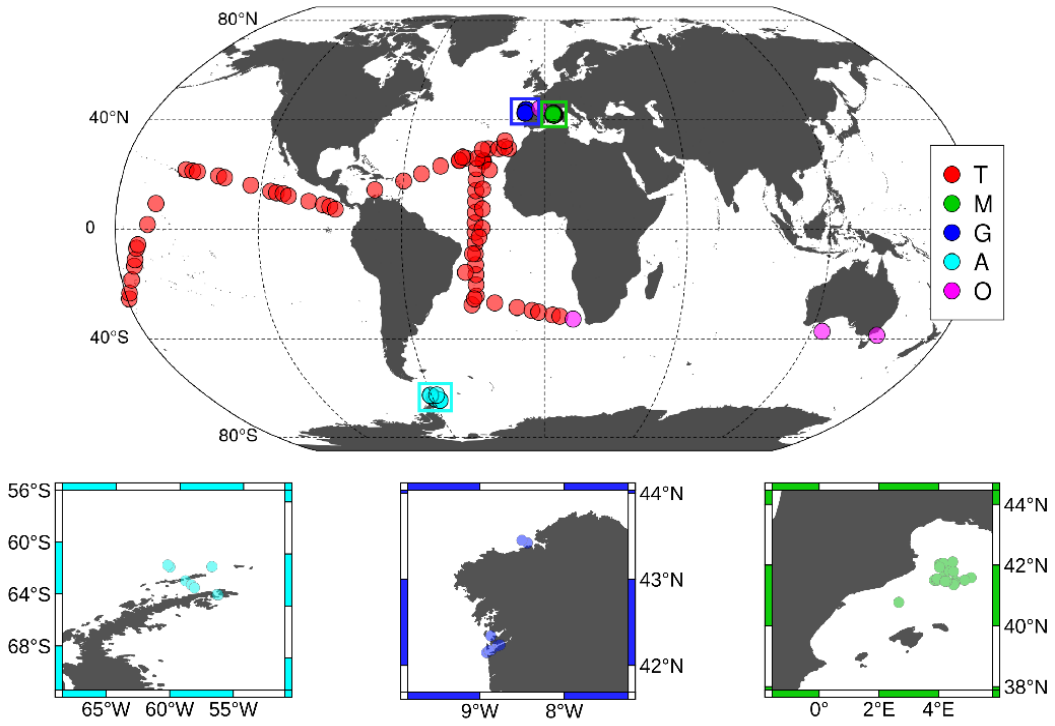

Figure 4.1 *Location of the stations sampled in tropical and subtropical regions (red), the Mediterranean Sea (green), the Galician coastal upwelling (dark blue), the Antartic Península (light blue) and other regions (pink). Small panels provide details about those stations sampled in the Antartic Península (light blue), the Galician coastal upwelling (dark blue) and the Mediterranean Sea (green).*

Table 4.1 *Details of the data included in this study. Domain refers to tropical and subtropical Atlantic, Pacific and Indian oceans (T), Northwestern Mediterranean Sea (M), Galician coastal upwelling (G), Antarctic Peninsula (A) and other regions (O). N indicates the number of stations sampled during each cruise. Duration (mean ± standard deviation, in minutes) is the time used for the turbulence profiler deployment at each station. Depth (mean ± standard deviation, in meters) is the maximum depth reached by the microstructure profiler. During the Malaspina expedition only 44 out of 47 stations were considered as tropical and subtropical.*

Domain	N	Cruise	Vessel	Date (dd/mm/yy)	Duration	Depth
NE Atlantic (T)	8	CARPOS	*Hespérides*	14/10/06–22/11/06	49 ± 25	137 ± 14
Atlantic (T)	18	TRYNITROP	*Hespérides*	14/04/08–02/05/08	32 ± 12	219 ± 19
Atlantic, Pacific and Indian (T)	47	MALASPINA	*Hespérides*	19/12/10 - 10/07/11	27 ± 9	234 ± 23
NW Mediterranean (M)	15	PERFILM	*García del Cid*	27/06/09-1/07/09	51 ± 22	201 ± 12
Liguro-Provençal Basin (M)	6	FAMOSO1	*Sarmiento de Gamboa*	14/3/09–22/3/09	66 ± 5	259 ± 38
Liguro-Provençal Basin (M)	10	FAMOSO2	*Sarmiento de Gamboa*	30/4/09–13/05/09	94 ± 4	273 ± 2
Liguro-Provençal Basin (M)	3	FAMOSO3	*Sarmiento de Gamboa*	16/09/09–20/09/09	133 ± 3	323 ± 24
Ría de A Coruña (G)	2	HERCULES II	*Lura*	28/09/11–29/09/11	11 ± 8	77 ± 11
Ría de A Coruña (G)	5	HERCULES III	*Lura*	16/07/12–20/07/12	8 ± 4	67 ± 24
Ría de Vigo (G)	10	DISTRAL & REIMAGE	*Mytilus*	14/02/12–24/1/2013	110 ± 76	38 ± 2
Ría de Vigo (G)	1	STRAMIX	*Mytilus*	5-6/8/2013	1614	38 ± 2
Ría de Vigo (G)	2	CHAOS	*Mytilus*	20/08/13–27/08/13	1515 ± 6	41 ± 1
Ría de A Coruña (G)	13	NICANOR	*Lura*	27/02/14–17/12/15	30 ± 5	62 ± 3
Rías de Vigo & Pontevedra (G)	4	ASIMUTH	*Ramón Margalef*	17/06/13–21/06/13	16 ± 7	54 ± 17
South Shetland Islands (A)	10	COUPLING	*Hespérides*	8/1/10 – 21/1/10	57 ± 5	442 ± 41
Bay of Biscay (O)	27	PERFILC	*García del Cid*	18/7/08-24/7/08	35 ± 13	226 ± 39

During all cruises except COUPLING hydrographic properties and turbulent mixing were derived from a MSS microstructure profiler (Prandke and Stips 1998b). The MSS is equipped with a high-precision Conductivity-Temperature-Depth (CTD) probe, two microstructure shear sensors (type PNS06), and also a sensor to measure the horizontal acceleration of the profiler. The fluorometer included in the MSS profiler was calibrated with fluorometrically determined chlorophyll a concentrations ranging from 0.03 to 8.60 mg m^{-3} (Chl a = 2.255 × fluorescence – 0.527; R^2 = 0.859, number of samples (ns) = 134), obtained during 12 cruises (see below). Measurements of dissipation rates of turbulent kinetic energy (ε) were conducted to the bottom, or to 243 ± 23 m over deep waters (Table 4.1). The MSS profiler was balanced to have negative buoyancy and a sinking velocity of ~ 0.4 to 0.7 m s^{-1}. The frequency of data sampling was 1024 Hz. The sensitivity of the shear sensors was checked after each use. Data processing and calculation of dissipation rates of ε was carried out using the commercial software MSSpro, as described in detail in Fernández-Castro et al. (2014). During COUPLING turbulent mixing was derived from a TurboMAP microstructure profiler (Wolk et al 2002). Data processing and calculation of dissipation rates of turbulent kinetic energy (ε) were carried out with the commercial software of the TurboMAP, as described in Sangrà et al. (2014).

Microstructure turbulence profiles used for computing nitrate fluxes at each station were always deployed successively. Sets include 2–11 in the tropical and subtropical regions, 6–94 in the Mediterranean, 2-402 in the Galician coastal upwelling and 2-3 in the Antarctic Peninsula. Due to significant turbulence generation close to the ship, only the data below 5 (HERCULES2, HERCULES3, DISTRAL, REIMAGE, STRAMIX, ASIMUTH, CHAOS, and NICANOR) and 10 m (CARPOS, TRYNITROP, COUPLING, MALASPINA, PERFILC, PERFILM, FAMOSO1, FAMOSO2, FAMOSO3) were considered reliable. Data were depth averaged within 1 m bins.

The squared Brunt Väisälä frequency (N^2) was computed from the CTD profiles according to the equation:

$$N^2 = -\left(\frac{g}{\rho_w}\right)\left(\frac{\partial \rho}{\partial z}\right)(s^{-2})$$

where g is the acceleration due to gravity (9.8 m s^{-2}), ρ_w is seawater density (1025 kg m^{-3}), and $\partial\rho/\partial z$ is the vertical potential density gradient. Vertical diffusivity (K_z) was estimated as:

$$K_z = \Gamma \frac{\varepsilon}{N^2}\ (m^2 s^{-1})$$

where Γ is the mixing efficiency, here considered as 0.2 (Osborn 1980) for all cruises except MALASPINA and TRYNITROP. During both cruises vertical diffusivity including mechanical turbulence and the effect of salt-fingers mixing was calculated according to St. Laurent and Schmitt (1999) (see details in Fernández-Castro et al., 2015).

Nitrate supply

Samples for the determination of nitrate (NO_3) + nitrite (NO_2) were collected from 5 ± 2 (Galician coastal upwelling), 7 ± 1 (Mediterranean), 11 ± 2 (Antarctic Peninsula) and 11 ± 2 (tropical and subtropical regions) different depths in rinsed polyethylene tubes and stored frozen at -20 °C until analysis, according to standard methods using the automated colorimetric technique (Hansen and Koroleff 1999). Analyses were performed on land except during the MALASPINA expedition where the samples were analyzed on board.

When nitrate concentrations were not available, during STRAMIX and one sampling during the NICANOR cruises, concentration values were obtained by using a nitrate–density (σ_t) relationship built by using all samples collected during CHAOS (ns=624) and NICANOR (ns = 52), respectively. In CHAOS the nitrate-density relationship ($NO_3 = 11.93 \times \sigma_t - 310.60$; Adj-$R^2 = 0.92$; p-valor < 0.001) was valid for the density range between 25.9 and 27.2 kg m^{-3}. During NICANOR the relationship showed a linear behavior ($NO_3 = 9.78 \times \sigma t - 256.38$; Adj-$R^2 = 0.87$; p-valor < 0.001) for density ranging between 26.1 and 27.1 kg m^{-3} (Chapter II). Nitrate concentration profiles for PERFILM and PERFILC cruises were obtained from the World Ocean Atlas 2009 (WOA09, http://www.nodc.noaa.gov/) as the closest available bin to the averaged geographical location of each cruise (40.770ºN-2.675ºE and 43.865ºN-2.173ºW, respectively), and considering the average values for the month when each cruise was conducted.

Vertical diffusive fluxes of nitrate into the euphotic zone were calculated following the Fick's law as:

$$FluxNO_3 = \overline{K_z}\, \Delta NO_3$$

where ΔNO_3 is the nitrate vertical gradient obtained by linear fitting of nitrate concentrations in the nitracline, determined as a region of approximately maximum and constant gradient, and $\overline{K_z}$ is the averaged turbulent mixing in the same depth interval. In the Galician coastal

upwelling, nitrate diffusive fluxes were estimated between 10 and 40 m depth using the same procedure.

Most stations carried out in the Galician coastal upwelling were conducted inside three different Rías (Ría de Vigo, Ría de Pontevedra and Ría de A Coruña). The Rías are coastal embayments affected by seasonal wind-driven coastal upwelling of the cold, nutrient-rich North Atlantic Central water (Álvarez-Salgado et al. 2000). The total nitrate supply in the Galician Rías was computed as the sum of nitrate vertical diffusion plus nitrate vertical advection due to coastal upwelling. A simplified estimate of nitrate supply through vertical advection due to upwelling was computed considering the Galician Rías as single boxes divided into two layers, the deeper one influenced by upwelled inflowing waters and the surface layer dominated by the outgoing flow. Assuming that the bottom layer volume is conservative and stationary, the vertical advective flux (Q_Z, $m^3\ s^{-1}$), would be equivalent to the incoming bottom flux (Q_B, $m^3\ s^{-1}$), computed as the product of the upwelling index (I_W, $m^3\ s^{-1}\ km^{-1}$) and the lengths of the mouth of the Rías (ca. 10-11.5 km). I_W was averaged over the three-day period before each cruise from wind data recorded by meteorological buoys located in Cabo Vilano (HERCULES, NICANOR) and Cabo Silleiro (DISTRAL-REIMAGE, ASIMUTH, CHAOS, STRAMIX, REIMAGE), or modeled by the Fleet Numerical Meteorology and Oceanography Center (FNMOC) model when buoy data were not available (http://www.indicedeafloramiento.ieo.es). Finally, the transport of nitrate into the euphotic zone through vertical advection was computed as:

$$NO_3^- \ advective\ flux\ = \frac{Q_Z}{A_{basin}} [NO_3^-]_D$$

where A_{basin} is the surface area of the Galician Rías, Q_Z is the vertical advective flux, and $[NO_3]_D$ is the averaged nitrate concentration at the base of the euphotic layer. A_{basin} is 141 km^2 for Ría de Pontevedra (ASIMUTH), 174 km^2 for Ría de Vigo (CHAOS, ASIMUTH, DISTRAL-REIMAGE, STRAMIX), and 145 km^2 for Ría de A Coruña (HERCULES, NICANOR).

Total nitrate supply included diffusive and advective vertical processes in the Galician costal upwelling, and only the nitrate turbulent supply in the other regions.

Chlorophyll-a and primary production

Samples for the determination of chlorophyll-a were collected at four to eight depths during CARPOS (ns=8), TRYNITROP (ns=18), MALASPINA (ns=47), FAMOSO (ns=18),

NICANOR (ns=13), HERCULES III (ns=1), DISTRAL (ns=9), CHAOS (ns=2), and COUPLING (ns=9) cruises. 50-250 mL of seawater were filtered through 0.2 μm pore-size polycarbonate or Whatman GF/F (FAMOSO) filters which were later frozen at -20ºC until analysis. The fluorescence emitted by the chlorophyll-a was measured from pigments extracted in 90% acetone overnight. The fluorescence due to chlorophyll-a was measured using a Turner TD-700 fluorometer previously calibrated with pure chlorophyll-a. For those cruises where samples for the determination of chlorophyll-a were not collected, chlorophyll-a was derived from the calibrated fluorescence sensor included in the MSS profiler.

Samples for the determination of net primary production were collected at selected stations and several depths during TRYNITROP (ns=18), MALAPINA (ns=37), FAMOSO (ns=19), NICANOR (ns=13), HERCULES III (ns=1), DISTRAL (ns=8) and COUPLING (ns=3) cruises. During TRYNITROP, MALAPINA, NICANOR, HERCULES III, and DISTRAL water samples from two to seven depths were collected for the determination of primary production with the ^{14}C- uptake technique during on-deck incubations. For each depth, 75-mL (250-ml MALAPINA, NICANOR & HERCULES III) polystyrene bottles (3 light and 1 dark bottles, or 2 light and 1 dark bottles for FAMOSO, NICANOR & HERCULES III) were filled with seawater just before dawn and spiked with 2-15 μCi (50-100 μCi MALASPINA) of $NaH^{14}CO_3$. Samples were incubated during 2 h (DISTRAL), 24 h (MALASPINA, FAMOSO, NICANOR & HERCULES III) or from dawn to dusk (TRYNITROP) in flow-through incubators provided with neutral density and blue (Lee Mist Blue) filters that simulated the PAR levels experienced by the phytoplankton in their natural location within the water column. The incubators were cooled with running seawater pumped from the surface or with water circulating through a refrigerator. At the end of the incubations, samples were filtered through 0.2 μm polycarbonate filters under low-vacuum pressure (<100 mm Hg). Inorganic carbon on the filters was removed by exposing them to concentrated HCl fumes overnight. After removal of inorganic ^{14}C, filters were placed into scintillation vials to which 4 mL of scintillation cocktail were added. The radioactivity on each sample was determined on scintillation counters which used an internal standard for quenching correction. Detailed methods for the experiments conducted during these cruises is included in Mouriño-Carballido et al. (2011), Marañón et al. (2016), Estrada et al. (2014), (Moreira-Coello et al. 2017), and Cermeño et al. (2016).

During COUPLING primary production was measured using the ^{13}C method (Hama et al. 1983) at two sampling depths (surface and at the depth of the deep chlorophyll maximum).

Water samples were transferred to 2 L polycarbonate bottles, and after addition of $NaH^{13}CO_3$ at about 10% of total inorganic carbon in the ambient water, the samples were incubated for about 12 h in a tank on deck. Initial and final particulate organic carbon, and particulate material used for isotope analysis were filtered through GF/F filters. They were frozen and stored at -20ºC until analysis on land. Detailed methods are included in Teira et al. *(*2012).

For those experiments where incubations lasted less than 24 h, net primary production was computed assuming the ratio of phytoplankton respiration to gross photosynthesis (about 20%; Geider, 1992), and the number of light hours for each sampling date. Depth-integrated values were computed by trapezoidal integration considering the rates measured at the different depths.

Model regression variables and statistical analysis

At each station a set of physical, chemical and biological variables regularly obtained during oceanographic cruises was selected as potential predictors of the nitrate supply by turbulent diffusion: sea surface temperature (SST), sea surface salinity (SSS), vertical stratification in the pycnocline (defined as the maximum value of the square Brünt Väissälä frequency, $maxN^2$), depth of the pycnocline (depth of the maximum value of the square Brünt Väissälä frequency, $dmaxN^2$), average stratification in the nitracline (average squared Brunt Väissälä frequency in this layer, $avrN^2$), depth of the mixed layer (MLD, calculated using a density difference criterion of 0.1 Kg/m^3 for open ocean and 0.125 Kg/m^3 for coastal regions, with respect to the surface value), depth of the nitracline (depth were nitrate concentration was equal to 1 mmol $m^{-3,}$ nitraD), nitrate gradient across the nitracline ($grNO_3$), surface nitrate concentration (sNO_3), depth (DCM) and value (maxCHL) of the maximum chlorophyll-a, and surface chlorophyll-a (sCHL). The cluster analysis of the correlation matrix between the predictors showed that variables could be clustered into three groups (Figure 4.2). Among these clusters we selected three variables (SST, grNO3, and sCHL) to build more simple models (even models). The three selected predictors were chosen for being measured during oceanographic cruises on a regular basis, and also derived from satellite observations or available on databases.

A Multivariable Fractional Polynomial (MFP) method was used to select the predictors of nitrate turbulent diffusion in the four contrasting environments (tropical and subtropical At-

lantic Ocean, Northwestern Mediterranean Sea, Galician coastal upwelling ecosystem and Antarctic Peninsula), and for the complete dataset. Regression analyses commonly assume that relationships are linear between the predictors and the response variable, or assume a log-transform without assessing these assumptions. When addressed, nonlinear relationships are often based on generalized additive models or use standard polynomials. However, these models neither can be expressed as an explicit equation nor handle general nonlinearity, respectively. The MFP method solves these problems and determines whether a predictor is important for the model, and its functional form. The algorithm use fractional polynomials based on Box-Cox transformation (Box and Cox 1964) of predictors. It uses the eight powers −2, −1, −0.5, 0, 0.5, 1, 2 and 3 (with the 0 case corresponding to the natural log transform). A back-forward procedure is applied to include/exclude the terms of the model following the next steps: (I) backward elimination of predictors that are statistically insignificant, and (II) iterative examination of the scale of all continuous predictors. Therefore, we need two significance levels: α_1, for the exclusion and inclusion of a predictor, and α_2 for the determination of significance of fractional transformation of continuous predictors. Successive cycles improve the accuracy of the model until two cycles converge. Goodness of fit was assessed via quantile-quantile plots (Figure 4.3). All calculations were done using mfp package (Zhang 2016) in R (R Core Team 2015).

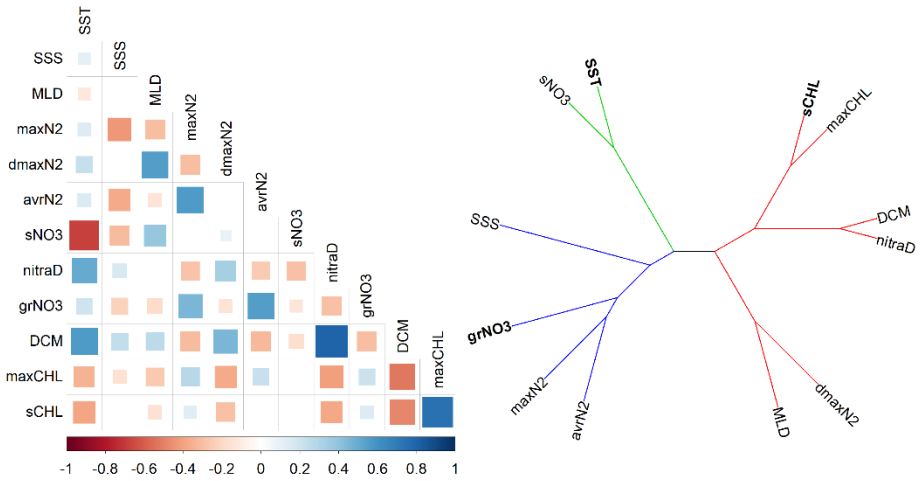

Figure 4.2 *Left: Correlogram of predictive variables and nitrate diffusive flux (dNO3f). Statistically significant correlations (statistical confidence level of 95%) are shown. The test was based on Pearson's product moment correlation, and alternative hypothesis include both sides. A Bonferroni correction was applied to p-values to control Type-I error. The color indicates the sign and the size indicate the magnitude of the correlation. Right: Dendrogram created using the correlations between predictive variables and nitrate diffusive flux. Dissimilarity was established as 1- |correlation|. Bold letters indicate the predictors selected to be used in the simplified (even) models.*

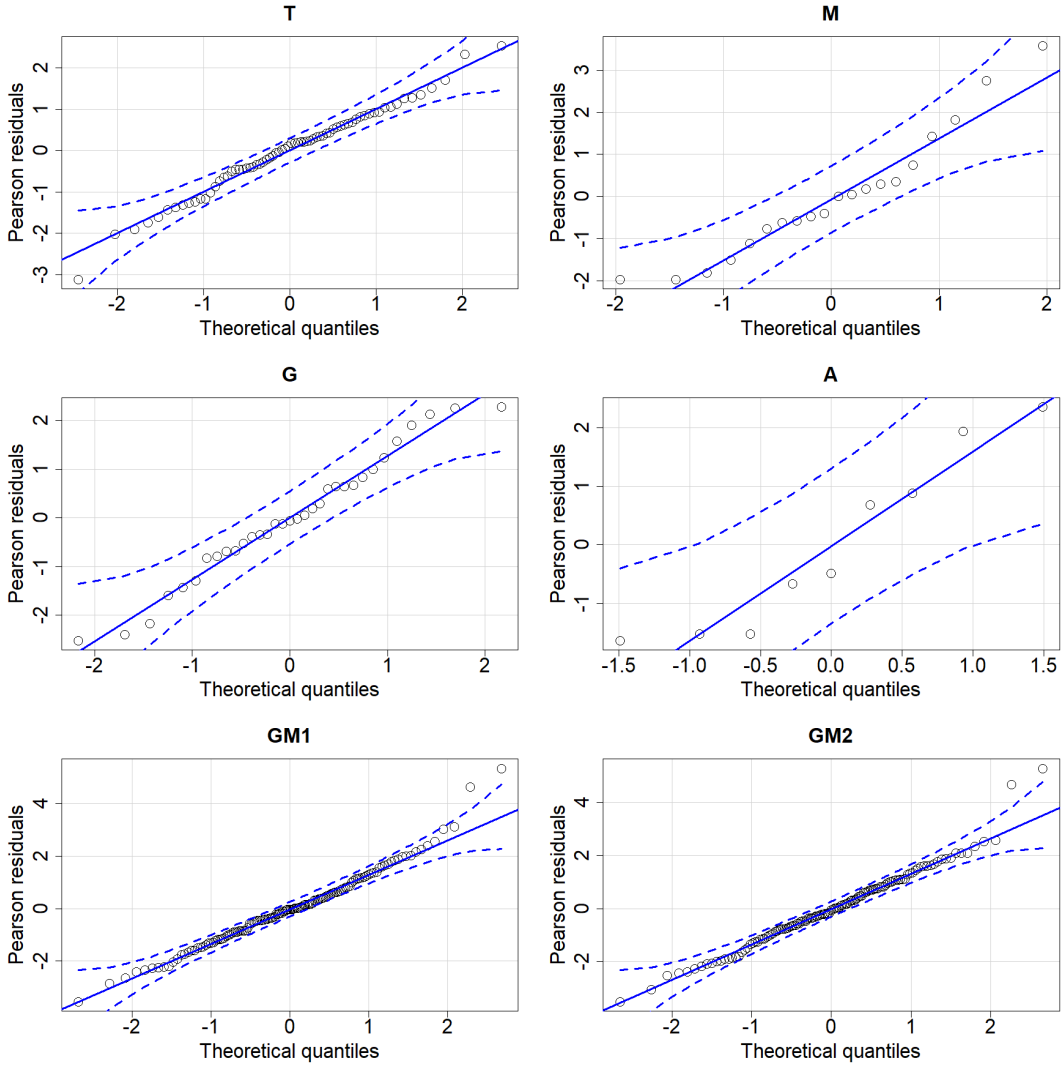

Figure 4.3 *Quantile-Quantile (QQ) plots obtained by the MFP method in each domain: tropical and subtropical regions (T), Mediterranean Sea (M), Galician coastal upwelling (G), Antarctic Peninsula (A); using the complete dataset (GM1); and using the complete dataset except those stations collected in the Antarctic Peninsula (GM2). The y-axes represent the Pearson residuals and the x-axes the theoretical quantiles. Solid blue lines indicate the theoretical quantile of the models and blue dashed lines the 95% confidence intervals.*

Global spatial distribution of nitrate turbulent diffusion

The large-scale spatial distribution of nitrate turbulent diffusion was computed by using the MFP model obtained by using the complete dataset (GM1), and including as predictors sea surface temperate and the vertical nitrate gradient across the nitracline derived from the World Ocean Atlas 2013 (WOA13, http://www.nodc.noaa.gov/), and surface chlorophyll-a provided by the European Space Agency (ESA, hermes.acri.fr). At each bin from WOA13 the vertical

nitrate gradient was calculated as the maximal vertical gradient between 0 and 250 meters. Regions where predictors data were outside the range covered by the dataset used to build the model were removed. Averaged nitrate fluxes for most of the biogeographical provinces defined by Longhurst (2007) were calculated using the even model built with the complete dataset (GM1). Averaged nitrate diffusive flux between 40ºN and 40ºS was calculated using the even model including the complete dataset except those stations collected in the Antarctic Peninsula (GM2), and only considering those regions where sCHL and nitrate diffusive fluxes were lower than 0.5 mg m^{-3} and 1 mmol m^{-2} d^{-1}, respectively.

Contribution of nitrate turbulent diffusion to total gross primary production

The contribution of nitrate turbulent diffusion to total gross primary production for most of the biogeographical provinces and the region between 40ºN and 40ºS was calculated by comparing the magnitude of both processes. Averaged total gross primary production for the biogeographical provinces and the region between 40ºN and 40ºS was derived from satellite monthly averaged net primary production (period 1998-2012) by using the model proposed by Uitz et al. (2008), which was depth-integrated down to the base of the photic layer, computed from the algorithm proposed by Morel et al. 2007). In order to convert net production to total production in nitrogen units we assumed mean values for the percentage of dissolved organic carbon production with respect to total integrated primary production (~23%; Teira et al., 2001), the ratio of phytoplankton respiration to gross photosynthesis (~ 20%; Geider, 1992), and the averaged stoichiometry relationship for carbon and nitrogen proposed by Galbraith and Martiny (2015).

Present and future distributions of the cyanobacteria to picoeukaryotes depth-integrated biomass ratio

In order to calculate the decrease in the vertical supply of nitrate by vertical diffusion into the euphotic zone in the next century we used the relative change in nitrogen flux for the periods 2000-1800 and 2100-1800 computed by Lewandowska et al. (2014). These authors used a global ocean model simulation under the A1F1 emission scenario of the Intergovernmental Panel on Climate Change (Nakicenovic and Swart 2000). This scenario assumes continuing exponential increase in global carbon emissions until the year 2100, and approximates current trends in emission growth. In order to extract the relative change in nitrogen flux from Figure 4.1 in Lewandowska et al. (2014) we used a 3-nearest neighbours (3-nn) algorithm (Ripley

1996).

Using a first order derivative filter in the x-direction of the colour bar we detected the edges, and we sampled 100 random points of each "brick" extracting the values in the three colour channels (RGB). The response variable was the value of relative change in nitrogen flux of the colour bar (calibration) and in the maps (prediction). To classify a new sample, 3-nn identifies that sample's K-Nearest Neighbours in the predictor space. Based on the Euclidean distance between samples, the predicted response was assigned by the 3 closest samples. Using this method in each pixel, the images information was extracted. We obtained the relative change in nitrogen flux between 2000 and 2100 subtracting the relative change of the periods 2000-1800 and 2100-1800 (Figure 4.4).

Finally, we calculated the average relative global change (~20%) and we applied it uniformly to the estimation of present nitrate turbulent diffusion. Finally, both estimates (present and future) of nitrate diffusive supply were used as inputs variables in the Generalized additive model proposed in Chapter 2, to compute the present and future distributions of the cyanobacteria to picoeukaryotes depth-integrated biomass ratio. All calculations were done using MASS package (Venables and Ripley 2002) in R (R Core Team 2015).

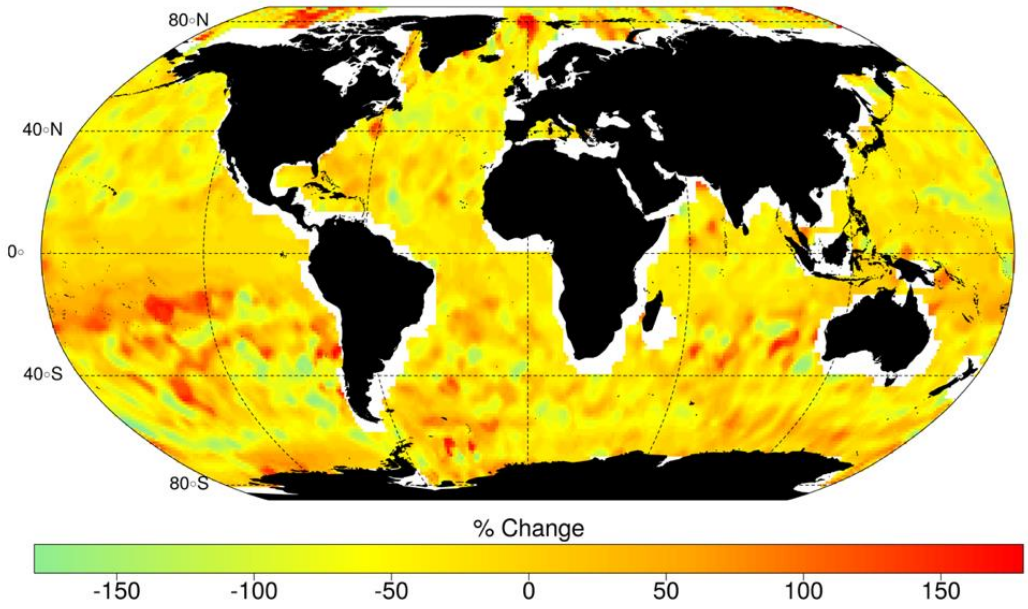

Figure 4.4 *Relative change in vertical nitrogen flux between 2000 and 2100 derived from Lewandowska et al. (2014).*

Results and discussion

Multivariable fractional polynomial models

The database covered a wide environmental gradient from oligotrophic to eutrophic conditions (Figure 4.5 & Table 4.2). The 71 stations sampled in the tropical and subtropical Atlantic, Pacific and Indian oceans during three different cruises were, on average, characterized by warm surface temperature (26 ± 3 ºC, mean ± SD), weak vertical diffusivity (0.04 ± 0.05 $x10^{-3}$ m^{-2} s^{-1}) and low nitrate diffusive supply (0.4 ± 1 mmol N m^{-2} d^{-1}). Accordingly, surface chlorophyll-a and photic layer depth-integrated net primary production were low (0.2 ± 0.1 mg m^{-3} and 202 ± 98 mgC m^{-2} d^{-1}, respectively). The Mediterranean Sea, sampled from March to September, was characterized by cooler surface waters (16 ± 4 ºC), and intermediate diffusivity (2 ± 6 $x10^{-3}$ m^{-2} s^{-1}) and nitrate diffusive supply (39 ± 110 mmolN m^{-2} d^{-1}). Surface chlorophyll-a and net primary production were also intermediate (0.9 ± 0.9 mg m^{-3} and 581 ± 454 mg C m^{-2} d^{-1}, respectively). The stations sampled in the Galician coastal upwelling system, which included year-round samples, were also characterized on average by relatively cold surface water (16 ± 2 ºC), and intermediate diffusivity (0.4 ± 0.5 $x10^{-3}$ m^{-2} s^{-1}) and nitrate diffusive supply (5.3 ± 7.1 mmol N m^{-2} d^{-1}). However, due to the influence of the coastal upwelling the total nitrate supply (including both diffusive and advective processes) was significantly higher (31 ± 42 mmol N m^{-2} d^{-1}). As the result of the input of new nitrogen by both processes this system was characterized by high values of surface chlorophyll a and net primary production (2.5 ± 2.9 mg m^{-3} and 2950 ± 2330 mg m^{-2} d^{-1}, respectively). Finally, the stations sampled in the Antartic Peninsula were characterized by cold surface water (0.1 ± 1 ºC), high diffusivity (66 ± 126 $x10^{-3}$ m^{-2} s^{-1}) and high nitrate diffusive supply (102 ± 165 mmol N m^{-2} d^{-1}). However, due to the limitation of control factors other than nitrate (Teira et al., 2012), these regions exhibited intermediate values of surface chlorophyll-a and relatively low net primary production (1.1 ± 0.8 mg m^{-3} and 153 ± 136 mg m^{-2} d^{-1}, respectively).

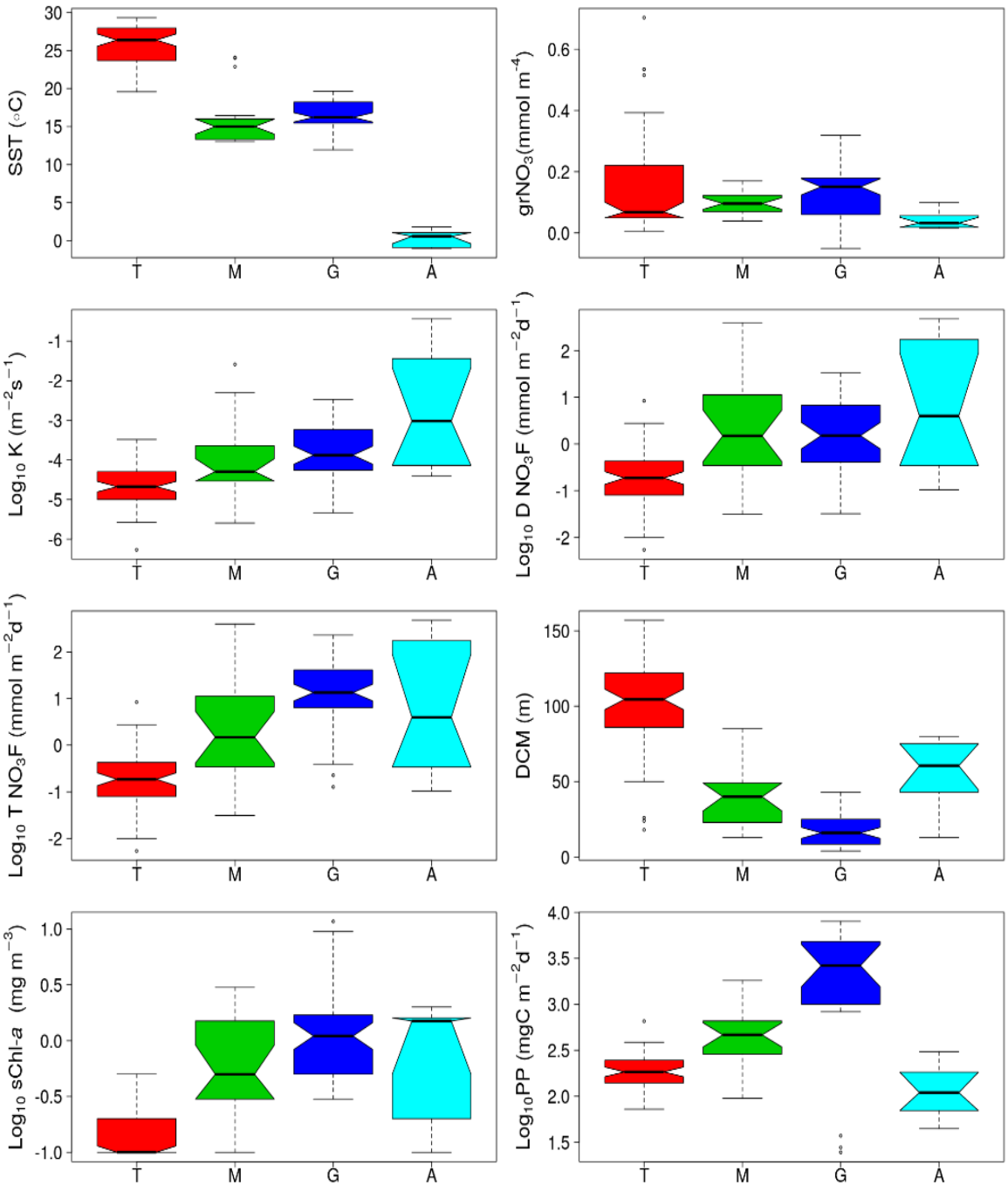

Figure 4.5 *Box-and-whisker plots of sea surface temperature (SST), vertical nitrate gradient ($grNO_3$), vertical diffusivity (Kz), nitrate diffusive flux (DNO_3F), total nitrate supply (including vertical diffusion plus advection, TNO_3F), depth of the deep chlorophyll maximum (DCM), surface chlorophyll-a (sChl-a), and photic layer depth-integrated net primary production (PP) computed for the tropical and sub-tropical regions (T), the Mediterranean (M), the Galician coastal upwelling (G) and the Antartic (A). On each box, the central mark indicates the median, the notches the 95% confidence interval for the median, and the bottom and top edges of the box indicate the 25th and 75th percentiles, respectively. The whiskers extend to the most extreme data points not considered outliers, and the outliers are plotted individually using white circles.*

Table 4.2 *Mean ± standard deviation of sea surface temperature (SST), sea surface salinity (SSS), vertical stratification in the pycnocline ($maxN^2$), depth of the pycnocline ($dmaxN^2$), average stratification in the nitracline ($avrN^2$), depth of the mixed layer (MLD), vertical turbulent diffusivity (K), depth of the nitracline (nitraD), nitrate gradient across the nitracline ($grNO_3$), surface nitrate concentration (sNO_3), diffusive nitrate supply (dNO_3), total nitrate supply (including diffusive and advective fluxes, TNO_3), depth (DCM) and value (maxCHL) of the maximum chlorophyll-a, surface chlorophyll-a (sCHL), and photic layer depth-integrated net primary production (PP), computed for the tropical and subtropical regions (T), the Mediterranean Sea (M), the Galician coastal upwelling (G), and the Antarctic Peninsula (A). A nonparametric one-way ANOVA (Kruskal–Wallis, KW) was performed to test the null hypothesis that independent groups come from the same distribution. The Bonferroni multiple comparison test was applied a posteriori to analyze the differences between every pair of groups.*

Variables (units)	T	M	G	A	K-W p_{value}	Post hoc Bonferroni
SST (ºC)	26 ± 3	16 ± 4	16 ± 2	0.1 ± 1.0	<0.001	T>M,G,A; G>A
SSS (PSU)	36 ± 1	38 ± 0.1	35 ± 0.4	34 ± 0.9	<0.001	M>T,G>A
$maxN^2$ $x10^{-4}$ (s^{-2})	7 ± 7	3 ± 5	11 ± 12	4 ± 10	<0.001	G>T>M,A
$dmaxN^2$ (m)	74 ± 43	35 ± 17	16 ± 14	94 ± 92	<0.001	T>M>G; A>G
$avrN^2$ $x10^{-4}$ (s^{-2})	2.1 ± 3	0.7 ± 0.5	1.9 ± 1.4	0.3 ± 0.6	<0.001	G>T,M,A; T>A
MLD (m)	53 ± 23	32 ± 29	15 ± 13	174 ± 198	<0.001	T,A>M,G
K $x10^{-3}$ (m^{-2} s^{-1})	0.04 ± 0.05	2 ± 6	0.4 ± 0.5	66 ± 126	<0.001	M,G,A>T
nitraD (m)	109 ± 59	9 ± 12	9 ± 16	5 ± 0	<0.001	T>M,G,A
$grNO_3$ (µmol m^{-4})	142 ± 149	92 ± 37	124 ± 86	42 ± 29	<0.05	T,G>A
sNO_3 (mM)	0.5 ± 1.2	2.3 ± 1.7	1.7 ± 1.7	31 ± 4	<0.001	M,G,A>T; A>G
dNO_3 (mmolN m^{-2} d^{-1})	0.4 ± 1.0	39 ± 110	5.3 ± 7.1	102 ± 165	<0.001	M,G,A>T
TNO_3 (mmolN m^{-2} d^{-1})	0.4 ± 1.0	39 ± 110	31 ± 42	102 ± 165	<0.001	M,G,A>T
DCM (m)	100 ± 32	41 ± 20	16 ± 11	54 ± 24	<0.001	T>M>G; A>G
maxCHL (mg m^{-3})	0.5 ± 0.2	1.1 ± 0.9	4.3 ± 3.7	1.3 ± 0.8	<0.001	G>T,M,A
sCHL-*a* (mg m^{-3})	0.2 ± 0.1	0.9 ± 0.9	2.5 ± 2.9	1.1 ± 0.8	<0.001	M,G,A>T
PP (mgC m^{-2} d^{-1})	202 ± 98	581 ± 454	2950 ± 2330	153 ± 136	<0.001	G>T,A; M>T

Proxy for nitrate diffusive flux

Multivariable fractional polynomial models were developed for each of the four investigated oceanographic domains, for the complete dataset (GM1), and for the complete dataset except those stations located in the Antarctic Peninsula (GM2) (Table 4.3). This last model was tried as our dataset includes only a few stations representing polar regions and surface temperature conditions below 15ºC (Figure 4.6). In a first exploratory step we allowed the models to introduce any of the twelve variables initially selected as potential predictors of nitrate diffusion

(odd models): sea surface temperature (SST), sea surface salinity (SSS), vertical stratification in the pycnocline ($maxN^2$), depth of the pycnocline ($dmaxN^2$), average stratification in the nitracline ($avrN^2$), depth of the mixed layer (MLD), depth of the nitracline (nitraD), nitrate gradient across the nitracline ($grNO_3$), surface nitrate concentration (sNO_3), depth (DCM) and value (maxCHL) of the maximum chlorophyll-a, and surface chlorophyll-a (sCHL). In tropical and subtropical regions a model including four predictors ($grNO_3$, SSS, $avrN^2$ and sNO_3) explained 70% of the variance in nitrate diffusive fluxes, whereas in the Mediterranean and the Galician coastal upwelling two predictors (SST and sCHL, and $grNO_3$ and MLD; respectively) explained more than 55% of the variance. In the Antarctic Peninsula a model including only SST explained 75% of the variance. Finally, five predictors were selected for the model using the complete dataset ($grNO_3$, SST, sCHL, $avrN^2$, $maxN^2$; Adj-R^2=0.61), and the one excluding the stations collected in the Antarctic Peninsula ($grNO_3$, $avrN^2$, DCM, sCHL, $maxN^2$; Adj-R^2=0.60).

Table 4.3 *Regression equations obtained by the MFP method in each domain (D): tropical and subtropical regions (T), Mediterranean Sea (M), Galician Coastal Upwelling (G), Antartic Peninsula (A), using the complete dataset (GM1) and all the stations except those in the Antartic Peninsula (GM2). Odd models used all the predictors and even models only used sea surface temperature (SST), surface chlorophyll-a (sCHL) or vertical nitrate gradient (grNO3). Models (M) are identified by numbers from 1 to 12. Asterisks denote the existence of significant relationship with predictors (^ p<0.1, * p<0.05, ** p<0.01, *** p<0.001).*

D	Adj-R^2	Variable	Functional Form	Coef	Std Error	p_{value}
T	0.70	Intercept		-20.620	3.067	***
		$grNO_3$	$log(grNO_3/100)$	0.818	0.089	***
		SSS	SSS/100	47.130	8.389	***
		$avrN^2$	$(avrN^2/10^{-4})^3$	0.009	0.003	***
			$(avrN^2/10^{-4})^3 * log(avrN^2/10^{-4})$	-0.003	0.001	***
		sNO_3	$(sNO_3 + 0.1)^{-0.5}$	0.876	0.141	***
			$(sNO_3 + 0.1)^2$	0.049	0.010	***
	0.36	Intercept		1.307	1.285	
		$grNO_3$	$log(grNO_3/100)$	0.794	0.126	***
		SST	SST/10	-1.154	0.495	*
M	0.63	Intercept		5.210	2.300	*
		SST	SST/10	-3.420	1.188	*
		sCHL	sCHL	1.090	0.538	^
G	0.56	Intercept		-2.772	0.624	***
		$grNO_3$	$grNO_3/100$	1.940	0.305	***
		MLD	MLD/10	0.433	0.181	*
	0.49	Intercept		-1.702	0.468	***
		$grNO_3$	$grNO_3/100$	1.641	0.299	***
A	0.75	Intercept		5.410	0.842	***
		SST	SST + 1.1	-2.751	0.514	***

GM1	0.61	Intercept		-3.910	1.270	**
		grNO3	log($grNO_3$/100)	0.779	0.145	***
		SST	(SST + 1.1)/10	-0.478	0.251	^
		sCHL	log(sCHL + 0.1)	0.724	0.141	***
		$avrN^2$	$avrN^2/10^{-4}$	-0.238	0.065	***
		$maxN^2$	$\log(maxN^2/10^{-3})$	-1.820	0.326	***
			$(maxN^2/0.001)^{0.5}$	4.957	1.009	***
	0.57	Intercept		1.942	0.335	***
		SST	$((SST + 1.1)/10)^{-1}$	0.044	0.008	***
			$((SST + 1.1)/10)^3$	-0.075	0.018	***
		$grNO_3$	$(grNO_3/100)^{-0.5}$	-1.006	0.184	***
		sCHL	log(sCHL + 0.1)	0.705	0.147	***
GM2	0.60	Intercept		0.035	0.329	
		$grNO_3$	log($grNO_3$/100)	0.760	0.138	***
		$avrN^2$	$avrN^2/10^{-4}$	-0.178	0.053	**
		DCM	DCM/100	-1.668	0.315	***
		sCHL	sCHL + 0.1	0.231	0.070	**
		$maxN^2$	$(maxN^2/10^{-3})^{-1}$	0.115	0.019	***
	0.52	Intercept		4.444	0.521	***
		SST	SST/10	-2.377	0.239	***
		$grNO_3$	log($grNO_3$/100)	0.800	0.132	***

In a next step we simplified the models by limiting the number of potential predictors to exclusively three variables ($grNO_3$, SST, sCHL, even models) (see Methods). This was not necessary for the Mediterranean and the Antarctic, where the odd models already selected a combination of these predictors. For tropical and subtropical regions the algorithm retained two variables ($grNO_3$ and SST), which explained 36% of the variance, about half of the variance explained by model with all the potential predictors included. In the Galician coastal upwelling only $grNO_3$ was retained, but the decrease in explained variance was smaller (Adj-R^2=0.49). Both global models maintained their accuracy very close after the reduction in the number of predictors (Adj-R^2 reduced by <0.1). The model including the complete dataset retained the three variables, whereas the model excluding those stations collected in the Antarctic Peninsula only SST and $grNO_3$.

Several factors could explain the variability in the variance explained by the different even regional models. First, the dataset collected in the Antarctic and, specially, in the Mediterranean included contrasting hydrographic conditions and a wider range of nitrate diffusive fluxes than the other regions (Figure 4.5). Second, in the Galician upwelling nitrate turbulent diffusion represents, on average, a minor source of new nitrogen into the euphotic zone compared to the nitrate flux driven by vertical advection of deeper waters through upwelling

(Moreira-Coello et al. 2017). Moreover, it is remarkable the reduction in the explained variance in the tropical and subtropical regions when comparing odd and even models (from 70% down to 36%), whereas the reduction in the number of predictors had a limited effect in the other regions.

All models in which SST was included exhibited negative relationships between nitrate diffusive fluxes and this variable (Figure 4.6). These relationships were close to linear except for the global model including the complete dataset (GM1). The vertical nitrate gradient exhibited a positive linear correlation with nitrate diffusive flux in the model built for the Galician coastal upwelling. For tropical and subtropical regions and both global models the relationship was also positive but logarithmic. Finally, surface chlorophyll-a showed a linear or nearly linear positive relationship with nitrate diffusive fluxes in the Mediterranean and global models.

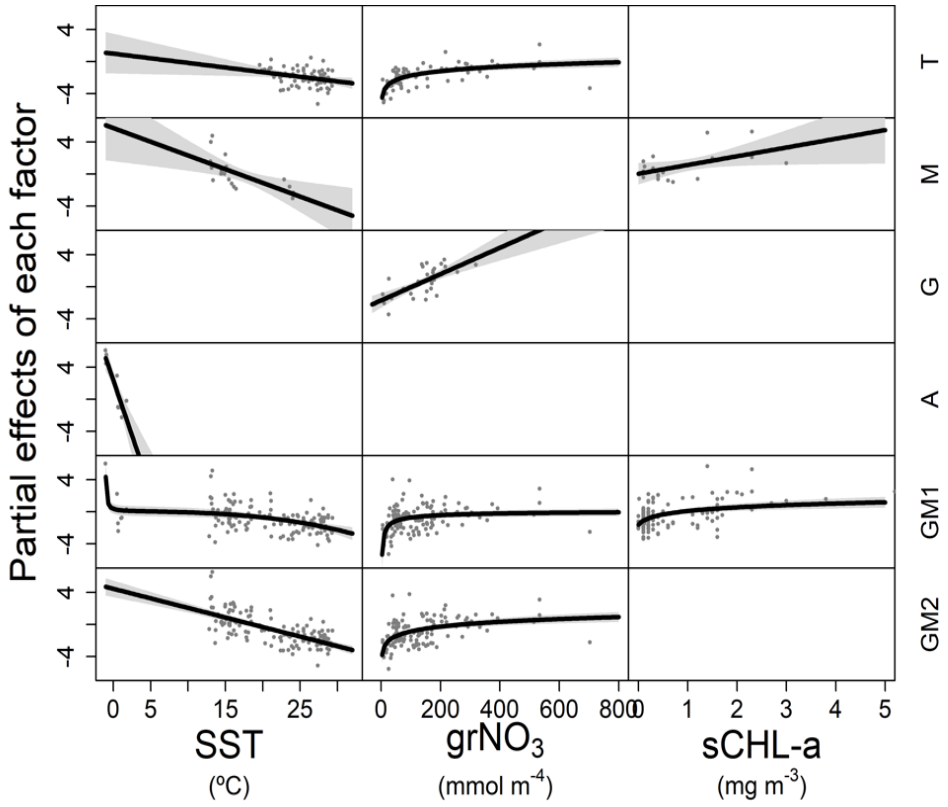

Figure 4.6 *Partial effects and residuals of the response variable (Nitrate diffusive flux) as a smooth function of sea surface temperature (SST), vertical nitrate gradient ($grNO_3$) and surface chlorophyll-a (sCHL-a) computed for tropical and subtropical regions (T), the Northwest Mediterranean (M), Galician coastal upwelling (G), Antartic Peninsula (A), using the complete dataset (GM1) and all the stations except those collected in the Antartic Peninsula (GM2). All terms were centered in zero. Significant relationships are indicated as solid (p-value<0.05) black lines. Intercepts and parameters are indicated in Table 4.3.*

Sea surface temperature is related to vertical stratification, as stratification usually increases with higher surface temperature. As expected a statistically significant positive correlation was found between the two variables in our dataset (Figure 4.2). In turn, assuming no changes in dissipation rates of turbulent kinetic energy, vertical mixing decrease when stratification increases (see methods). This could explain the negative relationship observed between surface temperature and nitrate diffusive flux for all models where this predictor was included. The relationship between the vertical nitrate gradient and nitrate diffusive flux was positive, as this term is directly involved in the calculation of diffusive fluxes (see methods). Finally, when included, the relationship between surface chlorophyll-a and nitrate diffusive fluxes was positive, as this predictor is an estimator of phytoplankton biomass, and therefore reflects the response of these organisms to nitrate availability.

Inferred global distribution of nitrate diffusion into the photic zone

By using the even model built with the complete dataset (GM1) applied to climatologies of SST, $grNO_3$ and sCHL, we computed a large-scale climatological distribution of the supply of nitrate into the photic zone by vertical turbulent diffusion (Figure 4.7). As expected, based on the regional differences observed in our estimates of nitrate diffusive fluxes derived from observations (Figure 4.5), regional patterns of this distribution revealed an increase in the magnitude of nitrate supply from open ocean tropical and subtropical regions to upwelling, coastal and temperate regions. In general, a good correspondence was found between our climatological estimates and the limited number of studies that so far have quantified the magnitude of nitrate diffusive fluxes derived from observations of microstructure, tracer release experiments and acoustic Doppler (Figure 4.7 & Figure 4.8). Averaged nitrate fluxes for the biogeographical provinces defined in the tropical and subtropical Atlantic ocean (Longhurst 2007), where most stations were collected, were 0.50 ± 0.24 mmolN m^{-2} d^{-1} for NASE (NE Atlantic Subtropical Gyral), 0.21 ± 0.14 mmolN m^{-2} d^{-1} for NASW (NW Atlantic Subtropical Gyral), 0.26 ± 0.24 mmolN m^{-2} d^{-1} for NATR (NorthAtlantic Tropical Gyral), 0.48 ± 0.24 mmolN m^{-2} d^{-1} for ETRA (Eastern tropical Atlantic), 0.29 ± 0.06 mmolN m^{-2} d^{-1} for WTRA (Western Tropical Atlantic), and 0.43 ± 0.34 mmolN m^{-2} d^{-1} for SATL (South Atlantic Gyral). A detailed list of averaged

nitrate fluxes for most biogeographical provinces defined by Longhurst (2007) is included in Table 4.5.

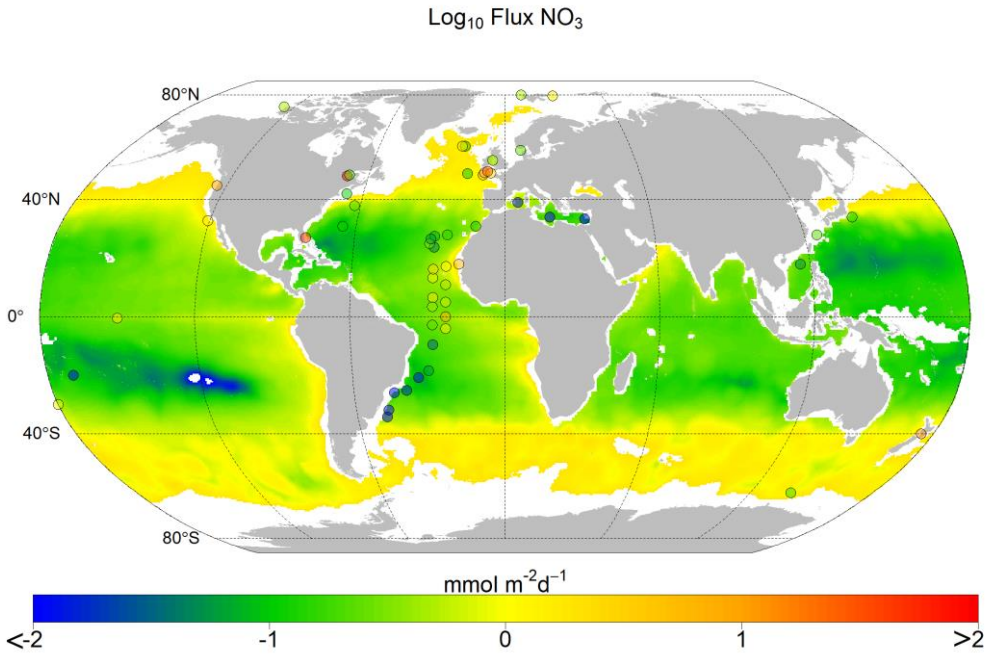

Figure 4.7 *Global climatology of the decimal logarithm of nitrate diffusive fluxes derived by using the GM1 model specified in Table 4.3. The colored dots represent nitrate diffusive fluxes previously reported in the literature and described in Table 4.4. Regions in white color represent data that was outside of the range covered by the dataset used to build the prediction model.*

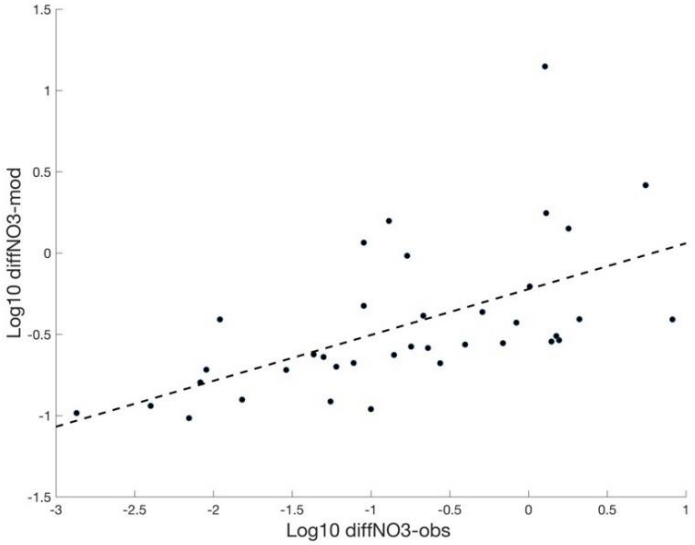

Figure 4.8 *Nitrate diffusive flux derived from observations (Log10 diffNO3-obs, see Table S3) versus nitrate diffusive flux derived from the global model GM1 (Log10 diffNO3-obs) for the same geographical locations. The dashed line represents the statistically significant relationship (y=0.28x-0.22; R^2 = 0.33; p-value < 0.001) calculated using all data except the lowest two values reported by* Planas et al. (1999) *in the North Atlantic (3.75-4.85 x 10^{-5} mmolN m^{-2} d^{-1}) by using indirect methods based on acoustic Doppler.*

Table 4.4 *Compilation of nitrate diffusive fluxes (diffNO3) previously reported in the literature in several domains (D): tropical and subtropical regions (T) (40º N – 40ºS), Mediterranean Sea (M), shelf seas and upwelling regions (Te), and Polar regions (P). The average (and the range, between brackets) of estimates reported at each study are indicated. When the average was not provided this value was calculated considering the published range. Publications reporting the dataset included in this analysis are not listed. When several frontiers for the calculation were used, the nitracline was choose. A molar mass of 62 gmol^{-1} was used for converting nitrate concentration from mg to mmol used in some of the references listed. * indicates estimates derived from acoustic Doppler and † from tracer release experiments.*

D	Reference	Region	diffNO_3 (mmolN m^{-2} d^{-1})
T	Lewis et al. [1986]	Subtropical Northeast Atlantic	0.14 (0.002-0.89)
	Planas et al. [1999]*	North, equatorial and south Atlantic	0.38 (0.00004-2.11)
	Dietze et al. [2004]*	Subtropical North Atlantic	0.28 (0.14–0.41)
	Painter et al, [2013]	Subtropical Northeast Atlantic	0.06 (0.04–0.09)
	Ledwell et al. [2008]†	Sargasso Sea	0.1
	Sandel et al. [2015]	Tropical Atlantic	2.4 (0.51-8.2)
	Carr et al. [1995]	Equatorial Pacific	1.5 (0.01–3)
	Kaneko et al. [2013]	Subtropical North Pacific	0.18 (0.02–0.35)
	Bouruet-Aubertot et al. [2018]	Subtropical South Pacific	0.007 (0.003–0.011)
	Ellwood et al. [2018]	Subtropical South Pacific	0.84 (0.02-1.65)
	Du et al. [2017]	South China Sea	0.05 (0.00004–0.1)
M	Bonnet et al. [2011]	Mediterranean Sea	0.002–0.013
Te	Horne et al. [1996]	Georges Bank	0.12 (0.05-0.18)
	Hales et al. [2009]	New England (Shelf Break)	0.22 (0.17-0.26)
	Cyr et al. [2015]	Lower St. Lawrence Estuary	0.12–300
	Zhang et al. [2017]	Florida Straits	42 (0.002–83.7)
	Forryan et al. [2012]	Iceland Basin	0.13 (0.08–0.22)
	Martin et al. [2010]	Porcupine Abyssal Plain	0.09 (0.05-0.16)
	Bendtsen & Richardson [2018]	North Sea (Shelf Edge)	0.25 (0.1–2)
	Law et al. [2001]†	North Atlantic	1.8
	Rippeth et al. [2009]	Irish Sea	1.5
	Williams et al. [2013a]	Irish Sea	0.31 (0.22-0.43)
	Sharples et al. [2007]	Celtic Sea (Shelf Edge)	5.1 (1.3–9)
	Williams et al. [2013b]	Celtic Sea	12 (1.3–22)
	Sharples et al. [2001b]	English Channel	2 (0.8-3.2)
	Tweddle et al. [2013]	Celtic Sea (Jones Bank)	26.4 (0.8–52)
	Schafstall et al. [2010]	Mauritanian Upwelling Region	5.5 (1-10.1)
	Arcos-Pulido et al. [2014]	Cape Ghir upwelling region	0.09
	Hales et al. [2005]	Oregon Shelf	8.6
	Li et al. [2012]	California current	1.3 (0–41.5)
	Sharples et al. [2001]	New Zealand Shelf	12
	Liu et al. [2013]	China Sea (Shelf Edge)	0.22 (0.02–1.54)
P	Sundfjord et al. [2007]	Barents Sea	1.3 (0.15-2.4)
	Law et al. [2003]†	Antarctic Circumpolar Current	0.17
	Bourgault et al. [2011]	Amundsen Gulf	0.5 (0.3-0.8)
	Randelhoff et al. [2016]	Artic Ocean	0.5 (0.3-0.5)

A meaningful comparison between our climatological estimates of nitrate diffusive fluxes with those derived from local observations, whose representativeness is limited in space and time, is very difficult to achieve. Turbulent mixing is highly intermittent in time and patchy in space due to its chaotic nature, and the multiple scales of variability of the forcing mechanisms. In the upper ocean energy dissipation and mixing are linked to the exchange of momentum and buoyancy with the atmosphere, which varies between seasons, day and night and also following the synoptic weather patterns (Moum et al. 2001). In the pycnocline mixing also depends on highly unpredictable processes, such as the generation of shear by internal waves (Nash et al. 2005; Rippeth et al. 2005). In coastal systems tidal forcing can be a predictable source of mixing (Simpson et al. 1990), but it can also produces complex dissipation patters as a result of the production of non-linear internal waves (Sharples et al. 2007; Villamaña-Rodríguez et al. 2015), and the interaction with wind-driven circulation (Fernández-Castro et al. 2018). Furthermore, the magnitude of nitrate fluxes is very sensitive to the different choices made for the calculation, in particular to the depth-interval. Different criteria used for the estimates reported in Figure 4.7 & Table 4.4, include the base of the euphotic zone, the base of the mixed layer, and also the nitracline. In fact the comparison of nitrate diffusive fluxes computed during the TRYNITROP cruise by using as a boundary the base of the euphotic zone (Mouriño-Carballido et al. 2011) or the nitracline (Fernández-Castro et al., 2015) demonstrates the large effect of the chosen criteria in the calculation.

A few studies have presented similar attempts to model nitrate availability in the surface waters by using different oceanographic predictors. In an early paper Kamykowski and Zentara [1986] investigated the capability to predict nutrient concentrations from temperature or density using a global dataset. With satellite SST observations, Switzer et al. [2003] generated an index of nitrate availability in the surface waters of the global ocean. Steinhoff et al. [2010] proposed a proxy for nitrate in the North Atlantic Ocean, using multiple linear regression and observed nitrate and SST, and model-based MLD. Arteaga et al. (Arteaga et al. 2015) developed a method for estimating global monthly mean surface nitrate by using local multiple linear regressions and including satellite SST and sCHL, and modelled MLD. Finally, Liang et al. [2018] used multivariate empirical orthogonal functions constructed from modeled nitrate, salinity, and potential temperature fields to build nitrate maps in the Southern Ocean. All these studies have

assumed implicitly that the nitrate concentration alone is sufficient to characterize the variability in the supply of this limiting resource for phytoplankton growth. Whereas in our case we computed the flux of nitrate being supplied to the euphotic zone by turbulent diffusion.

Table 4.5 *Mean ± standard deviation of nitrate diffusive fluxes (dNO_3, mmolN m^{-2} d^{-1}), gross primary production (GPP, mmolN m^{-2} d^{-1}), and contribution of nitrate diffusive fluxes to gross primary production (%) calculated for some of the biogeographical provinces defined in the Antartic, Atlantic, Pacific and Indian ocean by Longhurst (2007). Nitrate diffusive fluxes were calculated using the global model GM1.*

Biogeographical Province	Ocean	Domain	dNO_3	GPP	%
SANT (Subantarctic water ring)	Antarctic	Westerly	1.18 ± 0.29	6.85 ± 1.32	17
SSTC (South subtropical convergence)	Antarctic	Westerly	1.02 ± 0.38	6.69 ± 1.72	15
BENG (Benguela current coast)	Atlantic	Coastal	1.43 ± 1.01	11.83 ± 5.61	12
BRAZ (Brazilian current coast)	Atlantic	Coastal	0.60 ± 0.78	9.11 ± 5.89	7
CNRY (Canary current coast)	Atlantic	Coastal	1.77 ± 1.01	15.57 ± 6.89	11
GUIA (Guianas coast)	Atlantic	Coastal	0.20 ± 0.04	8.20 ± 6.42	2
GUIN (Guinea current coast)	Atlantic	Coastal	1.09 ± 0.96	13.01 ± 7.09	8
NWCS (Northwest Atlantic shelves)	Atlantic	Coastal	0.87 ± 0.74	11.49 ± 3.19	8
CARB (Caribbean)	Atlantic	Trade wind	0.21 ± 0.10	6.03 ± 1.75	3
ETRA (Eastern tropical Atlantic)	Atlantic	Trade wind	0.48 ± 0.24	7.58 ± 2.58	6
NATR (North Atlantic tropical gyral)	Atlantic	Trade wind	0.26 ± 0.24	4.87 ± 2.08	5
SATL (South Atlantic gyral)	Atlantic	Trade wind	0.43 ± 0.34	4.87 ± 1.73	9
WTRA (Western tropical Atlantic)	Atlantic	Trade wind	0.29 ± 0.06	6.09 ± 1.17	5
GFST (Gulf Stream)	Atlantic	Westerly	0.93 ± 0.49	7.77 ± 1.51	12
MEDI (Mediterranean Sea)	Atlantic	Westerly	0.48 ± 0.53	5.35 ± 1.02	9
NASE (Northeast Atlantic subtropical gyral)	Atlantic	Westerly	0.50 ± 0.24	5.61 ± 1.40	9
NASW (Northwest Atlantic subtropical gyral)	Atlantic	Westerly	0.21 ± 0.14	4.46 ± 0.92	5
AUSW (Western Australian and Indonesian coast)	Indian	Coastal	0.32 ± 0.19	6.13 ± 0.96	5
EAFR (Eastern African coastal Province)	Indian	Coastal	0.45 ± 0.35	6.21 ± 1.53	7
INDE (Eastern India coast)	Indian	Coastal	0.32 ± 0.05	7.43 ± 0.96	4
INDW (Western India coast)	Indian	Coastal	0.51 ± 0.02	10.42 ± 2.58	5
ISSG (Indian South subtropical gyre)	Indian	Trade wind	0.25 ± 0.15	4.39 ± 0.85	6
MONS (Indian monsoon gyre)	Indian	Trade wind	0.23 ± 0.05	5.81 ± 0.95	4

ARAB (Northwest Arabian Sea upwelling)	Indian	Westerly	0.57 ± 0.24	10.27 ± 2.56	6
AUSE (East Australian coast)	Pacific	Coastal	0.30 ± 0.25	5.44 ± 1.41	6
CAMR (Central American coast)	Pacific	Coastal	0.50 ± 0.16	9.21 ± 2.02	5
CCAL (Coastal Californian current)	Pacific	Coastal	1.09 ± 0.65	6.94 ± 2.61	16
CHIL (Chile-Peru Current Coastal Province)	Pacific	Coastal	1.61 ± 3.14	10.25 ± 3.21	16
CHIN (China Sea)	Pacific	Coastal	0.24 ± 0.70	14.53 ± 5.90	2
NEWZ (New Zealand coast)	Pacific	Coastal	1.60 ± 0.45	7.87 ± 1.48	20
SUND (Sunda-Arafura shelves)	Pacific	Coastal	0.20 ± 0.06	7.74 ± 3.47	3
BERS (North Pacific epicontinental sea)	Pacific	Polar	1.92 ± 0.18	16.00 ± 4.50	12
ARCH (Archipelagic deep basins)	Pacific	Trade wind	0.20 ± 0.09	5.19 ± 0.95	4
NPTG (North Pacific Tropical gyre)	Pacific	Trade wind	0.29 ± 0.12	3.91 ± 0.58	7
PEQD (Pacific equatorial divergence)	Pacific	Trade wind	0.37 ± 0.18	7.10 ± 0.79	5
PNEC (North Pacific equatorial counter)	Pacific	Trade wind	0.32 ± 0.11	6.28 ± 1.47	5
SPSG (South Pacific gyre)	Pacific	Trade wind	0.27 ± 0.24	3.99 ± 1.31	7
WARM (Western Pacific warm pool)	Pacific	Trade wind	0.13 ± 0.03	4.35 ± 1.04	3
KURO (Kuroshio current)	Pacific	Westerly	0.78 ± 0.68	7.46 ± 2.63	10
NPPF (North Pacific polar front)	Pacific	Westerly	0.99 ± 0.28	6.55 ± 0.95	15
NPSW (Northwest Pacific subtropical)	Pacific	Westerly	0.14 ± 0.11	3.74 ± 0.91	4
TASM (Tasman Sea)	Pacific	Westerly	0.85 ± 0.23	7.25 ± 0.75	12

The contribution of nitrate diffusive flux to primary production in tropical and subtropical regions

We next investigated how our estimates fit in the nitrogen budget for tropical and subtropical regions, where most of our observations were collected. We first computed the spatial average of nitrate diffusive fluxes between 40ºN and 40ºS. In order to limit our calculation to open ocean oligotrophic waters, we selected those regions where surface chlorophyll-a and nitrate diffusive fluxes were lower than 0.5 mg m^{-3} and 1 mmol m^{-2} d^{-1}, respectively. For that we used the global model built with the complete dataset but excluding the stations collected in the Antarctic Peninsula (GM2), where surface temperature was below 15º. Average nitrate diffusive flux for this region (~20 Tmol N y^{-1}) was comparable to the sum of global estimates of nitrogen fixation derived from models and observations (~11-14 Tmol N y^{-1} (Jickells et al.

2017; Tang et al. 2019)), fluvial nitrogen fluxes (1.2-2 Tmol N y^{-1}) (Sharples et al. 2017) and atmospheric nitrogen deposition (~2.1 Tmol N y^{-1} (Jickells et al. 2017)) to the ocean. These results contradict previous studies (Caffin et al. 2018) and reveal that nitrate diffusive flux represents the main entry of new nitrogen into the euphotic zone in these regions.

Comparing these estimates to the amount of total production derived from satellite net primary production (Uitz et al. 2008), considering the percentage of dissolved organic carbon production with respect to total primary production (Teira et al. 2001), the ratio of phytoplankton respiration to gross photosynthesis (Geider 1992), and the averaged stoichiometry relationship for carbon and nitrogen (Galbraith and Martiny 2015) (see methods), we calculated a rough estimation of the f-ratio (the ratio of new production to total production) for these regions. The sum of our estimate of nitrate diffusion for the region 40ºN-40ºS, and the global estimates of nitrogen fixation, fluvial nitrogen fluxes and atmospheric nitrogen deposition (~34-38 Tmol N y^{-1}) represented ~11-13% (f-ratio=0.11-0.13) of the averaged total (dissolved plus particulate) gross primary production (304 ± 178 Tmol N y^{-1}) derived from satellite data. This estimate neglects other potential relevant sources of new nitrogen into the system, such as horizontal and vertical transport of organic and inorganic forms through surface Ekman transport (Williams and Follows 1998) and mesoscale and submesoscale eddies (McGillicuddy 2016; Lévy et al. 2018). For this reason it probably represents a lower-end estimate of the f-ratio in these regions, which by several studies using sediment traps and modelling studies has been reported to be ~0.1-0.2 (Dugdale et al. 1967; Eppley and Peterson 1979; Dunne et al. 2005; Laws et al. 2011). A detailed list of the contribution of nitrate diffusive flux to total gross primary production for the biogeographical provinces defined by Longhurst (2007) is included in Table 4.5.

The ratio cyanobacteria to picoeukaryotes in a global change scenario

Two genera of picocyanobacteria (*Prochlorococcus* and *Synechococcus*) and one or two subgroups of autotrophic picoeukaryotes of different sizes (small and large) can be distinguished by using flow cytometric techniques (Gasol and Del Giorgio 2000). The analysis of a dataset partially collected in the same stations used in this study demonstrate that nitrate supply plays an important role in the distribution of picoplankton subgroups (Chapter 2). In general, autotrophic picoplankton biomass was dominated by *Prochlorococcus* in warmer waters where the availability of nitrate was low, and by *Synechococcus* and picoeukaryotes in cooler waters with medium to high nitrate availability. According to these results, in a future ocean where global

change scenarios predict an increase in surface temperature and stratification (Howes et al. 2015), the resulting decrease in nitrate supply across the thermocline would lead to the dominance of autotrophic picoplankton by cyanobacteria, whereas the picoeukaryotes would decrease their contribution.

By using the climatology of nitrate turbulent diffusion derived from this study and the General Additive Model proposed in Chapter 2, we computed the present ratio cyanobacteria to picoeukaryotic biomass (see Methods) (Figure 4.9). To compute the same ratio in a future global change scenario, we followed the same procedure but used the averaged global decrease in dissolved nitrogen flux into the euphotic zone estimated by Lewandowska et al. (2014) between years 2000 and 2100 (ca. 20%). According to this analysis, the projected decrease in nitrate supply would lead to an average increase of ca. 8 % in the ratio cyanobacteria to picoeukaryotes. Due to the smaller contribution of cyanobacteria, compared to picoeukaryotes, to the transfer of carbon to the deep ocean, this could have important implications regarding the contribution of the smaller cells to the biological carbon pump (Corno et al. 2007)

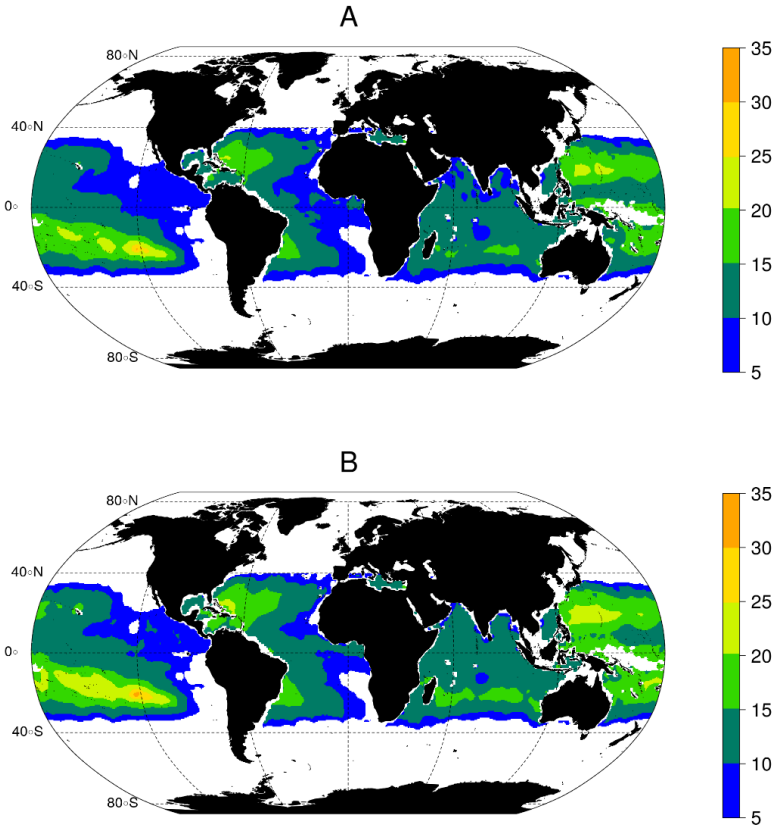

Figure 4.9 *Present (A) and future (B) distributions of the cyanobacteria to picoeukaryotes depth-integrated biomass ratio (see methods). Regions in white color represents data that was outside of the range covered by the dataset used to build the prediction model.*

Chapter 5

Conclusions

1. Temperature and nitrate supply were more relevant than light in predicting the biomass of most picoplankton subgroups, except for *Prochlorococcus* and low- nucleic-acid (LNA) prokaryotes, for which irradiance also played a significant role.
2. Nitrate supply was the only factor that allowed the distinction among the ecological niches of all autotrophic and heterotrophic picoplankton subgroups.
3. *Prochlorococcus* and LNA prokaryotes were more abundant in warmer waters where the nitrate fluxes were low, *Synechococcus* and high-nucleic-acid (HNA) prokaryotes prevailed in cooler environments characterized by intermediate or high levels of nitrate supply, and finally the niche of picoeukaryotes was defined by low temperatures and high nitrate supply.
4. Nitrate supply dynamics controlled the outcome of competition between the cyanobacterium *Synechococcus* and the picoeukaryote*M. pusilla*.
5. Under continuous nitrate limitation conditions (steady-state), *M. pusilla* was outcompeted by *Synechococcus* sp., the result of the competition was reversed when the steady-state was interrupted by nitrate pulses.
6. The rate of competitive exclusion of *Synechoccocus* was a linear function of the frequency of nitrate pulses, demonstrating that there is a window of opportunity for the coexistence of both species.
7. A model including three predictors (surface temperature, nitrate vertical gradient, and surface chlorophyll-a) explained 57% of the variance in the nitrate diffusive flux.
8. Average nitrate diffusion for oligotrophic regions between 40ºN-40ºS (~20 Tmol N y^{-1}) was comparable to the sum of global estimates of nitrogen fixation, fluvial fluxes and atmospheric deposition.
9. The predicted decrease of nitrate supply in tropical and subtropical areas as the result of global change (~20%), would produce an increase in the cyanobacteria to picoeukaryotes biomass ratio of 8%.

Chapter 6

References

Agawin, N. S. R., C. M. Duarte, and S. Agustí. 2000. Nutrient and temperature control of the contribution of picoplankton to phytoplankton biomass and production. Limnol. Oceanogr. **45**: 591–600. doi:10.4319/lo.2000.45.3.0591

Agustí, S., J. I. González-Gordillo, D. Vaqué, M. Estrada, M. I. Cerezo, G. Salazar, J. M. Gasol, and C. M. Duarte. 2015. Ubiquitous healthy diatoms in the deep sea confirm deep carbon injection by the biological pump. Nat. Commun. **6**: 7608. doi:10.1038/ncomms8608

Agusti, S., L. M. Lubián, E. Moreno-Ostos, M. Estrada, and C. M. Duarte. 2019. Projected Changes in Photosynthetic Picoplankton in a Warmer Subtropical Ocean. Front. Mar. Sci. **5**: 1–16. doi:10.3389/fmars.2018.00506

Aksnes, D., and J. Egge. 1991. A theoretical model for nutrient uptake in phytoplankton. Mar. Ecol. Prog. Ser. **70**: 65–72. doi:10.3354/meps070065

Alvarez-Salgado, X. A., A. V Borges, F. G. Figueiras, and L. Chou. 2009. Iberian margin: the Rías, p. 102–120. *In* Carbon and Nutrient Fluxes in Continental Margins: A Global Synthesis. Springer.

Álvarez-Salgado, X. A., J. Gago, B. M. Míguez, M. Gilcoto, and F. F. Pérez. 2000. Surface Waters of the NW Iberian Margin: Upwelling on the Shelf versus Outwelling of Upwelled Waters from the Rías Baixas. Estuar. Coast. Shelf Sci. **51**: 821–837. doi:10.1006/ecss.2000.0714

Alvarez-Salgado, X. A., G. Rosón, F. F. Pérez, and Y. Pazos. 1993. Hydrographic variability off the Rías Baixas (NW Spain) during the upwelling season. J. Geophys. Res. **98**: 14447. doi:10.1029/93JC00458

Aranguren-Gassis, M., P. Serret, E. Fernández, J. L. Herrera, J. F. Domínguez, V. Pérez, and J. Escanez. 2011. Production and respiration control the marine microbial metabolic balance in the eastern North Atlantic subtropical gyre. Deep Sea Res. Part I Oceanogr. Res. Pap. **58**: 768–775. doi:10.1016/j.dsr.2011.05.003

Arcos-Pulido, M., A. Rodríguez-Santana, M. Emelianov, and others. 2014. Diapycnal nutrient fluxes on the northern boundary of Cape Ghir upwelling region. Deep. Res. Part I Oceanogr. Res. Pap. **84**: 100–109. doi:10.1016/j.dsr.2013.10.010

Arteaga, L., M. Pahlow, and A. Oschlies. 2015. Global monthly sea surface nitrate fields estimated from remotely sensed sea surface temperature, chlorophyll, and modeled mixed layer depth. Geophys. Res. Lett. **42**: 1130–1138. doi:10.1002/2014GL062937

Azam, F., T. Fenchel, J. Field, J. Gray, L. Meyer-Reil, and F. Thingstad. 1983. The Ecological Role of Water-Column Microbes in the Sea. Mar. Ecol. Prog. Ser. **10**: 257–263. doi:10.3354/meps010257

Barber, R. T., and M. R. Hiscock. 2006. A rising tide lifts all phytoplankton: Growth response of other phytoplankton taxa in diatom-dominated blooms. Global Biogeochem. Cycles **20**: 1–12. doi:10.1029/2006GB002726

Barton, A. D., M. S. Lozier, and R. G. Williams. 2015. Physical controls of variability in North Atlantic phytoplankton communities. Limnol. Oceanogr. **60**: 181–197. doi:10.1002/lno.10011

Barton, A. D., B. A. Ward, R. G. Williams, and M. J. Follows. 2014. The impact of fine-scale turbulence on phytoplankton community structure. Limnol. Oceanogr. Fluids Environ. **4**: 34–49. doi:10.1215/21573689-2651533

Baudoux, A.-C., M. J. W. Veldhuis, H. J. Witte, and C. P. D. Brussaard. 2007. Viruses as mortality agents of picophytoplankton in the deep chlorophyll maximum layer during IRONAGES III. Limnol. Oceanogr. **52**: 2519–2529. doi:10.4319/lo.2007.52.6.2519

Bauer, S., G. L. Hitchcock, and D. B. Olson. 1991. Influence of monsoonally-forced Ekman dynamics upon surface layer depth and plankton biomass distribution in the Arabian Sea. Deep Sea Res. Part

A, Oceanogr. Res. Pap. **38**: 531–553. doi:10.1016/0198-0149(91)90062-K

Bendtsen, J., and K. Richardson. 2018. Turbulence measurements suggest high rates of new production over the shelf edge in the north-eastern North Sea during summer. Biogeosciences Discuss. **15**: 1–30. doi:10.5194/bg-2018-385

Berthelot, H., S. Duhamel, phane Lamp, J.-F. Maguer, S. Wang, I. Cetiniamp, and N. Cassar. 2018. NanoSIMS single cell analyses reveal the contrasting nitrogen sources for small phytoplankton. ISME J. doi:10.1038/s41396-018-0285-8

Berube, P. M., S. J. Biller, A. G. Kent, and others. 2015. Physiology and evolution of nitrate acquisition in Prochlorococcus. ISME J. **9**: 1195–1207. doi:10.1038/ismej.2014.211

Bonnet, S., O. Grosso, and T. Moutin. 2011. Planktonic dinitrogen fixation along a longitudinal gradient across the Mediterranean Sea during the stratified period (BOUM cruise). Biogeosciences **8**: 2257–2267. doi:10.5194/bg-8-2257-2011

Bonnet, S., C. Guieu, J. Chiaverini, J. Ras, and A. Stock. 2005. Effect of atmospheric nutrients on the autotrophic communities in a low nutrient, low chlorophyll system. Limnol. Oceanogr. **50**: 1810–1819. doi:10.4319/lo.2005.50.6.1810

Bouman, H. a, O. Ulloa, R. Barlow, W. K. W. Li, T. Platt, K. Zwirglmaier, D. J. Scanlan, and S. Sathyendranath. 2011. Water-column stratification governs the community structure of subtropical marine picophytoplankton. Environ. Microbiol. Rep. **3**: 473–482. doi:10.1111/j.1758-2229.2011.00241.x

Bourgault, D., C. Hamel, F. Cyr, J. E. Tremblay, P. S. Galbraith, D. Dumont, and Y. Gratton. 2011. Turbulent nitrate fluxes in the Amundsen Gulf during ice-covered conditions. Geophys. Res. Lett. **38**. doi:10.1029/2011GL047936

Bouruet-Aubertot, P., Y. Cuypers, A. Doglioli, and others. 2018. Longitudinal contrast in turbulence along a ∼ 19° S section in the Pacific and its consequences for biogeochemical fluxes. Biogeosciences **15**: 7485–7504. doi:10.5194/bg-15-7485-2018

Bouvier, T., P. A. del Giorgio, and J. M. Gasol. 2007. A comparative study of the cytometric characteristics of High and Low nucleic-acid bacterioplankton cells from different aquatic ecosystems. Environ. Microbiol. **9**: 2050–2066. doi:10.1111/j.1462-2920.2007.01321.x

Box, G. E. P., and D. R. Cox. 1964. An Analysis of Transformations. J. R. Stat. Soc. Ser. B **26**: 211–252.

Boyd, P. W., T. a Rynearson, E. a Armstrong, and others. 2013. Marine phytoplankton temperature versus growth responses from polar to tropical waters--outcome of a scientific community-wide study. PLoS One **8**: e63091. doi:10.1371/journal.pone.0063091

Brewin, R. J. W., S. Sathyendranath, G. Tilstone, P. K. Lange, and T. Platt. 2014. A multicomponent model of phytoplankton size structure. J. Geophys. Res. Ocean. **119**: 3478–3496. doi:10.1002/2014JC009859

Buitenhuis, E. T., W. K. W. Li, D. Vaulot, and others. 2012. Picophytoplankton biomass distribution in the global ocean. Earth Syst. Sci. Data **4**: 37–46. doi:10.5194/essd-4-37-2012

C Butcher John, B. J. 1987. The Numerical Analysis of Ordinary Differential Equations: Runge-Kutta and General Linear Methods. A Wiley Intersci. **7**: 5–12.

Caffin, M., T. Moutin, R. Ann Foster, and others. 2018. N2 fixation as a dominant new N source in the western tropical South Pacific Ocean (OUTPACE cruise). Biogeosciences **15**: 2565–2585. doi:10.5194/bg-15-2565-2018

Calvo-Díaz, A., and X. Morán. 2006. Seasonal dynamics of picoplankton in shelf waters of the southern Bay of Biscay. Aquat. Microb. Ecol. **42**: 159–174. doi:10.3354/ame042159

Capone, D. G. D. G., J. A. J. A. Burns, J. P. J. P. Montoya, A. Subramaniam, C. Mahaffey, T. Gunderson, A. F. A. F. Michaels, and E. J. E. J. Carpenter. 2005. Nitrogen fixation by Trichodesmium spp.: An important source of new nitrogen to the tropical and subtropical North Atlantic Ocean. Global Biogeochem. Cycles **19**: 1–17. doi:10.1029/2004GB002331

Capone, D. G., R. Popa, B. Flood, and K. H. Nealson. 2006. Follow the nitrogen. Science (80-.). **312**: 708–709. doi:10.1126/science.1111863

Capone, D., J. Zehr, H. W. Paerl, B. Bergman, and E. J. Carpenter. 1997. Trichodesmium, a Globally Significant Marine Cyanobacterium. Science (80-.). **276**: 1221–1229. doi:10.1126/science.276.5316.1221

Carr, M.-E., M. R. Lewis, D. Kelley, and B. Jones. 1995. A physical estimate of new production in the equatorial Pacific along 150°W. Limnol. Oceanogr. **40**: 138–147. doi:10.4319/lo.1995.40.1.0138

Cermeño, P., P. Chouciño, B. Fernández-Castro, and others. 2016. Marine Primary Productivity Is Driven by a Selection Effect. Front. Mar. Sci. **3**: 1–10. doi:10.3389/fmars.2016.00173

Cermeno, P., S. Dutkiewicz, R. P. Harris, M. Follows, O. Schofield, and P. G. Falkowski. 2008. The role of nutricline depth in regulating the ocean carbon cycle. Proc. Natl. Acad. Sci. **105**: 20344–20349. doi:10.1073/pnas.0811302106

Cermeño, P., J. Lee, K. Wyman, O. M. Schofield, and P. G. Falkowski. 2011. Competitive dynamics in two species of marine phytoplankton under non-equilibrium conditions. Mar. Ecol. Prog. Ser. **429**: 19–28. doi:10.3354/meps09088

Chen, B., H. Liu, M. Landry, M. Chen, J. Sun, L. Shek, X. Chen, and P. Harrison. 2009. Estuarine nutrient loading affects phytoplankton growth and microzooplankton grazing at two contrasting sites in Hong Kong coastal waters. Mar. Ecol. Prog. Ser. **379**: 77–90. doi:10.3354/meps07888

Chisholm, S. W. 1992. Phytoplankton Size, p. 213–237. *In* P.G. Falkowski, A.D. Woodhead, and K. Vivirito [eds.], Primary Productivity and Biogeochemical Cycles in the Sea. Springer US.

Chisholm, S. W., R. J. Olson, E. R. Zettler, R. Goericke, J. B. Waterbury, and N. A. Welschmeyer. 1988. A novel free-living prochlorophyte abundant in the oceanic euphotic zone. Nature **334**: 340–343. doi:10.1038/334340a0

Close, H. G., S. R. Shah, A. E. Ingalls, and others. 2013. Export of submicron particulate organic matter to mesopelagic depth in an oligotrophic gyre. Proc. Natl. Acad. Sci. **110**: 12565–12570. doi:10.1073/pnas.1217514110

Corno, G., D. M. Karl, M. J. Church, R. M. Letelier, R. Lukas, R. R. Bidigare, and M. R. Abbott. 2007. Impact of climate forcing on ecosystem processes in the North Pacific Subtropical Gyre. J. Geophys. Res. **112**: C04021. doi:10.1029/2006JC003730

Cullen, J. J., P. J. S. Franks, D. M. Karl, and A. R. Longhurst. 2002. Physical influences on marine ecosystem dynamics, p. 297–336. *In* A.R. Robinson, J.J. McCarthy, and B.J. Rotchschild [eds.], The Sea. John Wiley & Sons.

Cuypers, Y., P. Bouruet-Aubertot, C. Marec, and J.-L. Fuda. 2012. Characterization of turbulence from a fine-scale parameterization and microstructure measurements in the Mediterranean Sea during the BOUM experiment. Biogeosciences **9**: 3131–3149. doi:10.5194/bg-9-3131-2012

Cyr, F., D. Bourgault, P. S. Galbraith, and M. Gosselin. 2015. Turbulent nitrate fluxes in the Lower St. Lawrence Estuary, Canada. J. Geophys. Res. C Ocean. **120**: 2308–2330. doi:10.1002/2014JC010272

d'Ovidio, F., S. De Monte, S. Alvain, Y. Dandonneau, and M. Levy. 2010. Fluid dynamical niches of phytoplankton types. Proc. Natl. Acad. Sci. **107**: 18366–18370. doi:10.1073/pnas.1004620107

Díaz, P. A., M. Ruiz-Villarreal, B. Mouriño-Carballido, C. Fernández-Pena, P. Riobó, and B. Reguera.

2019. Fine scale physical-biological interactions during a shift from relaxation to upwelling with a focus on Dinophysis acuminata and its potential ciliate prey. Prog. Oceanogr. **175**: 309–327. doi:10.1016/j.pocean.2019.04.009

Dietze, H., A. Oschlies, and P. Kähler. 2004. Internal-wave-induced and double-diffusive nutrient fluxes to the nutrient-consuming surface layer in the oligotrophic subtropical North Atlantic. Ocean Dyn. **54**: 1–7. doi:10.1007/s10236-003-0060-9

Droop, M. R. 1973. Some thoughts on nutrient limitation in algae. J. Phycol. **9**: 264–272.

Du, C., Z. Liu, S. J. Kao, and M. Dai. 2017. Diapycnal Fluxes of Nutrients in an Oligotrophic Oceanic Regime: The South China Sea. Geophys. Res. Lett. **44**: 11,510-11,518. doi:10.1002/2017GL074921

Duce, R. A., J. LaRoche, K. Altieri, and others. 2008. Impacts of Atmospheric Anthropogenic Nitrogen on the Open Ocean. Science (80-.). **320**: 893–897. doi:10.1126/science.1150369

Ducklow, H. W., and S. C. Doney. 2013. What Is the Metabolic State of the Oligotrophic Ocean? A Debate. Ann. Rev. Mar. Sci. **5**: 525–533. doi:10.1146/annurev-marine-121211-172331

Dugdale, R. C., J. J. Goering, and N. Apr. 1967. UPTAKE OF NEW AND REGENERATED FORMS OF NITROGEN IN PRIMARY PRODUCTIVITY1. Limnol. Oceanogr. **12**: 196–206. doi:10.4319/lo.1967.12.2.0196

Dunne, J. P., R. A. Armstrong, A. Gnanadesikan, J. L. Sarmiento, A. Gnnadesikan, J. L. Sarmiento, A. Gnanadesikan, and J. L. Sarmiento. 2005. Empirical and mechanistic models for the particle export ratio. Global Biogeochem. Cycles **19**: 1–16. doi:10.1029/2004GB002390

Echevarria, F., L. Zabala, A. Corzo, G. Navarro, L. Prieto, and D. Macias. 2009. Spatial distribution of autotrophic picoplankton in relation to physical forcings: the Gulf of Cadiz, Strait of Gibraltar and Alboran Sea case study. J. Plankton Res. **31**: 1339–1351. doi:10.1093/plankt/fbp070

Edwards, K. F., M. K. Thomas, C. a. Klausmeier, and E. Litchman. 2012. Allometric scaling and taxonomic variation in nutrient utilization traits and maximum growth rate of phytoplankton. Limnol. Oceanogr. **57**: 554–566. doi:10.4319/lo.2012.57.2.0554

Ellwood, M. J., A. R. Bowie, A. Baker, and others. 2018. Insights Into the Biogeochemical Cycling of Iron, Nitrate, and Phosphate Across a 5,300 km South Pacific Zonal Section (153°E–150°W). Global Biogeochem. Cycles **32**: 187–207. doi:10.1002/2017GB005736

Eppley, R. W., and B. J. Peterson. 1979. Particulate organic matter flux and planktonic new production in the deep ocean. Nature **282**: 677–680. doi:10.1038/282677a0

Espinoza-González, O., F. Figueiras, B. Crespo, I. Teixeira, and C. Castro. 2012. Autotrophic and heterotrophic microbial plankton biomass in the NW Iberian upwelling: seasonal assessment of metabolic balance. Aquat. Microb. Ecol. **67**: 77–89. doi:10.3354/ame01584

Estrada, M., M. Latasa, M. Emelianov, and others. 2014. Seasonal and mesoscale variability of primary production in the deep winter-mixing region of the NW Mediterranean. Deep Sea Res. Part I Oceanogr. Res. Pap. **94**: 45–61. doi:10.1016/j.dsr.2014.08.003

Falkowski, P. G. 2012. Ocean Science: The power of plankton. Nature **483**: S17–S20.

Falkowski, P. G., D. Ziemann, Z. Kolber, and P. K. Bienfang. 1991. Role of eddy pumping in enhancing primary production in the ocean. Nature **352**: 55–58. doi:10.1038/352055a0

Farnelid, H., A. F. Andersson, S. Bertilsson, and others. 2011. Nitrogenase gene amplicons from global marine surface waters are dominated by genes of non-cyanobacteria. PLoS One **6**. doi:10.1371/journal.pone.0019223

Fawcett, S. E. S., M. W. Lomas, J. R. J. Casey, B. B. Ward, and D. M. Sigman. 2011. Assimilation of upwelled nitrate by small eukaryotes in the Sargasso Sea. Nat. Geosci. **4**: 717–722.

doi:10.1038/NGEO1265

Fenchel, T. 2008. The microbial loop – 25 years later. J. Exp. Mar. Bio. Ecol. **366**: 99–103. doi:10.1016/j.jembe.2008.07.013

Fernández-Castro, B., M. Gilcoto, A. C. Naveira-Garabato, M. Villamaña, R. Graña, and B. Mouriño-Carballido. 2018. Modulation of the Semidiurnal Cycle of Turbulent Dissipation by Wind-Driven Upwelling in a Coastal Embayment. J. Geophys. Res. Ocean. **123**: 4034–4054. doi:10.1002/2017JC013582

Fernández-Castro, B., B. Mouriño-Carballido, V. M. Benitez-Barrios, and others. 2014. Microstructure turbulence and diffusivity parameterization in the tropical and subtropical Atlantic, Pacific and Indian Oceans during the Malaspina 2010 expedition. Deep. Res. Part I Oceanogr. Res. Pap. **94**: 15–30. doi:10.1016/j.dsr.2014.08.006

Fernández-Castro, B., B. Mouriño-Carballido, E. Marañón, and others. 2015. Importance of salt fingering for new nitrogen supply in the oligotrophic ocean. Nat. Commun. **6**: 8002. doi:10.1038/ncomms9002

Fernández, E., X. A. Álvarez-Salgado, R. Beiras, A. Ovejero, and G. Méndez. 2016. Coexistence of urban uses and shellfish production in an upwelling-driven, highly productive marine environment: The case of the Ría de Vigo (Galicia, Spain). Reg. Stud. Mar. Sci. **8**: 362–370. doi:10.1016/j.rsma.2016.04.002

Field, C. B., M. J. Behrenfeld, J. T. Randerson, and P. G. Falkowski. 1998. Primary production of the biosphere: integrating terrestrial and oceanic components. Science **281**: 237–40. doi:10.1126/science.281.5374.237

Finkel, Z. V., J. Beardall, K. J. Flynn, A. Quigg, T. A. V Rees, and J. A. Raven. 2010. Phytoplankton in a changing world: cell size and elemental stoichiometry. J. Plankton Res. **32**: 119–137. doi:10.1093/plankt/fbp098

Flombaum, P., J. L. L. Gallegos, R. A. A. Gordillo, and others. 2013. Present and future global distributions of the marine Cyanobacteria Prochlorococcus and Synechococcus. Proc. Natl. Acad. Sci. **110**: 9824–9829. doi:10.1073/pnas.1307701110

Forryan, A., A. P. Martin, M. A. Srokosz, E. E. Popova, S. C. Painter, and M. C. Stinchcombe. 2012. Turbulent nutrient fluxes in the Iceland Basin. Deep. Res. Part I Oceanogr. Res. Pap. **63**: 20–35. doi:10.1016/j.dsr.2011.12.006

Fraga, F. 1981. Upwelling off the Galacian Coast, northwest Spain, p. 176–182. *In* F.A. Richards [ed.], Coastal and Estuarine Sciences. American Geophysical Union.

Froján, M., B. Arbones, D. Zúñiga, C. Castro, and F. Figueiras. 2014. Microbial plankton community in the Ría de Vigo (NW Iberian upwelling system): impact of the culture of Mytilus galloprovincialis. Mar. Ecol. Prog. Ser. **498**: 43–54. doi:10.3354/meps10612

Galbraith, E. D., and A. C. Martiny. 2015. A simple nutrient-dependence mechanism for predicting the stoichiometry of marine ecosystems. Proc. Natl. Acad. Sci. **112**: 201423917. doi:10.1073/pnas.1423917112

Gardner, W. D., S. P. Chung, M. J. Richardson, and I. D. Walsh. 1995. The oceanic mixed-layer pump. Deep. Res. Part II **42**. doi:10.1016/0967-0645(95)00037-Q

Gasol, J. M. 1999. How to count picoalgae and bacteria with the FACScalibur flow cytometer.

Gasol, J. M., and P. A. Del Giorgio. 2000. Using flow cytometry for counting natural planktonic bacteria and understanding the structure of planktonic bacterial communities. Sci. Mar. **64**: 197–224. doi:10.3989/scimar.2000.64n2197

Gasol, J., E. Vázquez-Domínguez, D. Vaqué, S. Agustí, and C. Duarte. 2009. Bacterial activity and

diffusive nutrient supply in the oligotrophic Central Atlantic Ocean. Aquat. Microb. Ecol. **56**: 1–12. doi:10.3354/ame01310

Gause, B. Y. G. F. 1932. Experimental Studies on the Struggle for Existence: I. Mixed Population of Two Species of Yeast. J. Exp. Biol. **9**: 389–402.

Geange, S. W., S. Pledger, K. C. Burns, and J. S. Shima. 2011. A unified analysis of niche overlap incorporating data of different types. Methods Ecol. Evol. **2**: 175–184. doi:10.1111/j.2041-210X.2010.00070.x

Geider, R. J. 1992. Respiration: Taxation Without Representation?, p. 333–360. *In* P.G. Falkowski and A.D. Woodhead [eds.], Primary Productivity and Biogeochemical Cycles in the Sea. Springer US.

Gomes, A., J. M. Gasol, M. Estrada, L. Franco-Vidal, L. Díaz-Pérez, I. Ferrera, and X. A. G. Morán. 2015. Heterotrophic bacterial responses to the winter–spring phytoplankton bloom in open waters of the NW Mediterranean. Deep Sea Res. Part I Oceanogr. Res. Pap. **96**: 59–68. doi:10.1016/j.dsr.2014.11.007

Grob, C., O. Ulloa, W. Li, G. Alarcón, M. Fukasawa, and S. Watanabe. 2007. Picoplankton abundance and biomass across the eastern South Pacific Ocean along latitude 32.5°S. Mar. Ecol. Prog. Ser. **332**: 53–62. doi:10.3354/meps332053

Grover, J. P. J. 1991. Resource competition in a variable environment: phytoplankton growing according to the variable-internal-stores model. Am. Nat. **138**: 811–835.

Guasto, J. S., R. Rusconi, and R. Stocker. 2012. Fluid Mechanics of Planktonic Microorganisms. Annu. Rev. Fluid Mech. **44**: 373–400. doi:10.1146/annurev-fluid-120710-101156

Guidi, L., S. Chaffron, L. Bittner, and others. 2016. Plankton networks driving carbon export in the oligotrophic ocean. Nature **532**: 465–470. doi:10.1038/nature16942

Guillard, R. R. L., and J. H. Ryther. 1962. Studies of marine planktonic diatoms, I, *Cyclotella nanna* (Hustedt) and *Detonula convervacea* (Cleve). Can. J. Microbiol. **8**: 229–239.

Gundersen, K., M. Heldal, S. Norland, D. A. Purdie, and A. H. Knap. 2002. Elemental C, N, and P cell content of individual bacteria collected at the Bermuda Atlantic Time-series Study (BATS) site. Limnol. Oceanogr. **47**: 1525–1530. doi:10.4319/lo.2002.47.5.1525

Haario, H., M. Laine, A. Mira, and E. Saksman. 2006. DRAM: Efficient adaptive MCMC. Stat. Comput. **16**: 339–354. doi:10.1007/s11222-006-9438-0

Hales, B. 2005. Irreversible nitrate fluxes due to turbulent mixing in a coastal upwelling system. J. Geophys. Res. **110**: C10S11. doi:10.1029/2004JC002685

Hales, B., D. Hebert, and J. Marra. 2009. Turbulent supply of nutrients to phytoplankton at the New England shelf break front. J. Geophys. Res. Ocean. **114**: 1–10. doi:10.1029/2008JC005011

Halsey, K. H., and B. M. Jones. 2015. Phytoplankton Strategies for Photosynthetic Energy Allocation. Ann. Rev. Mar. Sci. **7**: 265–297. doi:10.1146/annurev-marine-010814-015813

Hama, T., T. Miyazaki, Y. Ogawa, T. Iwakuma, M. Takahashi, A. Otsuki, and S. Ichimura. 1983. Measurement of photosynthetic production of a marine phytoplankton population using a stable 13C isotope. Mar. Biol. **73**: 31–36. doi:10.1007/BF00396282

Hansen, H. P., and F. Koroleff. 1999. Determination of nutrients, p. 159–228. *In* K. Grasshoff, K. Kremling, and M. Ehrhardt [eds.], Methods of Seawater Analysis. Wiley-VCH Verlag GmbH.

Harrison, P. J., J. Parslow, and H. Conway. 1989. Determination of nutrient uptake kinetic parameters: a comparison of methods. Mar. Ecol. Prog. Ser. Oldend. **52**: 301–312.

Hastie, T. J., and R. Tibshirani. 1993. Varying-coefficient Models. J. R. Stat. Soc. Ser. B **55**: 757–796.

Hibiya, T., M. Nagasawa, and Y. Niwa. 2007. Latitudinal dependence of diapycnal diffusivity in the

thermocline observed using a microstructure profiler. Geophys. Res. Lett. **34**: 1–4. doi:10.1029/2007GL032323

Hobbie, J. El, R. J. Daley, and S. Jasper. 1977. Use of nuclepore filters for counting bacteria by fluorescence microscopy. Appl. Environ. Microbiol. **33**: 1225–1228.

Horne, E. P. W., J. W. Loder, C. E. Naimief, and N. S. Oakey. 1996. Turbulence dissipation rates and nitrate supply in the upper water column on Georges Bank. Deep. Res. Part II Top. Stud. Oceanogr. **43**: 1683–1712. doi:10.1016/S0967-0645(96)00037-9

Howes, E. L., F. Joos, C. M. Eakin, and J.-P. Gattuso. 2015. An updated synthesis of the observed and projected impacts of climate change on the chemical, physical and biological processes in the oceans. Front. Mar. Sci. **2**: 1–27. doi:10.3389/fmars.2015.00036

Hutchinson, G. E. 1957. Concluding Remarks. Cold Spring Harb. Symp. Quant. Biol. **22**: 415–427. doi:10.1101/SQB.1957.022.01.039

Hutchinson, G. E. 1961. The Paradox of the Phytoplankton. Am. Nat. **95**: 137–145.

Hydes, D. J., P. M. Holligan, M. C. Moore, N. R. Fisher, T. P. Rippeth, J. Sharples, and J. H. Simpson. 2010. Phytoplankton distribution and survival in the thermocline. Limnol. Oceanogr. **46**: 486–496. doi:10.4319/lo.2001.46.3.0486

Jenkins, W. J., and S. C. Doney. 2003. The subtropical nutrient spiral. Global Biogeochem. Cycles **17**: n/a-n/a. doi:10.1029/2003GB002085

Jickells, T. D., E. Buitenhuis, K. Altieri, and others. 2017. A reevaluation of the magnitude and impacts of anthropogenic atmospheric nitrogen inputs on the ocean. Global Biogeochem. Cycles. doi:10.1002/2016GB005586

Johnson, P. W., and J. M. Sieburth. 1982. In-situ morphology and occurrence of eukaryotic phototrophs of bacterial size in the picoplankton of estuarine and oceanic waters. J. Phycol. **18**: 318–327. doi:10.1111/j.1529-8817.1982.tb03190.x

Johnson, Z. I., E. R. Zinser, A. Coe, N. P. McNulty, E. M. S. Woodward, and S. W. Chisholm. 2006. Niche Partitioning Among Prochlorococcus Ecotypes Along Ocean-Scale Environmental Gradients. Science (80-.). **311**: 1737–1740. doi:10.1126/science.1118052

Jumars, P. A., J. H. Trowbridge, E. Boss, and L. Karp-Boss. 2009. Turbulence-plankton interactions: a new cartoon. Mar. Ecol. **30**: 133–150. doi:10.1111/j.1439-0485.2009.00288.x

Jurado, E., H. A. Dijkstra, and H. J. Van Der Woerd. 2012. Microstructure observations during the spring 2011 STRATIPHYT-II cruise in the northeast Atlantic. Ocean Sci. **8**: 945–957. doi:10.5194/os-8-945-2012

Kamykowski, D., and S. J. Zentara. 1986. Predicting plant nutrient concentrations from temperature and sigma-t in the upper kilometer of the world ocean. Deep Sea Res. **33**: 89–105.

Kaneko, H., I. Yasuda, K. Komatsu, and S. Itoh. 2013. Observations of vertical turbulent nitrate flux across the Kuroshio. Geophys. Res. Lett. **40**: 3123–3127. doi:10.1002/grl.50613

Kark, S., T. Mukerji, U. N. Safriel, I. Noy-Meir, R. Nissani, and A. Darvasi. 2002. Peak morphological diversity in an ecotone unveiled in the chukar partridge by a novel Estimator in a Dependent Sample (EDS). J. Anim. Ecol. **71**: 1015–1029. doi:10.1046/j.1365-2656.2002.00665.x

Karl, D. M., R. R. Bidigare, and R. M. Letelier. 2001. Long-term changes in plankton community structure and productivity in the North Pacific Subtropical Gyre: The domain shift hypothesis. Deep Sea Res. Part II Top. … **48**: 1449–1470. doi:10.1016/S0967-0645(00)00149-1

Karp-Boss, L., E. Boss, and P. A. Jumars. 1996. Nutrient fluxes to planktonic osmotrophs in the presence of fluid motion. Oceanogr. Mar. Biol. an Annu. Rev. Vol. 34 71–107.

Kiørboe, T. 1993. Turbulence, Phytoplankton Cell Size, and the Structure of Pelagic Food Webs, p. 1–72. *In* Advances in Marine Biology.

Kirchman, D. L. 1994. The uptake of inorganic nutrients by heterotrophic bacteria. Microb. Ecol. **28**: 255–271. doi:10.1007/BF00166816

Kirk, J. T. O. 1994. Light and photosynthesis in aquatic ecosystems, Cambridge University Press.

Kunze, E., J. F. Dower, I. Beveridge, R. Dewey, and K. P. Bartlett. 2006. Observations of biologically generated turbulence in a coastal inlet. Science **313**: 1768–1770. doi:10.1126/science.1129378

Kwon, E. Y., F. Primeau, and J. L. Sarmiento. 2009. The impact of remineralization depth on the air–sea carbon balance. Nat. Geosci. **2**: 630–635. doi:10.1038/ngeo612

Langlois, R. J., J. LaRoche, and P. A. Raab. 2005. Diazotrophic diversity and distribution in the tropical and subtropical Atlantic Ocean. Appl. Environ. Microbiol. **71**: 7910–9. doi:10.1128/AEM.71.12.7910-7919.2005

Laufkötter, C., M. Vogt, N. Gruber, and others. 2016. Projected decreases in future marine export production: the role of the carbon flux through the upper ocean ecosystem. Biogeosciences **13**: 4023–4047. doi:10.5194/bg-13-4023-2016

St. Laurent, L. C., and R. W. Schmitt. 1999. The Contribution of Salt Fingers to Vertical Mixing in the North Atlantic Tracer Release Experiment *. J. Phys. Ocean. **29**: 1404–1424.

Law, C. S., E. R. Abraham, A. J. Watson, and M. I. Liddicoat. 2003. Vertical eddy diffusion and nutrient supply to the surface mixed layer of the Antarctic Circumpolar Current. J. Geophys. Res. **108**: 3272. doi:10.1029/2002JC001604

Law, C. S., A. P. Martin, M. I. Liddicoat, A. J. Watson, K. J. Richards, and E. M. S. Woodward. 2001. A Lagrangian SF 6 tracer study of an anticyclonic eddy in the North Atlantic: Patch evolution, vertical mixing and nutrient supply to the mixed layer. Deep. Res. Part II Top. Stud. Oceanogr. **48**: 705–724. doi:10.1016/S0967-0645(00)00112-0

Laws, E. A., E. D'Sa, and P. Naik. 2011. Simple equations to estimate ratios of new or export production to total production from satellite-derived estimates of sea surface temperature and primary production. Limnol. Oceanogr. Methods **9**: 593–601. doi:10.4319/lom.2011.9.593

Lazier, J. R. N., and K. H. Mann. 1989. Turbulence and the diffusive layers around small organisms. Deep Sea Res. Part A. Oceanogr. Res. Pap. **36**: 1721–1733. doi:10.1016/0198-0149(89)90068-X

Ledwell, J. R., D. J. McGillicuddy, and L. A. Anderson. 2008. Nutrient flux into an intense deep chlorophyll layer in a mode-water eddy. Deep. Res. Part II Top. Stud. Oceanogr. **55**: 1139–1160. doi:10.1016/j.dsr2.2008.02.005

Lévy, M., P. J. S. Franks, and K. S. Smith. 2018. The role of submesoscale currents in structuring marine ecosystems. Nat. Commun. **9**: 4758. doi:10.1038/s41467-018-07059-3

Lewandowska, A. M., D. G. Boyce, M. Hofmann, B. Matthiessen, U. Sommer, and B. Worm. 2014. Effects of sea surface warming on marine plankton G. Fussmann [ed.]. Ecol. Lett. **17**: 614–623. doi:10.1111/ele.12265

Lewis, M. R., E. P. W. Horne, J. J. Cullen, N. S. Oakey, and T. Platt. 1984. Turbulent motions may control phytoplankton photosynthesis in the upper ocean. Nature **311**: 49–50. doi:10.1038/311049a0

Lewis, M. R. M. R., D. Hebert, W. G. G. Harrison, and others. 1986. Vertical Nitrate Fluxes in the Oligotrophic Ocean. Science (80-.). **234**: 870–873. doi:10.1126/science.234.4778.870

Li, Q. P., P. J. S. Franks, M. D. Ohman, and M. R. Landry. 2012. Enhanced nitrate fluxes and biological processes at a frontal zone in the southern California current system. J. Plankton Res. **34**: 790–801. doi:10.1093/plankt/fbs006

Li, W. K. W. 2002. Macroecological patterns of phytoplankton in the northwestern North Atlantic Ocean. Nature **419**: 154–157. doi:10.1038/nature00983.1.

Li, W. K. W. 2009. Plankton populations and communities, p. 29–64. *In* J.D. Witman and K. Roy [eds.], Marine Macroecology.

Li, W. K. W., E. J. H. Head, and W. Glen Harrison. 2004. Macroecological limits of heterotrophic bacterial abundance in the ocean. Deep Sea Res. Part I Oceanogr. Res. Pap. **51**: 1529–1540. doi:10.1016/j.dsr.2004.06.012

Li, W. K. W., J. F. Jellett, and P. M. Dickie. 1995. DNA distributions in planktonic bacteria stained with TOTO or TO-PRO. Limnol. Oceanogr. **40**: 1485–1495. doi:10.4319/lo.1995.40.8.1485

Liang, Y. C., M. R. Mazloff, I. Rosso, S. W. Fang, and J. Y. Yu. 2018. A multivariate empirical orthogonal function method to construct nitrate maps in the Southern Ocean. J. Atmos. Ocean. Technol. **35**: 1505–1519. doi:10.1175/JTECH-D-18-0018.1

Lipschultz, F., N. R. Bates, C. A. Carlson, and D. A. Hansell. 2002. New production in the Sargasso Sea: History and current status. Global Biogeochem. Cycles **16**: 1-1-1–17. doi:10.1029/2000gb001319

Litchman, E., and C. a. Klausmeier. 2008. Trait-Based Community Ecology of Phytoplankton. Annu. Rev. Ecol. Evol. Syst. **39**: 615–639. doi:10.1146/annurev.ecolsys.39.110707.173549

Liu, X., K. Furuya, T. Shiozaki, and others. 2013. Variability in nitrogen sources for new production in the vicinity of the shelf edge of the East China Sea in summer. Cont. Shelf Res. **61**–**62**: 23–30. doi:10.1016/j.csr.2013.04.014

Llabrés, M., S. Agustí, P. Alonso-Laita, and G. Herndl. 2010. Synechococcus and Prochlorococcus cell death induced by UV radiation and the penetration of lethal UVR in the Mediterranean Sea. Mar. Ecol. Prog. Ser. **399**: 27–37. doi:10.3354/meps08332

Lomas, M. W., and S. B. Moran. 2011. Evidence for aggregation and export of cyanobacteria and nano-eukaryotes from the Sargasso Sea euphotic zone. Biogeosciences **8**: 203–216. doi:10.5194/bg-8-203-2011

Longhurst, A. R. 2007. Ecological geography of the sea, Elservier.

Longhurst, A. R. 2010. Ecological geography of the sea, Academic Press.

MacArthur, R. H. 1972. Geographical ecology. Patterns in the distribution of species,.

Mackey, K. R. M., A. Paytan, K. Caldeira, A. R. Grossman, D. Moran, M. McIlvin, and M. A. Saito. 2013. Effect of Temperature on Photosynthesis and Growth in Marine Synechococcus spp. PLANT Physiol. **163**: 815–829. doi:10.1104/pp.113.221937

Malmstrom, R. R., S. Rodrigue, K. H. Huang, and others. 2013. Ecology of uncultured Prochlorococcus clades revealed through single-cell genomics and biogeographic analysis. ISME J. **7**: 184–198. doi:10.1038/ismej.2012.89

Marañón, E. 2005. Phytoplankton growth rates in the Atlantic subtropical gyres. Limnol. Oceanogr. **50**: 299–310.

Marañón, E. 2010. Degree of oligotrophy controls the response of microbial plankton to Saharan dust. Limnol. Oceanogr. **55**: 2339–2352. doi:10.4319/lo.2010.55.6.2339

Marañón, E. 2015. Cell Size as a Key Determinant of Phytoplankton Metabolism and Community Structure. Ann. Rev. Mar. Sci. **7**: 241–264. doi:10.1146/annurev-marine-010814-015955

Marañón, E., W. M. Balch, P. Cermeño, and others. 2016. Coccolithophore calcification is independent of carbonate chemistry in the tropical ocean. Limnol. Oceanogr. **61**: 1345–1357. doi:10.1002/lno.10295

Marañón, E., P. Cermeño, M. Latasa, and R. D. Tadonléké. 2015. Resource supply alone explains the variability of marine phytoplankton size structure. Limnol. Oceanogr. **60**: 1848–1854. doi:10.1002/lno.10138

Marañón, E., P. Cermeño, D. C. López-Sandoval, T. Rodríguez-Ramos, C. Sobrino, M. Huete-Ortega, J. M. Blanco, and J. Rodríguez. 2013. Unimodal size scaling of phytoplankton growth and the size dependence of nutrient uptake and use G. Fussmann [ed.]. Ecol. Lett. **16**: 371–379. doi:10.1111/ele.12052

Marañón, E., M. P. Lorenzo, P. Cermeño, and B. Mouriño-Carballido. 2018. Nutrient limitation suppresses the temperature dependence of phytoplankton metabolic rates. ISME J. **12**: 1836–1845. doi:10.1038/s41396-018-0105-1

Margalef, R. 1978. Life-forms of phytoplankton as survival alternatives in an unstable environment. Oceanol. acta **1**: 493–509.

Marie, D., and F. Partensky. 2006. Analyse de micro-organismes marins, p. 211–233. *In* X. RONOT, D. GRUNWALD, J.-F. MAYOL, and J. BOUTONNAT [eds.], La cytométrie en flux. Lavoisier.

Marie, D., F. Rigaut-Jalabert, and D. Vaulot. 2014. An improved protocol for flow cytometry analysis of phytoplankton cultures and natural samples. Cytom. Part A **85**: 962–968. doi:10.1002/cyto.a.22517

Marra, G., and S. N. Wood. 2012. Coverage Properties of Confidence Intervals for Generalized Additive Model Components. Scand. J. Stat. **39**: 53–74. doi:10.1111/j.1467-9469.2011.00760.x

Martin, A. P., M. I. Lucas, S. C. Painter, R. Pidcock, H. Prandke, H. Prandke, and M. C. Stinchcombe. 2010. The supply of nutrients due to vertical turbulent mixing: A study at the Porcupine Abyssal Plain study site in the northeast Atlantic. Deep. Res. Part II Top. Stud. Oceanogr. **57**: 1293–1302. doi:10.1016/j.dsr2.2010.01.006

Martínez-García, S., E. Fernández, X. Álvarez-Salgado, J. González, C. Lønborg, E. Marañón, X. Morán, and E. Teira. 2010. Differential responses of phytoplankton and heterotrophic bacteria to organic and inorganic nutrient additions in coastal waters off the NW Iberian Peninsula. Mar. Ecol. Prog. Ser. **416**: 17–33. doi:10.3354/meps08776

Martiny, A. C., S. Kathuria, and P. M. Berube. 2009. Widespread metabolic potential for nitrite and nitrate assimilation among Prochlorococcus ecotypes. Proc. Natl. Acad. Sci. **106**: 10787–10792. doi:10.1073/pnas.0902532106

Mary, I., G. A. Tarran, P. E. Warwick, M. J. Terry, D. J. Scanlan, P. H. Burkill, and M. V. Zubkov. 2008. Light enhanced amino acid uptake by dominant bacterioplankton groups in surface waters of the Atlantic Ocean. FEMS Microbiol. Ecol. **63**: 36–45. doi:10.1111/j.1574-6941.2007.00414.x

McGillicuddy, D. J. 2016. Mechanisms of Physical-Biological-Biogeochemical Interaction at the Oceanic Mesoscale. Ann. Rev. Mar. Sci. **8**: 125–159. doi:10.1146/annurev-marine-010814-015606

McGillicuddy, D. J., A. R. Robinson, D. A. Siegel, and others. 1998. Influence of mesoscale eddies on new production in the Sargasso Sea. Nature **394**: 263–266. doi:10.1038/28367

Mella-Flores, D., C. Six, M. Ratin, and others. 2012. Prochlorococcus and Synechococcus have Evolved Different Adaptive Mechanisms to Cope with Light and UV Stress. Front. Microbiol. **3**: 1–20. doi:10.3389/fmicb.2012.00285

Moisander, P. H., R. A. Beinart, I. Hewson, A. E. White, K. S. Johnson, C. A. Carlson, J. P. Montoya, and J. P. Zehr. 2010. Unicellular Cyanobacterial Distributions Broaden the Oceanic N2 Fixation Domain. Science (80-.). **327**: 1512–1514. doi:10.1126/science.1185468

Monger, B. C., and M. R. Landry. 1993. Flow cytometric analysis of marine bacteria with hoechst

33342. Appl. Environ. Microbiol. **59**: 905–11.

Moore, C. M., M. M. Mills, K. R. Arrigo, and others. 2013. Processes and patterns of oceanic nutrient limitation. Nat. Geosci. **6**: 701–710. doi:10.1038/ngeo1765

Moore, L., R. Goericke, and S. Chisholm. 1995. Comparative physiology of Synechococcus and Prochlorococcus: influence of light and temperature on growth, pigments, fluorescence and absorptive properties. Mar. Ecol. Prog. Ser. **116**: 259–275. doi:10.3354/meps116259

Moore, L. R., A. Coe, E. R. Zinser, and others. 2007. Culturing the marine cyanobacterium Prochlorococcus. Limnol. Oceanogr. Methods **5**: 353–362. doi:10.4319/lom.2007.5.353

Moore, L. R., A. F. Post, G. Rocap, and S. W. Chisholm. 2002. Utilization of different nitrogen sources by the marine cyanobacteria Prochlorococcus and Synechococcus. Limnol. Oceanogr. **47**: 989–996. doi:10.4319/lo.2002.47.4.0989

Van Mooy, B. A. S., G. Rocap, H. F. Fredricks, C. T. Evans, and A. H. Devol. 2006. Sulfolipids dramatically decrease phosphorus demand by picocyanobacteria in oligotrophic marine environments. Proc. Natl. Acad. Sci. **103**: 8607–8612. doi:10.1073/pnas.0600540103

Morán, X. 2007. Annual cycle of picophytoplankton photosynthesis and growth rates in a temperate coastal ecosystem: a major contribution to carbon fluxes. Aquat. Microb. Ecol. **49**: 267–279. doi:10.3354/ame01151

Morán, X. A. G., L. Alonso-Sáez, E. Nogueira, and others. 2015. More, smaller bacteria in response to ocean's warming? Proc. R. Soc. B Biol. Sci. **282**: 1–9. doi:10.1098/rspb.2015.0371

Morán, X. A. G., Á. López-Urrutia, A. Calvo-Díaz, and W. K. W. Li. 2010. Increasing importance of small phytoplankton in a warmer ocean. Glob. Chang. Biol. **16**: 1137–1144. doi:10.1111/j.1365-2486.2009.01960.x

Moreira-Coello, V., B. Mouriño-Carballido, E. Marañón, and others. 2019. Temporal variability of diazotroph community composition in the upwelling region off NW Iberia. Sci. Rep. **9**: 1–13. doi:10.1038/s41598-019-39586-4

Moreira-Coello, V., B. Mouriño-Carballido, E. Marañón, A. Fernández-Carrera, A. Bode, and M. M. M. Varela. 2017. Biological N2 Fixation in the Upwelling Region off NW Iberia: Magnitude, Relevance, and Players. Front. Mar. Sci. **4**: 1–16. doi:10.3389/fmars.2017.00303

Morel, A., Y.-H. Ahn, F. Partensky, D. Vaulot, and H. Claustre. 1993. <I>Prochlorococcus</I> and <I>Synechococcus</I>: A comparative study of their optical properties in relation to their size and pigmentation. J. Mar. Res. **51**: 617–649. doi:10.1357/0022240933223963

Morel, A., Y. Huot, B. Gentili, P. J. Werdell, S. B. Hooker, and B. a. Franz. 2007. Examining the consistency of products derived from various ocean color sensors in open ocean (Case 1) waters in the perspective of a multi-sensor approach. Remote Sens. Environ. **111**: 69–88. doi:10.1016/j.rse.2007.03.012

Mouillot, D., W. Stubbs, M. Faure, O. Dumay, J. A. Tomasini, J. B. Wilson, and T. Do Chi. 2005. Niche overlap estimates based on quantitative functional traits: a new family of non-parametric indices. Oecologia **145**: 345–353. doi:10.1007/s00442-005-0151-z

Moum, J. N., W. D. Smyth, and J. H. Steele. 2001. Upper Ocean Mixing Processes, p. 3093–3100. *In* Encyclopedia of Ocean Sciences. Academic Press.

Mouriño-Carballido, B., R. Graña, A. Fernández, and others. 2011. Importance of N 2 fixation vs. nitrate eddy diffusion along a latitudinal transect in the Atlantic Ocean. Limnol. Oceanogr. **56**: 999–1007. doi:10.4319/lo.2011.56.3.0999

Mouriño-Carballido, B., E. Hojas, P. Cermeño, and others. 2016. Nutrient supply controls picoplankton community structure during three contrasting seasons in the northwestern Mediterranean Sea. Mar.

Ecol. Prog. Ser. **543**: 1–19. doi:10.3354/meps11558

Mulholland, M. R., and M. W. Lomas. 2008. Nitrogen Uptake and Assimilation, p. 303–384. *In* D. Capone, D. Bronk, M. Mulholl, and E. Carpenter [eds.], Nitrogen in the Marine Environment. Elsevier.

Nakicenovic, N., and R. Swart. 2000. Emission Scenarios IPCC Special Report on Emission Scenarios. Cambridge Univ. Press. 598 598.

Nash, J. D., M. H. Alford, and E. Kunze. 2005. Estimating Internal Wave Energy Fluxes in the Ocean. J. atmoshperic Ocean. Technol. 1551–1570.

Olson, R. J., D. Vaulot, and S. W. Chisholm. 1985. Marine phytoplankton distributions measured using shipboard flow cytometry. Deep Sea Res. Part A. Oceanogr. Res. Pap. **32**: 1273–1280. doi:https://doi.org/10.1016/0198-0149(85)90009-3

Omand, M. M., E. A. D'Asaro, C. M. Lee, M. J. Perry, N. Briggs, I. Cetini, and A. Mahadevan. 2015. Eddy-driven subduction exports particulate organic carbon from the spring bloom. Science (80-.). **348**: 222–225. doi:10.1126/science.1260062

Osborn, T. R. 1980. Estimates of the Local Rate of Vertical Diffusion from Dissipation Measurements. J. Phys. Oceanogr. **10**: 83–89. doi:10.1175/1520-0485(1980)010<0083:EOTLRO>2.0.CO;2

Paerl, H. W. 1997. Coastal eutrophication and harmful algal blooms: Importance of atmospheric deposition and groundwater as "new" nitrogen and other nutrient sources. Limnol. Oceanogr. **42**: 1154–1165. doi:10.4319/lo.1997.42.5_part_2.1154

Paerl, H. W., R. L. Dennis, and D. R. Whitall. 2002. Atmospheric deposition of nitrogen: Implications for nutrient over-enrichment of coastal waters. Estuaries **25**: 677–693. doi:10.1007/BF02804899

Paerl, H. W., W. S. Gardner, K. E. Havens, A. R. Joyner, M. J. McCarthy, S. E. Newell, B. Qin, and J. T. Scott. 2016. Mitigating cyanobacterial harmful algal blooms in aquatic ecosystems impacted by climate change and anthropogenic nutrients. Harmful Algae **54**: 213–222. doi:10.1016/j.hal.2015.09.009

Painter, S. C., M. D. Patey, A. Forryan, and S. Torres-Valdes. 2013. Evaluating the balance between vertical diffusive nitrate supply and nitrogen fixation with reference to nitrate uptake in the eastern subtropical North Atlantic Ocean. J. Geophys. Res. Ocean. **118**: 5732–5749. doi:10.1002/jgrc.20416

Partensky, F., J. Blanchot, and D. Vaulot. 1999. Differential distribution and ecology of Prochlorococcus and Synechococcus in oceanic waters : a review. Bull. l'Institut océanographique **19**: 457–475.

Partensky, F., and L. Garczarek. 2010. Prochlorococcus : Advantages and Limits of Minimalism. Ann. Rev. Mar. Sci. **2**: 305–331. doi:10.1146/annurev-marine-120308-081034

Paulsen, M. L., H. Doré, L. Garczarek, L. Seuthe, O. Müller, R.-A. Sandaa, G. Bratbak, and A. Larsen. 2016. Synechococcus in the Atlantic Gateway to the Arctic Ocean. Front. Mar. Sci. **3**: 1–14. doi:10.3389/fmars.2016.00191

Pinhassi, J., E. F. DeLong, O. Béjà, J. M. González, and C. Pedrós-Alió. 2016. Marine Bacterial and Archaeal Ion-Pumping Rhodopsins: Genetic Diversity, Physiology, and Ecology. Microbiol. Mol. Biol. Rev. **80**: 929–954. doi:10.1128/MMBR.00003-16

Planas, D., S. Agustí, C. M. Duarte, T. C. Granata, and M. Merino. 1999. Nitrate uptake and diffusive nitrate supply in the Central Atlantic. Limnol. Oceanogr. **44**: 116–126. doi:10.4319/lo.1999.44.1.0116

Porter, K. K. G., and Y. Y. S. Feig. 1980. The use of DAPI for identifying and counting aquatic microflora 1. Limnol. Oceanogr. **25**: 943–948.

Prandke, H., and A. Stips. 1998a. Microstructure profiler to study mixing and turbulent transport

processes. Ocean. Conf. Proc. 179–183.

Prandke, H., and A. Stips. 1998b. Test measurements with an operational microstructure-turbulence profiler: Detection limit of dissipation rates. Aquat. Sci. **60**: 191–209. doi:10.1007/s000270050036

R Core Team. 2015. R: A Language and Environment for Statistical Computing.

Randelhoff, A., F. Ilker, A. Sundfjord, J.-E. Tremblay, and M. Reigstad. 2016. Vertical fluxes of nitrate in the seasonal nitracline of the Atlantic sector of the Arctic Ocean. J. Geophys. Res. Ocean. 2286–2313. doi:10.1002/2015JC011486.Received

Raven, J. A. 1986. Physiological consequences of extremely small size for autotrophic organisms in the sea. Photosynth. Picoplankton. Can. Bull. Fish. Aquat. Sci. **214**: 1–70.

Raven, J. A. 1994. Why are there no picoplanktonic O 2 evolvers with volumes less than 10 −19 m 3 ? J. Plankton Res. **16**: 565–580. doi:10.1093/plankt/16.5.565

Raven, J. A. 1998. The twelfth Tansley Lecture. Small is beautiful: the picophytoplankton. Funct. Ecol. **12**: 503–513. doi:10.1046/j.1365-2435.1998.00233.x

Reckermann, M., and M. J. W. Veldhuis. 1997. Trophic interactions between picophytoplankton and micro- And nanozooplankton in the western Arabian Sea during the NE monsoon 1993. Aquat. Microb. Ecol. **12**: 263–273. doi:10.3354/ame012263

Redfield, A. C. 1958. The biological control of chemical factors in the environment. Am. Sci **46**: 205–221.

Richardson, T. L., and G. a Jackson. 2007. Small Phytoplankton and Carbon Export from the Surface Ocean. Science (80-.). **315**: 838–840. doi:10.1126/science.1133471

Riemann, L., H. Farnelid, and G. F. Steward. 2010. Nitrogenase genes in non-cyanobacterial plankton: Prevalence, diversity and regulation in marine waters. Aquat. Microb. Ecol. **61**: 235–247. doi:10.3354/ame01431

Ripley, B. D. 1996. Pattern Recognition and Neural Networks, Cambridge University Press.

Rippeth, T. P. 2005. Mixing in seasonally stratified shelf seas: A shifting paradigm. Philos. Trans. R. Soc. A Math. Phys. Eng. Sci. **363**: 2837–2854. doi:10.1098/rsta.2005.1662

Rippeth, T. P., M. R. Palmer, J. H. Simpson, N. R. Fisher, and J. Sharples. 2005. Thermocline mixing in summer stratified continental shelf seas. Geophys. Res. Lett. **32**: 1–4. doi:10.1029/2004GL022104

Rippeth, T. P., P. Wiles, M. R. Palmer, J. Sharples, and J. Tweddle. 2009. The diapcynal nutrient flux and shear-induced diapcynal mixing in the seasonally stratified western Irish Sea. Cont. Shelf Res. **29**: 1580–1587. doi:10.1016/j.csr.2009.04.009

Rippka, R., T. Coursin, W. Hess, and others. 2000. Prochlorococcus marinus Chisholm et al. 1992 subsp. pastoris subsp. nov. strain PCC 9511, the first axenic chlorophyll a2/b2 -containing cyanobacterium (Oxyphotobacteria). Int. J. Syst. Evol. Microbiol. **50**: 1833–1847.

Ritz, C., and J. C. Streibig. 2005. Bioassay Analysis using R. J. Stat. Softw. **12**: 1–22. doi:10.18637/jss.v012.i05

Rusch, D. B., A. C. Martiny, C. L. Dupont, A. L. Halpern, and J. C. Venter. 2010. Characterization of Prochlorococcus clades from iron-depleted oceanic regions. Proc. Natl. Acad. Sci. **107**: 16184–16189. doi:10.1073/pnas.1009513107

Sakamoto, C. M. 2004. Influence of Rossby waves on nutrient dynamics and the plankton community structure in the North Pacific subtropical gyre. J. Geophys. Res. **109**: C05032. doi:10.1029/2003JC001976

Sandel, V., R. Kiko, P. Brandt, M. Dengler, L. Stemmann, P. Vandromme, U. Sommer, and H. Hauss.

2015. Nitrogen fuelling of the pelagic food web of the Tropical Atlantic. PLoS One **10**. doi:10.1371/journal.pone.0131258

Sangrà, P., C. García-Muñoz, C. García, and others. 2014. Coupling between upper ocean layer variability and size-fractionated phytoplankton in a non-nutrient-limited environment. Mar. Ecol. Prog. Ser. **499**: 35–46. doi:10.3354/meps10668

Sarmiento, J. L., and N. Gruber. 2013. Organic Matter Production, p. 102–172. *In* Ocean Biogeochemical Dynamics. Princeton University Press.

Sarthou, G., K. R. Timmermans, S. Blain, and P. Tréguer. 2005. Growth physiology and fate of diatoms in the ocean: a review. J. Sea Res. **53**: 25–42. doi:10.1016/j.seares.2004.01.007

Scanlan, D. J., and N. J. West. 2002. Molecular ecology of the marine cyanobacterial genera Prochlorococcus and Synechococcus. FEMS Microbiol. Ecol. **40**: 1–12. doi:10.1111/j.1574-6941.2002.tb00930.x

Schafstall, J., M. Dengler, P. Brandt, and H. Bange. 2010. Tidal-induced mixing and diapycnal nutrient fluxes in the Mauritanian upwelling region. J. Geophys. Res. Ocean. **115**. doi:10.1029/2009JC005940

Schattenhofer, M., J. Wulf, I. Kostadinov, F. O. Glöckner, M. V. Zubkov, and B. M. Fuchs. 2011. Phylogenetic characterisation of picoplanktonic populations with high and low nucleic acid content in the North Atlantic Ocean. Syst. Appl. Microbiol. **34**: 470–475. doi:10.1016/j.syapm.2011.01.008

Schott, F., M. Visbeck, U. Send, J. Fischer, L. Stramma, and Y. Desaubies. 1996. Observations of Deep Convection in the Gulf of Lions, Northern Mediterranean, during the Winter of 1991/92. J. Phys. Oceanogr. **26**: 505–524. doi:10.1175/1520-0485(1996)026<0505:OODCIT>2.0.CO;2

Sharples, J., J. J. Middelburg, K. Fennel, and T. D. Jickells. 2017. What proportion of riverine nutrients reaches the open ocean? Global Biogeochem. Cycles **31**: 39–58. doi:10.1002/2016GB005483

Sharples, J., C. M. Moore, and R. Abraham. 2001. Internal tide dissipation, mixing, and vertical nitrate flux. J. Geophys. Res. **106**: 69–81.

Sharples, J., J. F. Tweddle, J. A. Mattias Green, and others. 2007. Spring-neap modulation of internal tide mixing and vertical nitrate fluxes at a shelf edge in summer. Limnol. Oceanogr. **52**: 1735–1747. doi:10.4319/lo.2007.52.5.1735

Sheldon, R. W., and T. R. Parsons. 1967. A continuous size spectrum for particulate matter in the sea. J. Fish. Board Canada **24**: 909–915.

Sherr, E. B., B. F. Sherr, and P. A. Wheeler. 2005. Distribution of coccoid cyanobacteria and small eukaryotic phytoplankton in the upwelling ecosystem off the Oregon coast during 2001 and 2002. Deep Sea Res. Part II Top. Stud. Oceanogr. **52**: 317–330. doi:10.1016/j.dsr2.2004.09.020

Simpson, J. H., J. Brown, J. Matthews, and G. Allen. 1990. Tidal Straining, Density Currents, and Stirring in the Control of Estuarine Stratification. Estuaries **13**: 125. doi:10.2307/1351581

Six, C., and J. Thomas. 2004. Photophysiology of the marine cyanobacterium Synechococcus sp. WH8102, a new model organism. Aquat. Microb. Ecol. **35**: 17–29.

Smayda, T. J. 1971. Normal and accelerated sinking of phytoplankton in the sea. Mar. Geol. **11**: 105–122. doi:10.1016/0025-3227(71)90070-3

Smayda, T. J. 1980. Phytoplankton species succession., p. 493–570. *In* I. Morris [ed.], The physiological ecology of phytoplankton. Blackwell Scientific Publications.

Smeti, E., D. L. Roelke, and S. Spatharis. 2016. Spatial averaging and disturbance lead to high productivity in aquatic metacommunities. Oikos **125**: 812–820. doi:10.1111/oik.02684

Sommaruga, R., J. S. Hofer, L. Alonso-Saez, and J. M. Gasol. 2005. Differential Sunlight Sensitivity of Picophytoplankton from Surface Mediterranean Coastal Waters. Appl. Environ. Microbiol. **71**: 2154–2157. doi:10.1128/AEM.71.4.2154-2157.2005

Sommer, U. 1986. Phytoplankton competition along a gradient of dilution rates. Oecologia **68**: 503–506. doi:10.1007/BF00378762

Sommer, U. 1989. The Role of Competition for Resources in Phytoplankton Succession, p. 57–106. *In* U. Sommer [ed.], Plankton Ecology: Succession in Plankton Communities. Springer Berlin Heidelberg.

Steinhoff, T., T. Friedrich, S. E. Hartman, A. Oschlies, D. W. R. Wallace, and A. Körtzinger. 2010. Estimating mixed layer nitrate in the North Atlantic Ocean. Biogeosciences **7**: 795–807. doi:10.5194/bg-7-795-2010

Stolte, W., and R. Riegman. 1995. Effect of phytoplankton cell size on transient-state nitrate and ammonium uptake kinetics. Microbiology **141**: 1221–1229. doi:10.1099/13500872-141-5-1221

Sundfjord, A., I. Fer, Y. Kasajima, and H. Svendsen. 2007. Observations of turbulent mixing and hydrography in the marginal ice zone of the Barents Sea. J. Geophys. Res. Ocean. **112**: 1–23. doi:10.1029/2006JC003524

Switzer, A. C., D. Kamykowski, and S.-J. Zentara. 2003. Mapping nitrate in the global ocean using remotely sensed sea surface temperature. J. Geophys. Res. **108**: 3280. doi:10.1029/2000JC000444

Takahashi, T., S. C. Sutherland, R. Wanninkhof, and others. 2009. Climatological mean and decadal change in surface ocean pCO2, and net sea–air CO2 flux over the global oceans. Deep Sea Res. Part II Top. Stud. Oceanogr. **56**: 554–577. doi:10.1016/j.dsr2.2008.12.009

Takeya, K., A. Kuwata, M. Yoshida, and T. Miyazaki. 2004. Effect of dilution rate on competitive interactions between the cyanobacterium Microcystis novacekii and the green alga Scenedesmus quadricauda in mixed chemostat cultures. J. Plankton Res. **26**: 29–35. doi:10.1093/plankt/fbh005

Tang, W., S. Wang, D. Fonseca-Batista, and others. 2019. Revisiting the distribution of oceanic N 2 fixation and estimating diazotrophic contribution to marine production. Nat. Commun. **10**: 1–10. doi:10.1038/s41467-019-08640-0

Teira, E., V. Hernando-Morales, A. Fernández, S. Martínez-García, X. Álvarez-Salgado, A. Bode, and M. Varela. 2015. Local differences in phytoplankton-bacterioplankton coupling in the coastal upwelling off Galicia (NW Spain). Mar. Ecol. Prog. Ser. **528**: 53–69. doi:10.3354/meps11228

Teira, E., B. Mouriño-Carballido, S. Martínez-García, C. Sobrino, J. Ameneiro, S. Hernández-León, and E. Vázquez. 2012. Primary production and bacterial carbon metabolism around South Shetland Islands in the Southern Ocean. Deep. Res. Part I Oceanogr. Res. Pap. **69**: 70–81. doi:10.1016/j.dsr.2012.07.002

Teira, E., M. J. Pazo, P. Serret, E. Fernandez, M. J. Pazó, P. Serret, and E. Fernández. 2001. Dissolved organic carbon production by microbial populations in the Atlantic Ocean. Limnol. Oceanogr. **46**: 1370–1377. doi:10.4319/lo.2001.46.6.1370

Thorpe, S. A. 2004. LANGMUIR CIRCULATION. Annu. Rev. Fluid Mech. **36**: 55–79. doi:10.1146/annurev.fluid.36.052203.071431

Thorpe, S. A. S. A. 2007. An introduction to ocean turbulence, Cambridge University Press.

Tilman, D. 1977. Resource competition between plankton algae: an experimental and theoretical approach. Ecology **58**: 338–348. doi:10.2307/1935608

Tilman, D. 1980. Resources: A Graphical-Mechanistic Approach to Competition and Predation. Am. Nat. **116**: 362–393. doi:10.1086/283633

Tilman, D. 1982. Resource competition and community structure.,.

Tozzi, S., O. M. Schofield, and P. G. Falkowski. 2004. Historical climate change and ocean turbulence as selective agents for two key phytoplankton functional groups. Mar. Ecol. Prog. Ser. **274**: 123–132.

Tremblay, J.-E., L. L. Bert Klein, R. B. . Rivkin, and J.-C. T. Source. 1997. Estimation of f-Ratios in Oceans Based on Phytoplankton Size Structure. Limnol. Oceanogr. **42**: 595–601.

Tweddle, J. F., J. Sharples, M. R. Palmer, K. Davidson, and S. McNeill. 2013. Enhanced nutrient fluxes at the shelf sea seasonal thermocline caused by stratified flow over a bank. Prog. Oceanogr. **117**: 37–47. doi:10.1016/j.pocean.2013.06.018

Uitz, J., Y. Huot, F. Bruyant, M. Babin, and H. Claustre. 2008. Relating phytoplankton photophysiological properties to community structure on large scales. Limnol. Oceanogr. **53**: 614–630. doi:10.4319/lo.2008.53.2.0614

Venables, W. N., and B. D. Ripley. 2002. Modern Applied Statistics with S, Fourth. Springer.

Vila-Costa, M., J. M. Gasol, S. Sharma, and M. A. Moran. 2012. Community analysis of high- and low-nucleic acid-containing bacteria in NW Mediterranean coastal waters using 16S rDNA pyrosequencing. Environ. Microbiol. **14**: 1390–1402. doi:10.1111/j.1462-2920.2012.02720.x

Villamaña-Rodríguez, M., B. Mouriño-Carballido, P. Cermeño, and others. 2015. Role of internal waves on mixing, nutrient supply and phytoplankton composition during spring and neap tides in the Ría de Vigo (NW Iberian Peninsula). *Aquatic Science Meeting, Granada (Spain)*.

Villamaña, M., P. J. S. Franks, B. Fernández-Castro, M. Gilcoto, E. Marañón, and B. Mouriño-Carballido. 2019a. A pseudo-Lagrangian transformation to study the spatial structure of a fluorescence patch in the Ría de Vigo (NW Iberian Peninsula). Prep.

Villamaña, M., E. Marañón, P. Cermeño, and others. 2019b. The role of mixing in controlling resource availability and phytoplankton community composition. Prog. Oceanogr. **178**: 102181. doi:10.1016/j.pocean.2019.102181

Villamaña, M., B. Mouriño-Carballido, E. Marañón, and others. 2017. Role of internal waves on mixing, nutrient supply and phytoplankton community structure during spring and neap tides in the upwelling ecosystem of Ría de Vigo (NW Iberian Peninsula). Limnol. Oceanogr. **62**: 1014–1030. doi:10.1002/lno.10482

Volk, T., and M. I. Hoffert. 2013. Ocean Carbon Pumps: Analysis of Relative Strengths and Efficiencies in Ocean-Driven Atmospheric CO 2 Changes, p. 99–110. *In*.

Voss, M., H. W. Bange, J. W. Dippner, J. J. Middelburg, J. P. Montoya, and B. Ward. 2013. The marine nitrogen cycle: Recent discoveries, uncertaintiesand the potential relevance of climate change. Philos. Trans. R. Soc. B Biol. Sci. **368**. doi:10.1098/rstb.2013.0121

Walsh, J. J., T. E. Whitledge, F. W. Barvenik, C. D. Wirick, S. O. Howe, W. E. Esaias, and J. T. Scott. 1978. Wind events and food chain dynamics within the New York Bight 1, 2. Limnol. Oceanogr. **23**: 659–683. doi:10.4319/lo.1978.23.4.0659

Ward, B. A., E. Marañón, B. Sauterey, J. Rault, and D. Claessen. 2017. The size dependence of phytoplankton growth rates: A trade-off between nutrient uptake and metabolism. Am. Nat. **189**: 170–177. doi:10.1086/689992

Waterbury, J. B., S. W. Watson, R. R. L. Guillard, and L. E. Brand. 1979. Widespread occurrence of a unicellular, marine, planktonic, cyanobacterium [10]. Nature **277**: 293–294. doi:10.1038/277293a0

Williams, C., J. Sharples, M. Green, C. Mahaffey, and T. Rippeth. 2013a. The maintenance of the subsurface chlorophyll maximum in the stratified western Irish Sea. Limnol. Oceanogr. Fluids Environ. **3**: 61–73. doi:10.1215/21573689-2285100

Williams, C., J. Sharples, C. Mahaffey, and T. Rippeth. 2013b. Wind-driven nutrient pulses to the subsurface chlorophyll maximum in seasonally stratified shelf seas. Geophys. Res. Lett. **40**: 5467–5472. doi:10.1002/2013GL058171

Williams, R. G., and M. J. Follows. 1998. The Ekman transfer of nutrients and maintenance of new production over the North Atlantic. Deep. Res. Part I Oceanogr. Res. Pap. **45**: 461–489. doi:10.1016/S0967-0637(97)00094-0

Winkler, M. K. H., P. Boets, B. Hahne, P. Goethals, and E. I. P. Volcke. 2017. Effect of the dilution rate on microbial competition: R-strategist can win over kstrategist at low substrate concentration. PLoS One **12**: 1–12. doi:10.1371/journal.pone.0172785

Wood, S. N. 2011. Fast stable restricted maximum likelihood and marginal likelihood estimation of semiparametric generalized linear models. J. R. Stat. Soc. Ser. B (Statistical Methodol. **73**: 3–36. doi:10.1111/j.1467-9868.2010.00749.x

Wood, S. N. 2017. Generalized Additive Models, Chapman and Hall/CRC.

Wood, S. N., N. Pya, and B. Säfken. 2016. Smoothing Parameter and Model Selection for General Smooth Models. J. Am. Stat. Assoc. **111**: 1548–1563. doi:10.1080/01621459.2016.1180986

Wooster, W. S., A. Bakun, and R. M. McLain. 1976. Seasonal upwelling cycle along the Eastern boundary of the North Atlantic. J. Mar. Res. **34**: 131–141.

Worden, A. Z., J. Lee, T. Mock, and P. Rouzé. 2009. Green evolution and dynamic adaptations revealed by genomes of the marine picoeukaryotes Micromonas. Science (80-.). **375**: 268–272.

Worden, A. Z., J. K. Nolan, and B. Palenik. 2004. Assessing the dynamics and ecology of marine picophytoplankton: The importance of the eukaryotic component. Limnol. Oceanogr. **49**: 168–179. doi:10.4319/lo.2004.49.1.0168

Wyatt, T. 2014. Margalef's mandala and phytoplankton bloom strategies. Deep. Res. Part II Top. Stud. Oceanogr. **101**: 32–49. doi:10.1016/j.dsr2.2012.12.006

Yool, A., A. P. Martin, C. Fernández, and D. R. Clark. 2007. The significance of nitrification for oceanic new production. Nature **447**: 999–1002. doi:10.1038/nature05885

Zehr, J. P., E. J. Carpenter, and T. A. Villareal. 2000. New perspectives on nitrogen-fixing microorganisms in tropical and subtropical oceans. Trends Microbiol. **8**: 68–73. doi:10.1016/S0966-842X(99)01670-4

Zehr, J. P., B. D. Jenkins, S. M. Short, and G. F. Steward. 2003. Nitrogenase gene diversity and microbial community structure: A cross-system comparison. Environ. Microbiol. **5**: 539–554. doi:10.1046/j.1462-2920.2003.00451.x

Zhang, J. Z., M. O. Baringer, C. J. Fischer, and V. J. A. Hooper. 2017. An estimate of diapycnal nutrient fluxes to the euphotic zone in the Florida Straits. Sci. Rep. **7**: 1–8. doi:10.1038/s41598-017-15853-0

Zhang, Z. 2016. Multivariable fractional polynomial method for regression model. Ann. Transl. Med. **4**: 174–174. doi:10.21037/atm.2016.05.01

Zimmermann, R. 1977. Estimation of bacterial number and biomass by epifluorescence microscopy and scanning electron microscopy, p. 103–120. *In* Microbial ecology of a brackish water environment. Springer.

Zubkov, M. V., M. A. Sleigh, P. H. Burkill, and R. J. G. Leakey. 2000. Picoplankton community structure on the Atlantic Meridional Transect: a comparison between seasons. Prog. Oceanogr. **45**: 369–386. doi:10.1016/S0079-6611(00)00008-2

Chapter 7

Summary in Spanish/Resumen en español

Introducción

El fitoplancton es responsable de aproximadamente el 90% de la producción primaria que tiene lugar en el océano, que representa casi la mitad de la producción primaria de la biosfera, y por lo tanto desempeña un papel clave en el intercambio de dióxido de carbono y otros gases radiativamente activos entre el océano y la atmósfera (Field et al. 1998; Falkowski 2012). Aunque la mayor parte de la producción primaria marina se recicla rapidamente dentro de la capa del océano iluminada por el sol, una fracción de esta producción primaria se hunde en las profundidades oceánicas. Esta exportación de materia orgánica hacia las capas profundas crea un déficit de carbono inorgánico en la parte superior del océano que se compensa por la entrada de CO_2 desde la atmósfera, dando lugar al proceso conocido como bomba biológica (Volk and Hoffert 2013; Sarmiento and Gruber 2013).

El nitrogeno es el principal nutriente limitante en la mayor parte de las regiones tropicales y subtropicales del océano abierto, así como en mares templados y polares durante períodos de estratificación estacional (Moore et al. 2013). Dado que una parte de la producción biológica en la capa fótica se exporta cara el oceano profundo (exportación), el mantenimiento de la producción biológica dependara de la entrada de nutrientes al sistema (producción nueva). Los mecanismos que contribuyen a la nueva producción incluyen la fijación biológica del nitrógeno, la deposición atmosférica (Paerl 1997; Paerl et al. 2002; Marañón 2010; Martínez-García et al. 2010) y el transporte vertical y horizontal difusivo y advectivo de formas orgánicas e inorgánicas de nitrógeno.

El cálculo del transporte difusivo vertical requiere de la estimación de la difusividad (Kz). Las dificultades metodológicas en la obtención de estimas de Kz motivaron la utilización de valores constantes de Kz (Capone et al. 2005), y parametrizaciones empíricas de difusividad vertical (Planas et al. 1999). Sin embargo, la comercialización de los perfiladores de turbulencia de microestructura ha facilitado la obtención de observaciones de turbulencia de microstructura, que revelaron una importante variabilidad de Kz en la capa superior del océano (Hibiya et al. 2007; Mouriño-Carballido et al. 2011, 2016; Jurado et al. 2012; Cuypers et al. 2012; Fernández-Castro et al. 2014; Villamaña et al. 2017; Bendtsen and Richardson 2018). Alternativamente se ha utilizado la concentración de nutrientes inorgánicos disueltos en la capa fótica como un estimador de la disponibilidad de nutrientes para las comunidades planctonicas (Agawin et al. 2000; Flombaum et al. 2013). Sin embargo, en condiciones de estado estacionario, como los giros subtropicales, donde el suministro de nutrientes por difusión hacia la zona eufótica es

lento puede no existir relación entre la concentración de nutrientes en la capa fótica y su suministro (Mouriño-Carballido et al. 2016).

El picoplancton hace referencia a la fracción del plancton menor de 2 µm y está constituido por *Synechococcus* (Waterbury et al. 1979), picoeukaryotes (Johnson and Sieburth 1982), *Prochlorococcus* (Chisholm et al. 1988) y bacterias heterótrofas. Estas últimas se pueden dividir entre bacterias con alto (HNA) o bajo (LNA) contenido en acidos nucleicos (Gasol and Del Giorgio 2000). Generalmente el picoplancton fotosintético domina la biomasa y la producción primaria en regiones oligotróficas tropicales y subtropicales (Chisholm 1992), mientras que su contribución es menor en regiones costeras ricas en nutrientes (Finkel et al. 2010; Marañón et al. 2015).

Prochlorococcus tiende a restringirse a aguas relativamente cálidas y pobres en nutrientes, a lo largo de la banda latitudinal 40N-40S (Partensky et al. 1999; Johnson et al. 2006). *Synechococcus* exhibe una distribución geográfica más amplia, incluyendo aguas ricas en nutrientes y ocasionalmente alcanzando latitudes polares (Paulsen et al. 2016). La contribución de los picoeucariotas a la biomasa de picoplancton es generalmente menor que la contribución de las cianobacterias (Zubkov et al. 2000; Buitenhuis et al. 2012) excepto en las regiones costeras donde su contribución suele aumentar (Grob et al. 2007). En general, los procariotas de bajo contenido en ácidos nucleicos (LNA) dominan la biomasa procariótica heterótrofa en el océano abierto oligotrófico, mientras que los de alto contenido (HNA) dominan en las regiones costeras (Li et al. 1995; Bouvier et al. 2007). Las diferentes distribuciones espaciales de estos subgrupos sugieren que estos ocupan diferentes nichos ecológicos. Sin embargo, a pesar de décadas de observaciones, por el momento se desconoce la importancia relativa de los factores que controlan su crecimiento y distribución espacial.

En los ecosistemas marinos, una fuente importante de heterogeneidad ambiental radica en la fluctuación temporal del suministros de nutrientes, que controla la diversidad de la comunidad de fitoplancton (Sommer 1989; Fawcett et al. 2011; Smeti et al. 2016). En condiciones de estado estacionario, el nivel mínimo de un recurso que puede sostener una población determina la competencia. Estudios experimentales y modelos numéricos de competición apoyan esta base teórica para el fitoplancton de gran tamaño (Tilman 1977, 1982; Sommer 1986; Stolte and Riegman 1995; Takeya et al. 2004; Tozzi et al. 2004; Cermeño et al. 2011; Winkler et al. 2017). Mientras que numerosos estudios han investigado el efecto de la dinámica del suministro

de nutrientes sobre la competencia interespecífica de especies de fitoplancton de gran tamaño, su efecto sobre los grupos que componen el picofitoplancton ha recibido mucha menos atención (Mouriño-Carballido et al. 2016; Villamaña et al. 2019b).

Hipótesis y objetivos

La hipótesis principal de esta tesis es que la dinámica del suministro de nutrientes controla la composición de las comunidades de picoplancton marino.

Para verificar esta hipótesis, se plantean los siguientes objetivos específicos:

1. Cuantificar el papel de la temperatura, la luz y el suministro de nitrato en la distribución de los subgrupos de picoplancton autotrófico y heterótrofo.

2. Describir los nichos ecológicos de los diferentes subgrupos de la comunidad del picoplancton.

3. Explorar el efecto de la dinámica de suministro de nitrato en la dinámica competitiva de dos especies de picofitoplancton marino: la cianobacteria *Synechoccocus sp.* y el picoeucariota *Micromonas pusilla*.

4. Construir un modelo predictivo y obtener la primera climatología del transporte difusivo de nitrato hacia la zona eufótica.

5. Predecir el cambio en la estructura de las comunidades de picoplancton (la relación entre cianobacterias y picoeucariotas) en un escenario futuro de cambio global.

Para lograr estos objetivos, utilizaré un enfoque multidisciplinar, combinando observaciones de campo realizadas durante 17 campañas oceanográficos realizadas en los océanos Atlántico, Pacífico e Índico tropicales y subtropicales, el Mar Mediterráneo Noroccidental, el ecosistema de afloramiento costero gallego y la Peninsula Antártica con experimentos de laboratorio y modelado ecológico de interacciones competitivas.

La tesis está estructurada de la siguiente manera. En el Capítulo II se evalúan los principales factores físicos que controlan la estructura de la comunidad de picoplancton en distintos ambientes marinos. En el Capítulo III se evalúa la dinámica competitiva de *Synechococcus* y un picoeucariota modelo (*Micromonas pusilla*) utilizando experimentos de competición por ni-

trato en biorreactores, experimentos de captación y modelos fisilogico del plancton. En el Capítulo IV se presentan datos aproximados del suministro de nitratos a nivel mundial y regional. Asimismo, se infieren estimaciones mundiales de las distribuciones oceánicas actuales y futuras de los subgrupos de picoplancton, basadas en los modelos de regresión presentados en el Capítulo II. Por último, en el Capítulo V se presentan las principales conclusiones de esta tesis.

Factores que controlan la estructura de la comunidad del picoplancton en distintos ambientes marinos

Aparte del efecto del control trófico, la distribución del plancton microbiano está primariamente determinada por la temperatura del agua de mar, la luz y los nutrientes (Li 2002, 2009; Barton et al. 2015). Cuantificar su influencia relativa en la distribución espacial y temporal de los diferentes grupos de picoplancton es complicado por el hecho de que dichos factores están a menudo correlacionados en el océano (Finkel et al. 2010). Por otro lado, tradicionalmente el efecto de los nutrientes inorgánicos sobre el plancton ha sido medido sobre las concentraciones y no sobre las estimaciones del suministro de nutrientes (Agawin et al. 2000; Flombaum et al. 2013). En este capitulo, se han combinado datos hidrográficos, de mezcla turbulenta, de concentración de nutrientes y de composición de la comunidad de picoplancton con el objetivo de (i) cuantificar el papel de la temperatura, la luz y el flujo de nitrato sobre la distribución de los grupos de picoplancton autotróficos y heterótrofos, determinados por citometría de flujo, y (ii) describir los nichos ecológicos de los diversos componentes de la comunidad de picoplancton. Se han recogido datos en 97 estaciones en el Océano Atlántico, incluyendo aguas tropicales y subtropicales en mar abierto, el noroeste del Mediterráneo y el sistema gallego de afloramiento costero del noroeste de la Península Ibérica. Se han utilizado modelos aditivo generalizado (Wood 2017) para predecir la biomasa integrada en profundidad de cada subgrupo de picoplancton sobre la base de tres predictores de nicho: temperatura superficial del mar, irradiancia superficial media diaria y el transporte de nitrato hacia la zona eufótica, tanto por difusión como por advección. Además, la superposición de nichos entre diferentes subgrupos de picoplancton se calculó utilizando funciones no paramétricas de densidad del núcleo (Mouillot et al. 2005). La temperatura y el suministro de nitrato fueron más relevantes que la luz en la predicción de la biomasa de la mayoría de los subgrupos de picoplancton, excepto en el caso de *Prochlorococcus* y procariotas de bajo contenido en ácido nucleico (LNA), para los cuales la irradiancia

también jugó un papel significativo. Por otro lado, el suministro de nitrato fue el único factor que permitió la distinción entre los nichos ecológicos de todos los subgrupos de picoplancton autotrófico y heterótrofo. Tanto *Prochlorococcus* como los procariotas de LNA fueron más abundantes en aguas cálidas (>20 ºC), caracterizadas por los flujos bajos de nitrato; mientras que *Synechococcus* y los procariotas de alto contenido en ácido nucleico (HNA) prevalecieron principalmente en ambientes más fríos caracterizados por niveles intermedios o altos de suministro de nitratos. Finalmente, el nicho de los picoeucariotas se definió por las bajas temperaturas y un elevado suministro de nitrato. Estos resultados apoyan el papel clave del suministro de nitrato, ya que no sólo promueve el crecimiento del fitoplancton a gran escala, sino que también determina la estructura de las comunidades de picoplancton marino.

Dinamica competitiva entre la cianobacteria *Synechococcus* y el picoeucariota *Micromonas pusilla* bajo una dinámica variable de suministro de nutrientes

El picoplancton fotosintético (<2 μm de diámetro esférico equivalente), también conocido como picofitoplancton, domina la biomasa autotrófica y la producción primaria en grandes regiones del océano tropical y subtropical (Chisholm 1992), sin embargo suelen ser un componente minoritario en regiones con un alto contenido en nutrientes, usualmente dominadas por grupos de mayor tamaño (Finkel et al. 2010; Marañón et al. 2015). Estudios previos sugieren que algunos grupos del picofitoplancton pueden contribuir significativamente a la producción nueva en estas regiones oceánicas (Richardson and Jackson 2007; Lomas and Moran 2011; Guidi et al. 2016). Sin embargo, nuestra comprensión de los mecanismos ecológicos subyacentes a los patrones de distribución espacial y temporal de los diferentes grupos de picofitoplancton es muy limitada. De acuerdo con la teoría de la competición por recursos (Gause 1932; MacArthur 1972; Tilman 1980, 1982), la especie con el requisito más bajo para el recurso más limitado será la mejor competidora en un sistema en estado estacionario, es decir, cuando la condición de limitación de recursos se mantiene a lo largo del tiempo. Sin embargo, el resultado de la competencia podría cambiar si el sistema se desvía del estado estacionario, que es el escenario más habitual en el océano superficial. Margalef (1978) demostró que el aporte de energía externa a los ecosistemas de plancton determina la sucesión ecológica de dinoflagelados, cocolitóforos y diatomeas, reconociendo que estos tres grupos funcionales de fitoplancton distintos responden de

manera diferente a los regímenes variables de suministro de nutrientes. Tanto experimentos de competición por nutrientes (Grover 1991; Cermeño et al. 2011) como modelado teórico (Tozzi et al. 2004) respaldan esta teoría en el plancton de gran tamaño. Con el fin de medir el efecto que tienen los nutrientes en estructura de la comunidad de picofitoplancton; dos cepas de picofitoplancton, la cianobacteria *Synechococcus* sp. y el picoeucariota *Micromonas pusilla*, fueron seleccionadas para realizar experimentos de competición por nutriente en fotobiorreactores. Estos experimentos fueron diseñados para simular diferentes escenarios de suministro de nitratos que van desde el suministro continuo hasta el intermitente (0, 0.5, 1, 2, 3 pulsos de nitrato por día). Complementariamente también se realizaron experimentos para determinar experimentalmente las tasas de captación de nitrato, el crecimiento y la estequiometría del carbono y nitrógeno de ambas cepas. En el estado estacionario, es decir, el suministro continuo, *M. pusilla* fue superada por *Synechococcus* sp. Sin embargo, el cambio de régimen hacia condiciones de pulsos de nitrato (es decir, no estacionario) o el aumento de las tasas de dilución del cultivo, llevó a la exclusión de *Synechococcus* sp. La tasa de exclusión competitiva fue una función lineal de la frecuencia de los pulsos de nitrato. Posteriomente, utilizando los parámetros fisiológicos que describen la cinética de captación de nitratos de cada una de las cepas seleccionadas, se llevaron a cabo simulaciones de modelos fisiológicos del proceso competitivo para expandir teóricamente nuestros ensayos experimentales a un rango más amplio de condiciones ambientales. Las simulaciones de los modelos fueron consistentes con los resultados experimentales y nos permitieron identificar escenarios de suministro de nitratos que promovieron la coexistencia de las especies a lo largo del tiempo. Estos resultados demuestran que los regímenes de suministro de nutrientes contribuyen a regular la estructura de las comunidades de picofitoplancton y, presumiblemente, la magnitud de la exportación de C orgánico al océano profundo.

Estimación del suministro vertical de la difusión turbulenta de nitratos en diferentes ambientes marinos

La producción primaria en el océano esta sustentada por aportes externos de nutrientes a la capa fótica (la llamada producción nueva, principalmente nitrato) o por nitrógeno remineralizado dentro de la capa fótica (producción regenerada) (Dugdale et al. 1967). La eficiencia de la bomba de carbono puede ser medida en términos de f-ratio, definido como el porcentaje de la producción total que es producción nueva (Eppley and Peterson 1979).

La difusión turbulenta de nitrato se ha considerado tradicionalmente uno de los principales mecanismos por los que se suministra nitrógeno al fitoplancton que habita en la superficie del océano, especialmente importante en regiones del oceáno que están permanentemente estratificadas, como es el caso de as regiones tropicales y subtropicales (Lipschultz et al. 2002) y zonas templadas durante la estratificación en verano (Rippeth et al. 2005; Bendtsen and Richardson 2018). Cuantificar la difusión de nitrato requiere de medidas de difusividad vertical (Kz) que pueden ser inferidas de observaciones microestructura. Sin embargo, esta aproximación experimental presenta dificultades metodológicas por las cuales se ha limitado nuestro conocimiento sobre la magnitud y la variabilidad geográfica de este proceso y muchas veces se ha usado una constante para estimarlo (Capone et al. 2005). En este capitulo, se han utilizado un gran conjunto de observaciones de turbulencia de microestructura recogidas en diferentes ambientes marinos para construir un modelo de predicción y obtener la primera climatología de la difusión de nitrato en la zona eufótica usando un modelo MFP (multivariable fractional polynomial). El objetivo de este modelo será 1) Hacer la estimación global del suministro de nutrientes por difusión por turbulencia en regiones tropicales y subtropicales, y 2) predecir el cambio de la relación cianobacteria/picoeucariotas en un escenario de cambio global (2100 mantiendo el incremento actual de emisiones). Debido a la alta correlación entre las variables y nuestro interés por usar variables que fuesen fácilmente medibles, se seleccionó el gradiente de nitrato en la nutriclina, la concentración de clorofila superficial y la temperatura supercial como representantes de cada uno de los clusters que formaban los datos. Un modelo que incluía tres predictores (temperatura superficial, gradiente vertical de nitrato y clorofila-*a* superficial) explica el 57% de la varianza en el flujo difusivo de nitrato. Este modelo se aplicó a los datos climatológicos para predecir la difusión de nitratos en el océano global. La difusión media de nitrato para regiones oligotróficas entre 40ºN-40ºS (~20 Tmol N y^{-1}) fue comparable a la suma de las estimaciones globales de fijación de nitrógeno, flujos fluviales y deposición atmosférica, y por lo tanto representa la principal entrada de nitrógeno nuevo en estas regiones. Finalmente, estimamos que con la disminución del suministro de nitrato debido al cambio global, la proporción de cianobacterias a picoeucariotas aumentará un 8% en un océano futuro, provocando implicaciones importantes, dada la contribución de las células más pequeñas a la bomba de carbono biológica.

Conclusiones

1. La temperatura y el suministro de nitrato fueron más relevantes que la luz para predecir la biomasa integrada en la capa fótica de la mayoría de los subgrupos de picoplancton, excepto en el caso del *Prochlorococcus* y los procariotas de bajo ácido nucleico (LNA), para los cuales la irradiancia también jugó un papel significativo.
2. El suministro de nitrato fue el único factor que permitió la distinción entre los nichos ecológicos de todos los subgrupos de picoplancton autotrófico y heterótrofo.
3. *Prochlorococcus* y los procariotas LNA fueron más abundantes en aguas cálidas donde el suministro de nitrato era bajo, *Synechococcus* y las bacterias de alto contenido en ácido nucleico (HNA) prevalecieron en ambientes más fríos caracterizados por niveles intermedios o altos de suministro de nitrato y, finalmente, el nicho de los picoeucariotas se definió por bajas temperaturas y elevado suministro de nitrato.
4. La dinámica de suministro de nitrato controló el resultado de la competencia entre la cianobacteria *Synechococcus* y el picoeucariota *Micromonas pusilla*.
5. En condiciones de limitación por nitrato *Synechococcus* superó a *Micromonas pusilla*, revirtiéndose el resultado de la competición en condiciones de pulsos de nitrato.
6. La tasa de exclusión competitiva de *Synechoccocus* fue una función lineal de la frecuencia de pulsos de nitrato, lo que demuestra la existencia de una ventana de oportunidad para la coexistencia de ambas especies.
7. Un modelo que incluyó tres predictores (temperatura superficial, gradiente vertical de nitrato y clorofila-*a*) explicó el 57% de la varianza en el flujo difusivo de nitrato.
8. El promedio de la difusión de nitrato para regiones oligotróficas entre 40ºN-40ºS (~20 Tmol N y^{-1}) fue comparable a la suma de las estimaciones globales de fijación de nitrógeno, transporte fluvial y deposición atmosférica.
9. La disminución prevista del suministro de nitrato en las zonas tropicales y subtropicales como resultado del cambio global (~20%), produciría un aumento en el ratio de la biomasa de cianobacterias y picoeucariotas del 8%.

Universidade Vigo